TAP2 - PAT2

Intelligent materials for energy conversion, storage and savings through soft chemistry

CHEMAT

R. CLOOTS (ULG)
K. DE BUYSSER (UGENT)
M. TRAIANIDIS (CRIBC)

STANDARDISATION

TELECOMMUNICATIONS

SPACE SECTOR

CLEAN TECHNOLOGIES

NEW MATERIALS

.be

PROGRAMME TO STIMULATE KNOWLEDGE TRANSFER IN AREAS OF STRATEGIC IMPORTANCE

TAP2

FINAL REPORT

INTELLIGENT MATERIALS FOR ENERGY CONVERSION, STORAGE AND SAVINGS THROUGH SOFT CHEMISTRY
CHEMAT

P02/00/03

Promoters

Rudi Cloots
Chimie des Matériaux Inorganiques, Chemistry Institute B6a, University of Liège
Sart-Tilman, B-4000 Liège
Serge Hoste, Klaartje De Buysser
Inorganic and Physical Chemistry Department, University of Ghent
Krijgslaan 281, B-9000 Gent
Maria Traianidis
Centre de Recherche de l'Industrie Belge de la Céramique
Avenue Gouverneur Cornez 4, B-7000 Mons

Authors
Rudi Cloots (ULg)
Klaartje De Buysser (UGent)
Maria Traianidis (CRIBC)

Université de Liège ULg   bcrccribc   UNIVERSITEIT GENT

R. Cloots, K. De Buysser, M. Traianidis, ***Intelligent materials for energy conversion, storage and savings through soft chemistry - CHEMAT***, Final Report, Belgian Science Policy (Programme to stimulate knowledge transfer in areas of strategic importance – TAP2), Brussels, 2011, 93 p.

TABLE OF CONTENTS

Summary

Context

Recent advances in solid state chemistry have resulted in substantial progress towards achieving a better understanding of the solid state, and have even led to the development of new predictive capabilities in crystal chemistry. Entirely new ways of preparing and studying advanced materials have resulting in pursuing the so-called "soft chemistry" approach to materials science and technology, getting access to a control of microstructure and heterogeneities at the nanoscale level.

Our aim is to set up a national expert consortium for the development of intelligent materials based on soft chemical production technology. Soft chemistry avoids the use of excessive heat or other energy input to produce chemicals by optimising the chemical structure and reactivity of the reagents and by promoting water as the preferred medium of reaction.

The scope of the CHEMAT task force is broad and encompasses many targeted actions such as the development of tailor made, soft chemical process on demand for the industry, for example research in space application of electroceramic materials or actions in education and dissemination of knowledge in this promising and emerging field of new materials technologies. The project will be launched by a Belgian academic consortium of two well established and highly specialised research laboratories, one at the University of Ghent, the other at the University of Liège, and a research center offering all the competences in the field of material sciences. Phase 1 of CHEMAT is at first enacted during 3 years, in the framework of this TAP2 proposal. It should develop during its growth stages in order to become a Belgian Federal Pole of Expertise with international ambition.

Deliverables cover the research and development of extremely efficient energy storage systems and converters (Li-ions batteries, superconductors, thermoelectric), of ecologically acceptable new chemistries for the industrial production of intelligent materials. In addition CHEMAT will closely monitor worldwide developments in this field and draft a roadmap for our local industries as priority.

Project description

The research will include the preparation and analysis of novel oxides and their use as potential candidates for the design of efficient energy storage or converting systems. As the introduction of clean technologies for energy production and storage has become a major concern throughout both industry and academia, oxides are presently undergoing an

upsurge of interest as heat-to-electricity converters, superconducting magnetic energy storage systems, batteries,... As ULg, CRIBC and UGent partners are also the stepping stone from bench to pilot plant, research will also include many engineering techniques (both chemical and electrical), like the device conception, its operation in a severe environment (for space applications for example) and the use of modelisation.

The relevance of the project is immediate and even double: the project aims at studies involving (i) the design and development of advanced engineering materials in an original research plan, and (ii) the use of energy and environment friendly materials for sustainable energy.

Résumé

Contexte

Les progrès récents réalisés dans le domaine de la chimie du solide ont permis d'une part des avancées importantes autorisant les chercheurs à une meilleure interprétation de l'état solide et des comportements liés des matériaux, et d'autre part la possibilité d'établir des prédictions se rapportant aux caractéristiques cristallochimiques requises pour un matériau en vision d'une propriété donnée. De nouvelles voies de synthèse ont émergé ouvrant le chemin à de nombreuses innovations en termes de matériaux grâce à une approche nouvelle basée sur l'utilisation de la "chimie douce" fortement inspirée des découvertes de la nature. Ces nouvelles voies de synthèse offrent la possibilité de contrôler la microstructure et les hétérogénéités de structure d'un matériau solide à l'échelle du nanomètre.

Notre but est de fédérer un consortium national d'experts actifs dans le domaine des matériaux intelligents préparés par voies de "chimie douce". Les techniques de "chimie douce" permettent de produire des matériaux sans apport conséquent d'énergie en optimisant les structures et la réactivité des composants et en favorisant l'eau comme milieu de synthèse.

Les objectifs rencontrés par CHEMAT sont ambitieux et sont orientés d'une part "développements de procédés par voies de chimie douce pour des matériaux d'intérêt industriel" comme dans les domaines du spatial et de l'électrotechnique, et d'autre part "actions dans les milieux éducationnels et scientifiques". Le projet est porté par deux laboratoires d'université (Gand et Liège) spécialisés dans la recherche sur les matériaux intelligents, et par un centre de recherche industriel (CRIBC Mons) compétent dans le domaine des matériaux inorganiques et doté de multiples expertises physico-chimiques de la science des matériaux. CHEMAT a été initié dans sa phase originelle grâce à un financement de la politique scientifique fédérale belge pour 3 ans dans le cadre du programme PAT2. L'objectif à terme est d'être reconnu comme pôle d'expertise dans le domaine des matériaux intelligents avec des ambitions internationales.

Les "délivrables" du projet concernent l'élaboration de systèmes performants dans le domaine du stockage et de la conversion d'énergie (accumulateurs au lithium, supraconducteurs, thermoélectriques) au travers de voies de synthèse par chimie douce des matériaux inorganiques intelligents qui les composent. CHEMAT a pour ambition également de dresser des perspectives nouvelles dans ces différents domaines de recherche pour aider les industries locales à maintenir et renforcer leur concurrence internationale.

Description du projet

Le projet concerne donc la mise en œuvre par voies de procédés "chimie douce" des composantes de systèmes compétitifs et durables de stockage et de conversion d'énergie, en l'occurrence les thermoélectriques pour la conversion de chaleur en électricité, et les matériaux supraconducteurs à haute température critique et les batteries Li-ion pour le stockage de l'énergie électrique. Les avancées récentes réalisées dans ces domaines l'ont été sur base des innovations réalisées dans le domaine des oxydes mixtes. Les partenaires du projet sont également armés pour concevoir et tester les démonstrateurs ou prototypes issus de la recherche sous contraintes environnementales sévères le cas échéant (pour des applications spatiales par exemple).

L'importance d'une telle action est double: elle offre la possibilité d'un développement nouveau dans le domaine des matériaux "électrocéramiques" compte tenu des méthodes de synthèse envisagées, mais aussi dans le domaine de l'utilisation rationnelle d'une énergie propre.

Samenvatting

Context

Recente ontdekkingen op het gebied van de vaste stof chemie hebben geleid tot het beter begrijpen van de vaste stof op zich en maken het zelfs mogelijk om een aantal nieuwe technieken te ontwikkelen die een voorspellend karakter hebben voor de kristalchemie van vaste stof materialen. Het ontwikkelen van nieuwe synthesemethodes en het bestuderen van geavanceerde materialen via de "soft chemistry" maken het mogelijk om de microstructuur en heterogeniteit van het materiaal op nanoschaal beter te kunnen controleren.

Het doel van dit project is om een nationaal expertise consortium op te richten met als doel de ontwikkeling van intelligente materialen gebaseerd op de "soft chemistry" productie technologie. Deze "soft chemistry" aanpak vermijdt het gebruik van erg hoge temperaturen of andere grote energie input bij het productieproces van de materialen door de chemische structuur en de reactiviteit van de reagentia zo aan te passen dat deze energie input niet langer nodig blijkt te zijn. Daarenboven wordt zoveel mogelijk water gebruikt als reactiemedium.

Het werkdomein van het CHEMAT consortium is breed en omvat een aantal werkpakketen zoals het ontwikkelen van een op maat gemaakt, "soft chemistry" proces op vraag van de industrie zoals: onderzoek naar het gebruik van elektrokeramische materialen voor ruimtevaart toepassingen of bijscholingen of het doorgeven van de kennis in dit veel belovend en groeiend gebied van nieuwe materialen. Het project wordt gedragen door een Belgisch academisch consortium bestaande uit 2 gevestigde en zeer gespecialiseerde onderzoeksgroepen (1 groep is gesitueerd aan Universiteit Gent en de andere onderzoeksgroep maakt deel uit van Universiteit Luik) en een onderzoekscentrum die alle competenties bezit op het vlak van de materiaal wetenschappen. Fase 1 van het CHEMAT consortium was gedurende 3 jaar actief in het kader van dit TAP2 project. Het CHEMAT consortium kan doorgroeien tot een Belgisch Federaal expertise centrum met internationale ambitie.

Dit project omvat het onderzoek en ontwikkelen van (i) extreme efficiënte energie opslag systemen en convertoren (Li-ion batterijen, supergeleidende materialen, thermo-elektrische materialen) en (ii) ecologisch verantwoorde nieuwe chemische synthesemethodes voor de industriële productie van intelligente materialen. Daarenboven zal CHEMAT de wereldwijde ontwikkeling in deze gebieden nauwlettend monitoren en prioriteit geven aan het uittekenen van een roadmap voor de lokale industrieën.

Project beschrijving

Het onderzoek omvat de bereiding van de analyse van nieuwe oxide materialen en hun gebruik als potentiële kandidaten voor de ontwikkeling van efficiënte energie opslag of conversie systemen. Het gebruik van "schone" technologie bij het produceren en de opslag van energie is een belangrijk onderzoekstopic voor zowel de industriële als de academische wereld. Hierdoor ontstaat er een grote interesse naar het gebruik van oxide materialen als warmte-elektriciteit convertoren, supergeleidende materialen, supergeleidende magnetische energie opslag systemen, batterijen,… Omdat de ULg, CRIBC en UGent partners de tussenpersonen vormen tussen laboschaal experimenten en een pilootopstelling zal het onderzoek ook een aantal technische ontwikkelingen (zowel chemisch als elektrisch) omvatten zoals materiaal prototypes ontwikkelen, het gebruik in extreme omstandigheden bestuderen (bijvoorbeeld in de ruimtevaart) en modellering allerhande.

De relevantie van dit project is tweeledig. Het project mikt (i) naar het ontwerpen en ontwikkelen van geavanceerde technologische materialen in een origineel onderzoeksplan en (ii) naar het gebruik energiezuinige en milieuvriendelijke materialen voor duurzame energiewinning.

I.   CONTEXT

Recent advances in solid-state chemistry have resulted in substantial progress towards achieving a better understanding of the solid state, and have even led to the development of new predictive capabilities in crystal chemistry. Entirely new ways of preparing and studying advanced materials have been the result of pursuing the so-called "soft chemistry" approach to materials science and technology, getting access to a control of microstructure and heterogeneities at the nanoscale level.

The vast majority of the technological benefits of today are the result of sustained investments in the development of materials during the previous decades. The first industrial revolution and the age of mechanical construction were based on iron and coal. The existence of a world-encompassing information technology is based on the development of materials like silicon, germanium, zinc, aluminium but a new stone age awaits: ceramics and, more generally, inorganic hybrid composites are the future.

Ceramics have already played a very big part in human activities since ages in enabling advances in construction (bricks), industry, health and leisure (classic ceramics) but their impact in electronics and space technology has been relatively recent and less profound. The discovery of copper-based superconducting ceramics in November 1986 has spurred the whole scientific community into considering a bewildering array of novel properties for this class of solids. Product properties like magneto-optics, thermo-electricity, magnetoresistance, piezo-optics, pyro-electricity and their applications in electronics, aeronautics, space, and safety technologies, in the clean production and distribution of energy, in improving the efficiency of transport or communications and in many other domains, can now be envisaged through sensitive applications of chemistry in the development of intelligent materials. These developments are based on the understanding that sophisticated, multi-component materials require more than the constructivist building block approach of mainly physical methods, i.e. "searching before constructing". Instead the natural but immense power of atomic self-arrangement into extremely complex arrays has hardly been harnessed for the controlled growth of intelligent materials. **This is the basis of intelligent chemical (nano)technology**.

This "material intelligence" is either passive (functional ceramics, integrated materials, composites) or active (sensors, actuators, self-cleaning films, reactive catalysts). Their control and benefits can be harvested thanks to the diligent combination of new methods in synthetic chemistry with the newest methods for materials analysis. This is the basis of the new "soft chemistry" approach.

Such a development obviously requires the guidance and support of its penultimate beneficiary: the manufacturing industry.

Thus, we propose to enact the creation of a <u>Federal Pole of Expertise</u> for the development and support of new, intelligent materials, CHEMAT. The objectives and operation of such a Pole of Expertise are described in details below.

This initiative is taken by two Belgian research groups at ULg and UGent with long standing co-operation in the field of inorganic materials chemistry, and by the Belgian Research Center in Ceramics. In the past these members have carried out joint research under federal funding and have benefited from regional governmental, international, and industrial supports. Their commitment to this proposal is fundamentally driven by the insight that the constellation of scientific knowledge, societal needs and technological demands is such that chemical ingenuity can be advantageously applied to many frontier fields and greatly improve today's capacities. Simultaneously, it is considered that such advances should aim to reduce the "scorned upon" total environmental impact of the present manufacturing industries while the users of new technologies should not bear excessive costs during or for their switch to this technological level.

II.   OBJECTIVES

In the present project, each of the partners will exploit one specific "soft chemistry" route (sol-gel, hydrothermal, templating, wet chemical synthesis) to prepare materials involved in energy conversion and storage. Two strategic applications have been selected: (i) compact energy storage systems (minimal energy consumption, high capacity, zero time constant) thanks to superconductors and mixed ionic-electronic conductors, and (ii) waste heat recovery using high temperature thermoelectric power units.

The objective of materials processing by means of soft solution processing is to fabricate or assemble functional products from technological materials with minimal consumption of energy at a low cost. In this proposal we will use various aspects of soft solution processing including sol-gel, hydrothermal, templating and wet chemical synthesis techniques.

Nowadays, a major challenge is the decreasing of pollutant emission and more efficient uses of our energy resources. With this aim in view, energy storage and energy conversion appear like a necessity, closely linked to the continuously growing electric energy demand, and there is no reason to think that this is going to change in the future.

(i) Electrochemical energy storage systems are already widely used. Among them, lithium accumulators offer all guarantees of success in the coming years, guided by the potential users needs and by security and environmental protection orientations of authorities. Although such accumulators are commercially successful, we are reaching the performances using current electrode materials. For applications in clean energy storage and use in hybrid electric vehicles, we need to improve materials performances. New intercalating electrodes are needed in order to improve life cycling by accommodating strain associated with lithium insertion/removal during operation.

(ii) A major challenge facing the commercialization of high temperature superconductor tapes is reducing the cost of manufacturing them while maintaining the performances required for practical applications like superconducting magnetic energy storage systems. Although solution-based deposition processes have been successfully developed for a wide variety of applications, continuous deposition of high-quality superconducting films over flexible substrate for electrical applications is a new aspect of innovation in the high-T_c superconductivity field of research.

(iii) Waste heat from automobiles, factories and other similar sources offers a high quality energy source equal to about 70% of the total primary energy source. Thermoelectric

generation systems offer the possibility to convert heat energy directly into electrical energy. Oxide materials are widely used due to their high chemical stability in air at 800-1000°C. Thanks to the soft chemistry approach the design of new functional oxides according to the concept of nanoblock integration will be envisaged (each block playing its own role in generating a specific function, one possessing a strongly correlated electron system serving as electronic transport region, and the other serving as phonon-scattering region to achieve low thermal conductivity, both being needed for getting high thermoelectric performances).

III.   PROJECT GOALS

One of the great challenges in the twenty-first century is energy storage and energy conversion. In response to the needs of modern society and emerging ecological concerns, it is now essential that new, low-cost and environmentally friendly energy conversion and storage systems are found. Performances of the devices are strongly dependent on the materials development. To produce materials with specific properties, the chemistry has to be fully controlled and modulated. This can be done through innovative processing routes thanks to the soft solution processing concept. Three targeted devices have been clearly identified.

Lithium-ion batteries are one of the great successes of modern materials electrochemistry field of research. Commercially available Li-ion batteries are successful today but are reaching the limits in performances using the current electrode and electrolyte materials. We must advance the science to advance the technology. Nanostructured materials offer the way of opening new concepts in getting advanced powerful energy conversion and storage devices. We will concentrate on the cathode, much less developed today than the nanoanodes. Different strategies have been suggested thanks to the chemistry which plays a central role in constructing appropriate materials. Innovative methods of producing nanopowders will be implemented (hydrothermal, sol-gel, GLA, templating,…) and tested. One of the big issues in using nanostructured cathodes is to overcome interactions between the cathode itself and the electrolyte. Coating particles with a stabilizing surface layer may help to alleviate such problems. By using a template it is also possible to produce porous and high surface area electrodes enhancing electrical capacities if cyclability is maintained. **All of these concepts have to be validated through the design of prototypes**, first lithium-ion batteries in the form of conventional electrochemical cells using liquid lithium salts as the electrolyte for the cathode to be fully characterized on an electrochemical point of view. Conventional batteries as those used in the market (coin cells) will be then produced thanks to the laboratory testing in ERACHEM (Tertre) for characterizing the performances of the material with respect to its use (cyclability, capacity, …).

The potential uses of high temperature superconducting cables for electric power applications include transmission cables, oil-free transformers, fault-current limiters, high-efficiency motors and compact generators, and superconducting magnetic-energy storage units. Even if superconducting wires of 10 to 100 m in length can be made, material and processing issues must be solved before an optimized production scheme can be achieved. The strategic goal is to achieve high temperature superconducting wires with a current capacity 100 times that of copper. One of the main obstacles to the manufacture of

commercial length of superconducting wires is the weak-links problem: grain boundaries formed by the misalignment of the superconducting grains create obstacles to current flow. Several methods have been developed to obtain biaxially textured substrates suitable for the production of high-performances superconducting cables. A low-cost manufacturing process for producing long lengths of high performances superconducting cable is also a challenge. Thanks again to the chemistry (sol-gel, hydrothermal and GLA) the development of a controlled superconducting material growth process can be achieved. Dip coating appears to be the most appropriate coating technique for industrial film-coating processes. Texture in the substrate will be induced by a pre-treatment under an external magnetic field giving access to a low-cost, high-rate deposition of high performance superconducting films on continuous length. **Precursor formulation, precursor coating and precursor decomposition will be the steps to fully control and improve for producing a low-cost scalable process**. The characteristics and performances of the superconducting films (texture, electrical properties, mechanical properties) will be evaluated first on short lengths samples. **A variety of coil demonstrations will be then tested** at different temperatures (from 4.2K to 77K) in different magnetic inductions depending on the application under consideration.

High-efficiency thermoelectric materials are important for power-generation devices that are designed to convert waste heat to electrical energy. The conversion of waste heat to electrical energy may play an important role in our current challenge to develop alternative energy technologies to reduce our dependence on fossil fuels and reduce greenhouse gas emissions. The demand for higher performance high temperature thermoelectric materials than those that are currently in use has generated an increased activity in this field of research during the last decade. Power-generation applications interest the automotive industry focalised on the development of electrical power from waste heat from the radiator and exhaust systems for use in the next generation of vehicles. A key factor in developing these technologies is the development of higher performance thermoelectric materials. A thermoelectric device is composed of an n-type (negative thermopower and electron carriers) and a p-type (positive thermopower and hole carriers) semiconductor material connected through metallic electrical contact pads. The goal of the current research is to find a thermoelectric material operating with high efficiency at high temperature (>400°C). A layered cobalt oxide for the p-type partner of the thermoelectric device is a good candidate. Improvement in the chemistry for producing controlled stoichiometry and texture bulks or thin films will be the central part of the current research. Soft solution processings open the way for producing nanostructured materials with a high control of the anisotropy and chemistry for providing different paths in space for electric current and thermal current flow enabling us to control the thermal conductivity and the electrical conductivity separately

(the nanoblock integration concept). For the n-type partner of the device, heavily doped strontium titanate or manganites will be used. For producing a thermoelectric oxide module both p-type and n-type materials have to be hot-pressed in order to align the grains and to correctly densify the materials. Silver paste will be used for providing good oxide/metal junctions. A prototype made of more than 20 legs connected in series will be tested for power-generation applications.

IV. WORK PLAN

IV.1 Work Package #1 "New electrode for next generation Li-ion batteries"

New technologies are needed to reduce the impact of our overall consumption of fossil fuels and aid the developed and developing countries as they adapt to future trends. In this WP we tackle one important element of energy management, that of energy storage!

Energy storage using new Li-ion batteries will be under consideration. For example Oxygen S.p.A., an Italian provider of electric transporters, has placed orders for Valence's new U-Charge XP lithium-ion battery systems which will power a new line of electric scooters designed for delivery fleets across Europe. Although widely used, the most promising Li-based technologies still suffer from a lack of suitable electrodes (cyclability versus capacity retention). There is therefore a need to seek new materials concepts to satisfy the increasing demands for energy storage. Fully reversible intercalation electrodes synthesized through soft chemical processes could provide a new direction for developing an alternative class of higher energy density Li storage systems. Moreover nanostructured materials are becoming increasingly important for electrochemical energy storage. Both concepts will be thus under consideration within this WP for developing a new generation of cathode for Li-ion batteries.

To sustain fast and reversible electrochemical reactions, intercalation compounds must be used, and that the electrochemical process is accompanied by a continuous solid solution on intercalation. Layered materials ($Bi_2Sr_2(CaCu_2)Co_2O_y$, $Ca_3Co_4O_9$ or $Li(Ni,Mn)O_2$) will be tested as it is well-known that such materials are very sensitive to lithium intercalation without creating internal stresses due to structural modifications. Soft solution processings are needed in order to fully control the stoichiometry of the compound and to enhance the formation of nanoparticulate materials. Due to the nanoparticulate forms of the precursor powder before shaping the electrode, greater reactions with the electrolyte can be expected and will probably need a stabilizing step consisting in modifying the surface of the nanoparticules. Carbon coating can be envisaged, moreover leading to a substantial increase of the electronic conductivity rendering these materials very attractive for this new generation of Li-ion batteries.

Based on the same new concept, manufacturing of nanostructured materials through templating is another way for increasing capacity and cyclability of Li-ion batteries. Nanopillars of more classical cathode materials like VO_2 or $LiMn_2O_4$ can be grown on a metal substrate and can first accommodate more easily volume changes and then support high intercalation reaction rates. Disordered mesoporous materials like aerogel can also be tested.

THE DELIVERABLES AND CHRONOGRAM ARE TO BE THE FOLLOWING:

- D1 Intercalation compounds I (month 1 to month 12): synthesis of layered Li(Ni,Mn)O$_2$ by soft solution processings and demonstration of easy conversion into LiMn$_2$O$_4$ through lithium deintercalation without any stress generation;

- D2 Intercalation compounds II (month 12 to month 24): synthesis of layered Bi$_2$Sr$_2$(CaCu$_2$)Co$_2$O$_y$ and Ca$_3$Co$_4$O$_9$ by soft solution processings and demonstration of their ability to incorporate lithium with great reversibility (higher than 99%);

- D3 Evaluation of performances (month 1 to month 24): Impedance spectroscopy measurements of ionic conductivity – Microstructural characterization of material evolution during operation and closer look at the interfaces electrodes-electrolyte to validate the concept;

- D4 Nanostructured materials (month 24 to month 36): synthesis of TiO$_2$ or VO$_2$ nanowires and nanotubes by templating – Evaluation of their performances (see D3);

- D5 Prototype conception (month 12 to month 24): elaboration of classical electrochemical cells to probe the intrinsic properties of the materials – Elaboration of a coin cell (to test the capacity and cyclability).

IV.2   Work Package #2 "Coated Conductors using superconducting materials"

High Temperature Superconductors (HTS) are known to be one of the most promising materials for the efficient storage and transmission of electrical energy. These materials are considered for a broad range of applications, i.e. from power engineering to communication technologies and also medical applications. Various programs are conducted to develop superconducting electric power apparatuses such as power cables, transformers, motors, current limiters, SMES, magnets,… Among practical materials, YBa$_2$Cu$_3$O$_7$ (YBCO) coated conductors exhibit a favourable critical current density dependence versus temperature and controlled external magnetic field dependence. They can be produced via reliable processing technologies, like vacuum deposition techniques. We propose to pursue chemical deposition methods, considered to be promising but still requiring optimization developments to reach the goal of a fully chemical based new generation of superconducting products with enhanced properties, e.g. high critical current density. The chemical solution deposition technique is an original, very promising, cheap, environment friendly and low cost method for producing such coated conductors. We pretend that its upscalability offers the possibility to produce long length superconducting YBCO wires or tapes. Such achievements are the major objectives to guarantee a widespread use of superconductivity in power applications. Specifically, a new method for producing strong biaxially textured YBCO coated conductors will be optimized and validated in the context of the TAP2 project, opening the way to a third generation of HTS conductors with high critical current density of the order of "MA/cm^2" at 77K and 0T, comparable to the critical current density for the best (but tiny)

single crystals. Finally it is relevant to maintain (and even to develop!) such an innovative technology in Europe, in general and in view of the ITER location.

Major advances have been made during the last decade in the processing of ceramics, high temperature superconductors. For most large-scale applications long lengths of flexible wires carrying large amounts of supercurrents are required. It has been now well established that in order to achieve such a level, long-range, biaxial or triaxial crystallographic texturing of the superconductor is necessary. Significant efforts have to be directed at attempts to fabricate long-lengths of near single crystal-like superconducting wires by epitaxial and controlled growth on biaxialy textured substrates.

Development of such coated conductors based on sol-gel technologies and related wet chemical processes is thus proposed in this WP. The task encompasses the application of established chemical experience in dip coating of ceramics to the elaboration of tailor made chemistries for coated conductor development. This encompasses definition of buffer layers, texture optimisation using chemical templating, developing process technology for multilayer deposition and compositional variation of coatings.

A new approach based on the magnetic field texturing of the substrate will be first implemented in order to produce biaxially textured YBCO films. Next a chemical solution deposition method for coated conductors applications will be developed. It bears upon Ni electrodeposition, achieved under external magnetic fields, giving easy access to "cube" textured Ni substrates; the control of the epitaxial growth of the YBCO and various buffer layers are to be investigated. In order to do so CeO_2 or $La_2Zr_2O_7$ buffer layers and YBCO will be deposited both by a dip (or spin)-coating process from a sol-gel or wet chemical precursor, with in mind the optimization of their rheological and physical properties (viscosity, wettability, adhesion, sol-gel stability, coating uniformity,…). Each layer will be thermally treated by controlling appropriate variables, i.e. temperature, atmosphere, and time. Optimization will be searched with respect to phase composition, substrate interaction, density and microstructure of the film, texture and finally the mechanical and superconducting properties (at least T_c and J_c). Connectivity between YBCO grains is a very important parameter to be optimized for getting the highest Jc values, and will be characterized through Hall-probe mapping, magneto-optical imaging, transport critical current. Manufacturing of long length YBCO coated conductors will be then performed through a scaling-up of the above chemical solution deposition process for producing in a continuous way successively long length biaxially textured substrates (more than 10 m long), buffer layer and biaxially textured YBCO film. Magnetic field dependence and mechanical

strain dependence of critical current density of these long length coated conductors will be evaluated in detail for optimizing and approaching commercial production.

THE DELIVERABLES AND CHRONOGRAM ARE TO BE THE FOLLOWING:

- D1 (month 1 to month 12): optimization of the electrodeposition of Ni under external magnetic field for producing biaxially textured substrates; method and tests: Pole figure measurements by X-ray and EBSD for characterizing the in-plane alignment and grain size uniformity;

- D2 (month 8 to month 24):
  - D21 (month 8 to month 18): sol-gel or wet chemical process deposition of CeO_2 and/or $La_2Zr_2O_7$ buffer layers;
  - D22 (month 8 to month 24): deposition of YBCO; method: spin or dip-coating on biaxially textured Ni recovered substrates ; tests: rheological behavior of the gel, microstructure, pole figures measurements for optimization and validation of the process;
  - D23 (month 8 to month 24): trial tests for the production of coatings through hydrothermal synthesis (CeO_2, $La_2Zr_2O_7$, YBCO);

- D3 (month 12 to month 36): superconducting properties evaluation for process optimization; methods and tests: Hall-probe mapping, magneto-optical imaging, transport critical current ; mechanical properties, ageing resistance measurements; magnetic properties:
  - D31 (month 1 to month 8): comparison of methods and normalisation for classical superconducting materials (bulks, thin films, single crystals);
  - D32 (month 8 to month 12): first evaluation of the lab-made YBCO coated conductors.

IV.3 Work Package #3 "Oxides for Heat-to-Electricity converter"

The elementary unit of a thermoelectric device is made of two "legs" that are linked together on one side, where hot temperature is applied. On the opposite side of the cell, exposed to a lower temperature, the f.e.m. appearing between the "legs" can be collected. One of the legs must be electron-conductive (N-type) and the other must be hole-conductive (P-type). To achieve a significant voltage potential across the output terminals of the device, these elementary units must be electrically connected in series and thermally connected in parallel. The thermoelectric efficiency of a material is called the "figure of merit" (ZT). ZT is a ratio involving, at the numerator, the electric conductivity, the operating temperature and the proportionality factor between the input thermal gradient and the output voltage potential (Seebeck coefficient) and, at the denominator, the thermal conductivity. A good

candidate has therefore to be highly electron or hole conductive and at the same time a very poor thermal conductor.

Thermoelectric devices are already commercialized either for cooling or for power generation. Most of these devices are limited to low temperatures (150-200°C). The thermoelectric material used in these components is bismuth telluride which exhibits a very high figure of merit (ZT ~ 1). Commercial power generation modules commercialized by Hi-Z (USA) are already operational for power generation through trucks waste heat conversion. The operating temperature is still low (temperature of exhausting gas is of about 900°C), these materials exhibit another drawback: under high temperature in air or any other oxidizing media, they oxidize. To overcome these problems, oxide materials were investigated.

Thermoelectric oxides for power generation is a recent field of investigation and most of this research is performed in Japan. $NaCo_2O_4$ is the first efficient material discovered in 1997 by Terasaki et al. A series of derived cobaltites followed the said "misfit cobaltite" $CaCo_3O_4$ either substituted or not with heavy atoms. These materials are of low dimensionality, naturally composed of alternately highly electric conductive layers and low thermal conductive ones. This particular structure is responsible for their high figure of merit. Cobaltites can be regarded as the most promising system for the P-type (hole conducting) leg of the thermoelectric unit. N-type are less investigated. Similarly, the most efficient system for the N-type (e- conducting) leg is the titanate or manganese oxides.

The challenge of creating novel thermoelectric oxides operating at high temperature with high chemical stability has thus recently motivated investigations from various materials concepts like the hybrid crystal to be effective in controlling electron and phonon transport separately, thus enhancing the total conversion efficiency. Layered cobaltites can be regarded as being composed of nanoblocks or nanosheets integrated into a "superlattice". Each block can play its own role in generating a specific function, and hence electron and phonon transport can be independently controlled. Moreover due to the high structural anisotropy of these cobaltites, the alignment of plate-like grains by mechanical or chemical means is necessary in attaining the best performances. One of the most promising techniques to obtain grain-oriented ceramics is the templated grain-growth (TGG). In this process large anisotropically shaped particles are used as templates for grain growth and are oriented in a fine particle size matrix by a shear gradient imposed during forming (tape casting, hot pressing or hot forging). The main research objective is thus the elaboration of cobaltite textured ceramics with high thermoelectric performances. The project will focus

mainly on $Bi_2Sr_2Co_2Ox$ and $Ca_3Co_4O_9$ polycrystalline materials, both in bulk and thin film forms.

THE DELIVERABLES AND CHRONOGRAM ARE TO BE THE FOLLOWING:

- D1: Processing and characterization of textured and non-textured $Bi_2Sr_2Co_2Ox$ and $Ca_3Co_4O_9$ ceramics (month 1 to month 24):
  - D11: selection of the cobaltite and the manganite or titanate materials and set up of the hydrothermal/sol-gel/GLA processing parameters. At the end of this period, a processing route for each product should have been identified. Hydrothermally processed platelet-like template particles should be available. At the same time, ultrafine powders produced either from sol-gel (citrate route) or from GLA methods should be available too (All these powders will be fully characterized for their crystallinity (XRD, DTA-TGA), chemical composition (XRF, ICP) physical properties (He pycnometry, BET, grain size distribution) and morphology (SEM, TEM));
  - D12: there is a need to find the most adequate elements to carry out the texturing by the TGG process (fine grain matrix through appropriate soft solution processings such as sol-gel or hydrothermal process, templates, liquid viscosity, precursor powder characteristics,...) – Structural, compositional and microstructural characterizations by X-ray diffraction, scanning electron microscopy and electron back scattering analyses;
- D2: Processing and characterization of textured $Bi_2Sr_2Co_2Ox$ and $Ca_3Co_4O_9$ thin films (month 1 to month 24): dip-coating of chemical solutions precursor followed by rapid heating - Structural, compositional and microstructural characterizations by X-ray diffraction, scanning electron microscopy and electron back scattering analyses;
- D3: Quantitative texture analysis of the resulting ceramics and thin films (month 12 to month 30): characterization by X-ray and neutron diffraction – EBSD texture analysis (mapping representation of the grain alignment and evaluation of an orientation distribution function);
- D4: Thermoelectric properties measurements of $Bi_2Sr_2Co_2Ox$ and $Ca_3Co_4O_9$ ceramics and thin films (month 12 to month 30): low and high temperature measurements will be performed on the elaborated materials. Electrical resistivity, Seebeck coefficient and thermal conductivity will be measured for investigating the transport behavior and thermoelectric performances of the materials. At the end of this period, a fabrication procedure leading to optimal thermoelectric behavior will be defined for each material. The influence of the sample size and shape on the thermoelectric response will also be investigated;

- D5: Prototype conception (month 30 to month 36): in accordance with the deliverable D4, an optimal design will be defined for the thermoelectric units that will be used for machining and connecting of N-type and P-type ceramics.

A demonstration system will then be built and its performance will be assessed. As an example, this system could be composed of an alumina tube heated above 600°C and surrounded by a metallic ring with an inner water flow. An assembly of thermoelectric units connected in series would be placed between the cold ring and the hot alumina tube generating by this way the thermal gradient. The output voltage would then be collected at each terminal of the assembly.

V.   RESULTS

V.1 Lithium-ions batteries

Soft-templating synthesized mesoporous thin film as positive electrode design for lithium battery: $NbVO_5$ as a probe – The best system for improving performances!

<u>V.1.1 Introduction</u>

Nowadays, Li battery technology appears as an unavoidable alternative to store energy in miniaturized devices. However Li-ion accumulators present low power rate as a result of the slow diffusion of Li^+ inside the electrode materials. Their nanoscalization decreases the diffusion distance improving the high rate capability of the batteries. Nevertheless problems appear during cycling because nanoparticles highly suffer from volume expansions occurring upon lithium insertion and extraction.

Mesoporous thin films (MTF) appear as interesting candidates as they offer high specific area. Pores are homogenously distributed in size, are interconnected and offer a large access to the inorganic network whose wall thickness is uniform.

This work aims at validating the MTF architecture as positive electrode material. The followed approach consists in selecting a material that is known, as bulk, to suffer from severe structural distortions after the first lithium insertion. Inserting lithium ion electrochemically in this candidate will test the ability of MTF to accommodate the as-induced mechanical stresses. $NbVO_5$ was chosen as candidate. $NbVO_5$ MTF were achieved by evaporation induced micelles packing from a precursor solution constituted of PS-b-PEO amphiphilic dibloc copolymer, VCl_4 and $NbCl_5$ in EtOH/THF in the presence of H_2O. The subsequent thermal treatment was adjusted on the basis of thermal ellipsometry analysis results. An ordered porous network presenting pores and wall sizes of 15 nm was highlighted by atomic force microscopy and transmission electron microscopy. These complex mixed oxides mesoporous network have been visualized in the three dimensions using electronic tomography. The connections between the pores could have been highlighted and comfort the assumption of the environmental ellipsometric characterization. The electrochemical behaviors of amorphous $NbVO_5$ MTF presenting three different pore sizes (15, 50 and 100 nm in diameter) were investigated by cyclic voltammetry. It has been shown that the MTF is able to better accommodate mechanical stresses compared to non porous film, and this ability is enhanced as the pore size decreases.

V.1.2 Context

As demonstrated by the market predominance of the lithium ion accumulators in many portable applications, this type of battery definitely plays a crucial role for enabling increasing miniaturization and mobility. (1)(2)(3)(4) The need of high power rechargeable lithium batteries, as means of delivering a large capacity at high discharge rate, has led to considerable interest in nanostructured electrodes (1)(2). Many factors influence the power of the battery, including transport of the Li^+ ions within the electrolyte between the particles of the active material, transport of Li^+ across the electrode/electrolyte interface, diffusion of Li^+ within the intercalation host, electron transport from the current collector to the active electrode particles, and diffusion of electrons within the active particles. (5)(3) Providing a large electrode–electrolyte contact area and shorter diffusion paths for both lithium ion and electron transportation, nanostructured electrodes has been reported to fasten kinetics for the lithium intercalation/deintercalation processes, leading to better rate performance. In addition, shortening the electron transport distances allows the use of otherwise poorly electron-conductive materials. (6)(7)(8) However such nanostructures amplify the role of interfaces, challenging the standard ways in which electrochemically active materials are used for energy storage, but widening the design of the battery. Recently, the concept of 3D microbattery has been introduced. (4)(9)(10) It is based on building architectures where electrodes and electrolyte are three-dimensionally interpenetrated at the nanometer scale. This would yield to improvements in power rate, the scaling up would permit to meet the desired energy density. Studies illustrating the feasibility of 3D solid-state electrochemical cells are now appearing (10)(4). Bruce et al. (8) develop 3D nanoarchitectured cells in which pillar anodes and cathodes are interdigitated.

The key point lies in the choice of the architecture of the positive/negative electrode material that acts as support and defines the design of the future 3D-battery (10). Due to their suitable 3D-interconnected morphology, mesoporous thin films (MTF) appear as promising candidates in this role. MTF present a large surface area and an excellent accessibility of the inner surface thanks to the high-quality void volume. The pores are monodisperse in size, also the walls have the same dimensions and because they are thin, they ensure short diffusion distances for Li^+. If this network appears to be mechanically robust and able to support cycling, this architecture should also overcome the loss of electrical which results from the volume expansions experienced during the intercalation/deintercalation reactions in the case of nanoparticles. Furthermore, as no extra conducting and binding reagents is added to the electrode, MTF are ideal models for understanding how the structural parameters influence the electrochemical performance (11).

Lithium insertion/extraction in MTF has already been investigated in a few works focused TiO_2 considering its potential application in electrochemical energy storage devices (12)(13) or to test the electrochemical accessibility to the porous inorganic network for its applications in photocatalysis (14), solar cells (Grätzel type) (15)(16) and sensors (17) displays. Among others, some works relate Li insertion in WO_3 MTF for electrochromic applications (18)(19).

In a recent work focused on ordered mesoporous micrometer-sized particles, Bruce et al. have demonstrated that mesopores act as a buffering layer to alleviate the adverse effect of volume expansion. They also show how the pore size and the wall thickness of the mesoporous particles can improve the cycling behavior (20). Therefore they have intentionally chosen β-MnO_2 as candidate. Its bulk is known to suffer from a poor cyclic stability: the first discharge of this electrode candidate is associated with a two-phase intercalation reaction, whereas on subsequent cycling lithium intercalation occurs within a single phase. Models created by Sayle et al. (21) predict at the atomistic level the openings of the tunnels into which Li inserts, deep inside the nanopores. This study confirms that for mesoporous MnO_2, there exists a wall thickness (between 10 and 100 nm) above which the strain associated with Li insertion is not accommodated via an elastic deformation of the host lattice leading to property fading upon cycling, supporting the results of Bruce et al. (20) This work tries to extend this approach to MTF, evaluating the ability of this architecture to accommodate important stresses, hence evaluating their ability to support cycling.

We therefore investigate the Li^+ intercalation/extraction into *NbVO_5* mesoporous thin films. $NbVO_5$ compound appears to be an ideal candidate in terms of its low ability to support cycling right after the first lithium insertion. Discovered in 1992 by Amarilla et al. (22)(23), this crystalline phase can only be prepared via a soft chemistry route. In 2003, these authors (23) have highlighted the potential use of $NbVO_5$ powder as a positive electrode material in a lithium accumulator arising from the existence of two types of empty channels for lithium insertion, one with a pentagonal cross-section and a smaller one presenting a rhombohedral cross-section. It appears that, upon the first Li^+ intercalation, the bulk overcomes an important structural distorsion which implies a drop of the capacity of about 90% of its initial value. This distorsion was attributed to the fact that, in the $NbVO_5$ structure, V^{5+} occupies tetrahedral sites. However the latter are too small to accommodate the V^{4+} species formed after Li^+ intercalation, leading to a deformation of the oxygen network and consequently to the trapping of Li^+ species inside the framework (24).

The synthesis of MTF of several transition metal oxides appears to be well-mastered, combining sol-gel and evaporation induced self-assembling of a block copolymer with

complexation of molecular inorganic species. (19) However it remains quite challenging to prepare vanadium oxides MTF. The main synthetic difficulty in achieving nanostructured compound, as for numerous other transition metal oxides, lies in the lack of thermal stability (25)(26). In the vanadium case, it results from the complexity of its chemistry in terms of valence and coordination states, added to the fact that the condensation reactions of the oxide network might be incomplete. (27)(28)

In 2005, Yuan et al. (29) obtained mixed MTF of Nb-V oxides (70-30 mol%) by EISA, but increasing the vanadium content to 50% remains a challenge. Sallard et al (18) have managed to obtain MTF of WO_3 using a KLE (poly(ethylene-co-butylene)-b-poly(ethylene oxide)) amphiphilic surfactant, whose weak interactions with the inorganic network allow their removal without destroying the mesoporous structure. Furthermore thanks to the high thermal stability of this kind of structuring agent, the inorganic network can get more condensed before the surfactant complete removal, comparing to the most widely used pluronic surfactant.

To achieve $NbVO_5$ MTF, we applied the self-assembling method using another amphiphilic diblock copolymer surfactant polystyrene-*b*-polyethylene (PS-*b*-PEO) whose PS part is also known to be calcined at higher temperature (30)(31). In-situ thermal ellipsometric analysis is used to elucidate the behavior of the film while heating. This technique gives access to the pyrolysis temperature of the surfactant and the crystallization temperature of the inorganic walls. Based on these results, we first discuss the possibility of obtaining amorphous and crystalline $NbVO_5$ mesoporous thin films.

Amorphous $NbVO_5$ MTF presenting three different pore sizes and wall thicknesses were achieved. The porous network was highlighted by atomic force microscopy, transmission electron microscopy and environmental ellisometic porosimetry. Part of the porous network have been rebuilt and can be visualized thanks to TEM-TOMO. Although no fully crystalline $NbVO_5$ MTF could have been achieved, amorphous ones present vanadium species and with the expected oxidation state +5 and in the right tetrahedral coordination, as confirmed by several structural characterizations (electronic paramagnetic resonance, X-ray photoelectron spectroscopy and [51]V nuclear magnetic resonance, respectively). For this reason amorphous $NbVO_5$ MTF would also suffer from the large structural distorsion induced by the first lithium insertion.

Cycling this material will definitely be a relevant test to evaluate the ability of the architecture to accommodate the mechanical stresses occurring during cycling. Amorphous $NbVO_5$ MTF were synthesized with three different sizes of pore and wall sizes and once

inserted in a Li cell, they were characterized by cyclic voltammetry. Their ability to maintain their capacity after the second cycle were compared to non porous films, **allowing to show up rapidly the potentialities of building 3D Li-microbattery from MTF positive electrode**.

V.1.3 Experimental part

Mesoporous thin films of $NbVO_5$ were prepared by the Evaporation-Induced Micelles Packing method (EIMP) (32). Three polystyrene-block-polyethyleneoxide (PS-b-PEO) structuring agents were used. The molecular weights of the PS and PEO blocks in hereafter-named PSA, PSB and PSC surfactants are 17,000 g/mol and 39,000 g/mol (PSA), 40,000 g/mol and 110,000 g/mol (PSB), and 105,000 g/mol and 190,000 g/mol (PSC). In a typical synthesis, 100 mg of surfactant (PSA/PSB/PSC) is dissolved in 1,4 g tetrahydrofuran (THF) and heated a few minutes at 70°C in order to achieve complete dissolution. After cooling, 1,5 g of EtOH, 2 ml of a $NbCl_5$ solution (0.9 M in ethanol) and 2 ml of a VCl_4 solution (0.9 M in ethanol) are added. The solution is then equilibrated for 1 hour before adding 0,32 g of distilled H_2O. The as obtained blue-green solution is kept one night at 10°C and is finally heated successively 3 times at 70°C for 1 minute just before dip coating. The substrate (superficially oxidized silicon wafer, FTO-coated glass or very 0,14 mm-thick glass) is dipped in the solution and withdrawn at a rate of 1 to 2,5 mm/s at a relative humidity of 10%. The film is then stabilized at 180°C for 10 minutes in air. The as-synthesized film thickness evaluated by ellipsometry is around 100 nm.

For multilayer films, each layer is subject to this stabilization at 180°C before the next dipping. The as-obtained single-layer and multilayer films are then calcined at 350°C for 10 minutes and finally annealed at 500°C for 1 minute in air.

Dense films were also prepared in the same conditions but without PS-*b*-PEO surfactants. Wettability of the substrate was improved by adding ~1 mg F127 (EO_{100}-PO_{65}-EO_{100}) to these solutions.

Metallic-free PSA/PSB/PSC based solutions were also prepared for DLS measurements following the previously described procedure except from the fact that 4 ml of EtOH are added in place of 4 ml of the vanadium / niobium chloride precursor solution.

Atomic Force Microscopy (AFM) was performed with a Veeco DI-CPII in non-contact mode. Scanning electron microscopy was performed using a Philips XL30 FEG-SEM. Transmission electron micrographs of fragments scratched from the films were obtained in a TECNAI G2 TWIN (LaB_6, 200 kV). An electronic tomogram was recorded thanks the *Suite Explore 3D (*from *FEI Company).* The sample was tilted from -60° to +60°, with a 1,5° step. The

treatment of the as-obtained TEM images to the reconstructed volume and then to the isosurface building was done with the program *Amirar (*from *Mercury).*

Ellipsometry measurements were performed on a UV-Visible (240-1000 nm) Variable Angle Spectroscopic Ellipsometer from Woollam and analysed with the WVase32 software. Environmental ellipsometric porosimetry measurements were conducted using a controlled relative humidity chamber at room temperature. Pore volumes and pore size distributions were obtained from the film refractive index and thickness data using the isotropic inorganic pore contraction model (IIC) and a modified Kelvin equation (33). In-situ thermal ellipsometric measurements were performed at 10°C/min using a previously described setup (34).

X-ray diffractograms were obtained using a Bruker D8 grazing incidence diffractometer (CuKα radiation, 1° incidence, 0.04 °/s step size, 3 s/step). ^{51}V static NMR patterns were recorded on powders with a Bruker Avance DSX 400WB spectrometer (B_0 = 9.04 T, pulse width = 0.8 µs; delay time = 0.2 s). The chemical shifts were referenced relative to Na_3VO_4. EPR measurements were recorded at 10K on a Bruker Elexsys-500 spectrometer operating in X band (v = 9.3813 GHz) spectrometer. The samples in powder form were loaded in quartz tube. The magnetic field was scanned from 2600 to 4600 G. The simulation of the spectra and the numerical double integration of the spectra were performed using EasySpin (35). The experimental data were simulated by a pseudo-Voigt function in order to take into account various broadening effects including potential unresolved magnetic dipolar interactions, short-range exchange interactions or inhomogeneous electronic environment. A strain contribution of the A parameter (A_{strain}) is also considered in the simulation to assume the asymmetrical environment of the vanadium. XPS analyses were performed on a Kratos Axis Ultra spectrometer (Kratos Analytical – Manchester – UK) equipped with a monochromatized aluminium X-ray source (powered at 10 mA and 15 kV). The pressure in the analysis chamber was about 10-6 Pa. The analysed area was 700 µm x 300 µm. The pass energy was set at 160 eV for the wide scan and 40 eV for narrow scans. Charge stabilization was achieved by using the Kratos Axis device. The following sequence of spectra was recorded: survey spectrum, C 1s, O 1s, V 2p, K 2p, Nb 3d and C1s again to check for charge stability as a function of time and the absence of degradation of the sample during the analyses. Accurate evaluation of the vanadium oxidation state requires to avoid a potential vanadium reduction during time under vacuum (36). Therefore, ''quick XPS analysis'' was performed in such a manner that for each sample a unique window with O 1s and V 2p peaks was recorded within less than 10 min. The C-(C,H) component of the C1s peak of carbon has been fixed to 284.8 eV to set the binding energy scale. Molar fractions (%) were calculated using peak areas normalized on the basis of acquisition parameters after a linear

background subtraction, experimental sensitivity factors, and transmission factors provided by the manufacturer. Spectra were decomposed with the CasaXPS program (Casa Software Ltd., UK) with a Gaussian/Lorentzian (70:30) product function.

Electrochemical tests were performed using a conventional three-dimension cell. Two Li foils were used as negative and reference electrodes; the film (deposited on FTO/glass substrates) was used as positive electrode (area = 4 cm^2). The electrolyte was 1 M LiPF$_6$ in ethylcarbonate/dimethylcarbonate (1/1 v/v). Cyclic voltammograms were measured using a PAR 263A potentiostat from 3.8 V to 1.8 V vs. Li$^+$/Li° at various scan rates (0.007, 0.05, 0.1, 0.5, 1, 5, 20, 50 and 100 mV/s). As convention, negative current corresponds to reduction processes. The effective active mass of the electrode can be deduced from the thickness and the porosity obtained from ellipsometric measurements.

V.1.4 Results and discussion

V.1.4.1 Solution characterization

Prior to Chemical Solution Deposition (CSD), in order to probe an organization in solution of the structuring agent molecules and the inorganic precursor, diffusion light scattering (DLS) measurements were performed on the three precursor solutions, containing the three different structuring agents PSA, PSB or PSC. In each case, micelles are present and exhibit a very small diameter size distribution centered at 40 nm, 100 nm and 350 nm, respectively. In order to confirm an expected interaction between the inorganic precursor and the micelle, DLS measurements were performed on the corresponding metallic-free PSA, PSB and PSC-solutions. It appears that the mean diameter of the micelles in the three latter solutions is much smaller, 20 nm, 60 nm and 100 nm respectively. The increase of the micelle apparent diameter when the vanadium and niobium precursors are added highlights the effective chelating role of PEO regarding the inorganic compound (37). On the other hand, the presence of micelles assesses that the formation of hybrid film by Chemical Solution Deposition results from an Evaporation Induced Micelles Packing process (EIMP), preferentially to the well-known Evaporation Induced Self Assembly (EISA) procedure.

V.1.4.2 Thermal behavior of the films

Going from hybrid films to crystalline mesoporous films requires a finely tuned thermal treatment. In order to throw some light on the temperature range of the removal of the template and crystallization of the vanadium niobium mixed oxide, the behavior of the hybrid films was followed *in situ* while heating by thermal ellipsometric analysis (TEA) (38). As an illustration, the variations of the thickness and the refractive index of PSB-based

hybrid films are reported in figure 1.1. The corresponding derivative curves are also shown in figure 1.1.
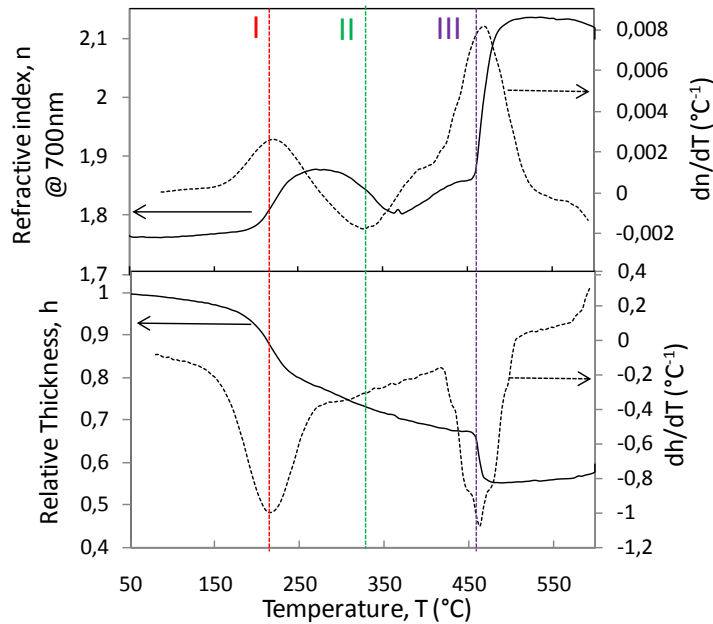
Fig. 1.1: In-situ thermal ellipsometry collected at a ramp of 10°C/min; Temperature dependence of the refractive index (up) and the relative thickness (down) for NbVO$_5$ PSB-films and the corresponding derivatives of the curves (dashed lines)

The derivative curve of the refractive index presents 3 maxima. This observation indicates that three main processes occur during the thermal treatment. These processes are further assigned to process I, II and III and are indicated in figure 1.1.

The process I is described by a large contraction and a rapid increase of the refractive index of the film, suggesting a significant densification of the inorganic walls allowed by the removal of the PEO shell part of the micelles. The process II is characterized by a large drop in the refractive index which means that porosity is generated after the removal of the PS core. Furthermore the corresponding thickness decreases because of the already reported thermally induced unidirectional contraction of the porous network (38).
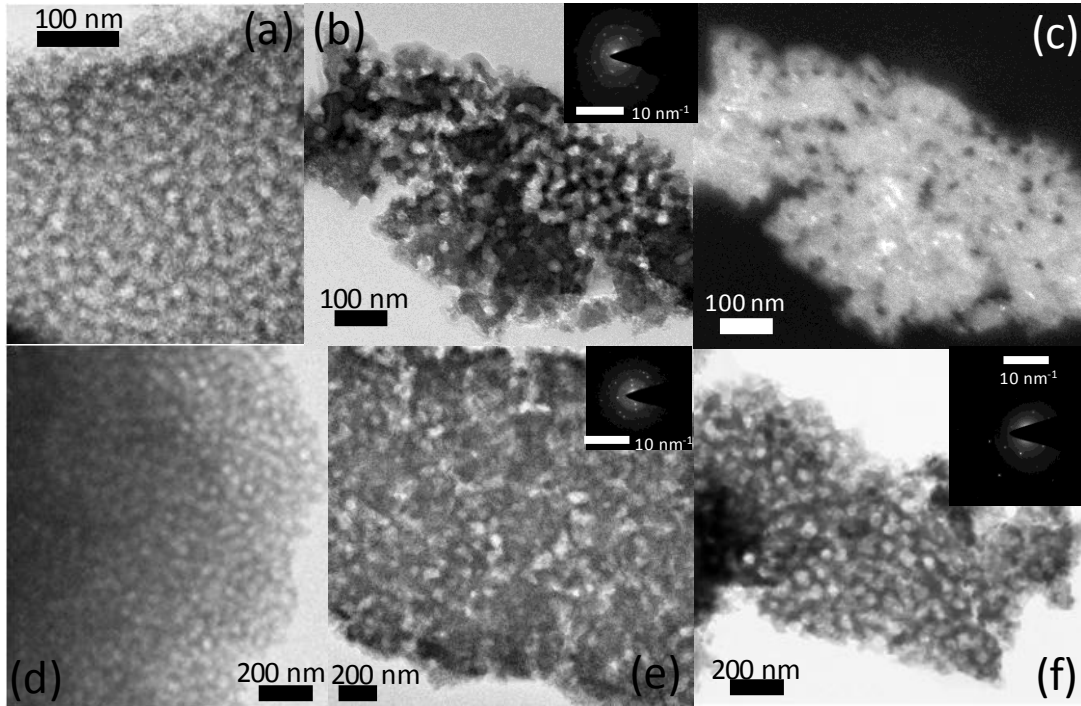
Fig. 1.2: (a, b) Bright field TEM micrographs of NbVO$_5$ PSA-films. The films were calcined at a rate of 10°C/min up to 435 (a) and to 445°C (b); Inset: Corresponding diffraction pattern; (c) Dark field image of (b); (d, e) Bright field TEM micrographs of NbVO$_5$ PSB-films calcined at a rate of 10°C/min up to 455 (d) and 465°C (e); (f) Bright field TEM micrograph of a PSB-film calcined at 500°C (60 s) - 510°C (30 s) - 520°C (30 s) - 530°C (30 s)

From the TEA results obtained for the PSA-, PSB- and PSC-hybrid films, it is deduced that the temperature range of template departure slightly depends on the copolymer size. It is equal to 180-350°C for PSA, 200-360°C for PSB and 200-390°C for PSC.

The process III is characterized by an abrupt decrease in the relative thickness together with a drastic increase in the refractive index. This corresponds to a rapid and large densification of the film resulting from the destruction of the porous framework. Such a collapse of the mesostructure at high temperature could be due to the fact that the porous network cannot sustain the extensive diffusive sintering process which follows the formation of crystallites in the inorganic walls. The temperature characteristic of the process III deduced from the thermal ellipsometric analysis is strongly dependent on the surfactant size, it is evaluated to 440, 460 and 465°C for PSA, PSB and PSC-based films. The high slope of the increase in the refractive index curve and the associated decrease in the film thickness suggest that the process III is very rapid.

In order to confirm that process III is correctly ascribed to the collapse of the mesoporous structure after crystallization of NbVO$_5$, *ex-situ* TEM images of PSB-films treated to 430 and 465°C are shown in figure 1.2(d) and (e), respectively. Figure 1.2(d) shows a well-defined

wormlike mesoporous network. However in the case of the treatment at a slightly higher temperature (figure 1.2(e)), the mesoporous network seems to be partially collapsed and the diffraction pattern indicate the presence of cristallites inside the inorganic walls. The same study was conducted for PSA-films and the results are presented figure 1.2(a) and 1.2(b). It appears that the collapse of the mesostructure is already observed at 445°C. Cristallites are detected on the diffraction pattern and highlighted by bright spots in the corresponding dark-field image (figure 1.2(c)). Furthermore, as the $NbVO_5$ crystallization temperature is not pore size dependent (T_{crist} = 440°C), and as the temperature of the process III increases from PSA to PSC-based films, it is deduced that mesoarchitecture presenting thicker walls (typically PSB and PSC) should be able to better accommodate diffusive sintering, being thus able to enclose $NbVO_5$ small crystallites. This behavior has already been reported in the literature for other transition metal oxides (26)(39)(40).

The TEA has shown that a fine tuning of the thermal treatment was of utmost importance in order to preserve the mesoporous network. On the basis of TEA curves, a rapid and efficient thermal treatment was developed to obtain mesoporous niobium vanadium mixed oxide films from the hybrid ones. Films were first treated at 350°C for 10 min in order to condense the inorganic mixed oxide network, while removing the main part of organic. A short treatment at a higher temperature (1 min at 500°C) is then applied to strengthen the inorganic framework, to erase last residue of surfactant, whereas its amorphous character is remained. It has to be noted that 500°C is higher than the temperature of the process III deduced from TEA, however a film heated progressively to 450°C and one quenched at 500°C for 1 min have different thermal histories, and thus different energy inputs, which can explain why a film flashed at 500°C is still amorphous.

The as-treated films obtained from PSA, PSB and PSC-based hybrid films were investigated by TEM, AFM and poro-ellipsometric measurements (for PSA only). These results are presented in figure 1.3 and 1.4.
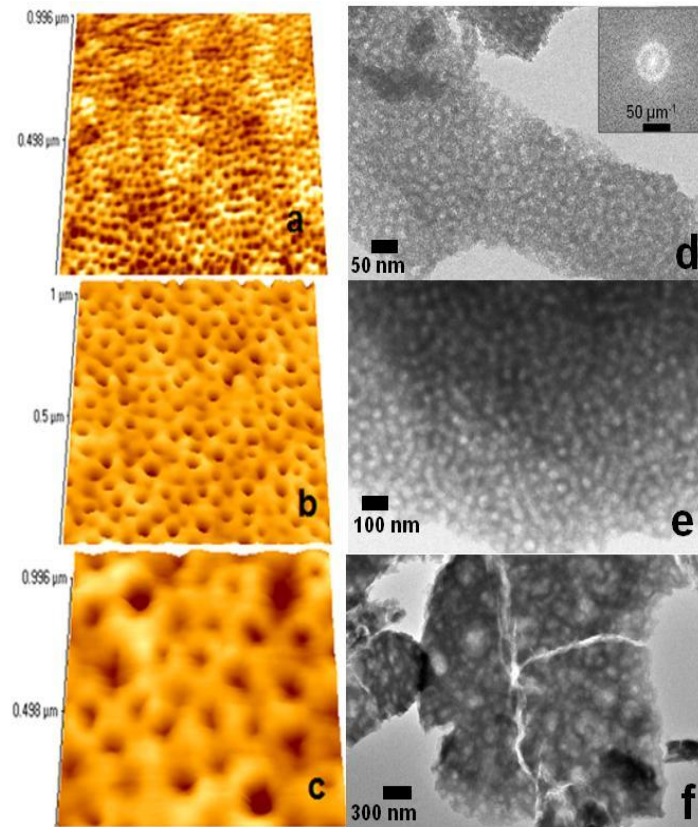
Fig. 1.3: AFM (a, b, c) and TEM (d, e, f) images of mesoporous $NbVO_5$ films prepared by EIMP using (a, d) PSA, (b, e) PSB and (c, f) PSC surfactant. The films are heated at 350°C for 10 min and 500°C for 1 min.

A porous architecture appears to be successfully achieved whatever the structuring agent. The pore size increases when the size of the copolymer blocks increase. Typical pore sizes are ~15 nm, ~50 nm, ~100 nm (macroporous) for PSA, PSB and PSC-based films, respectively. The pore size distribution appears to be quite narrow for PSA and PSB-based films, however it is quite large for the PSC-based even though the micelles sizes distribution was narrow in the solution. The thickness of the inorganic walls is in the same size range as the pore size. The increased pore size (from PSA to PSC) is related to the larger effective size of the micelles, while the increased thickness of the inorganic walls is related to the increasing molar proportion between M_T and PS-PEO (M_T/PS-PEO). In the case of PSA and PSB-based films, the pores appear to be worm-like structured.
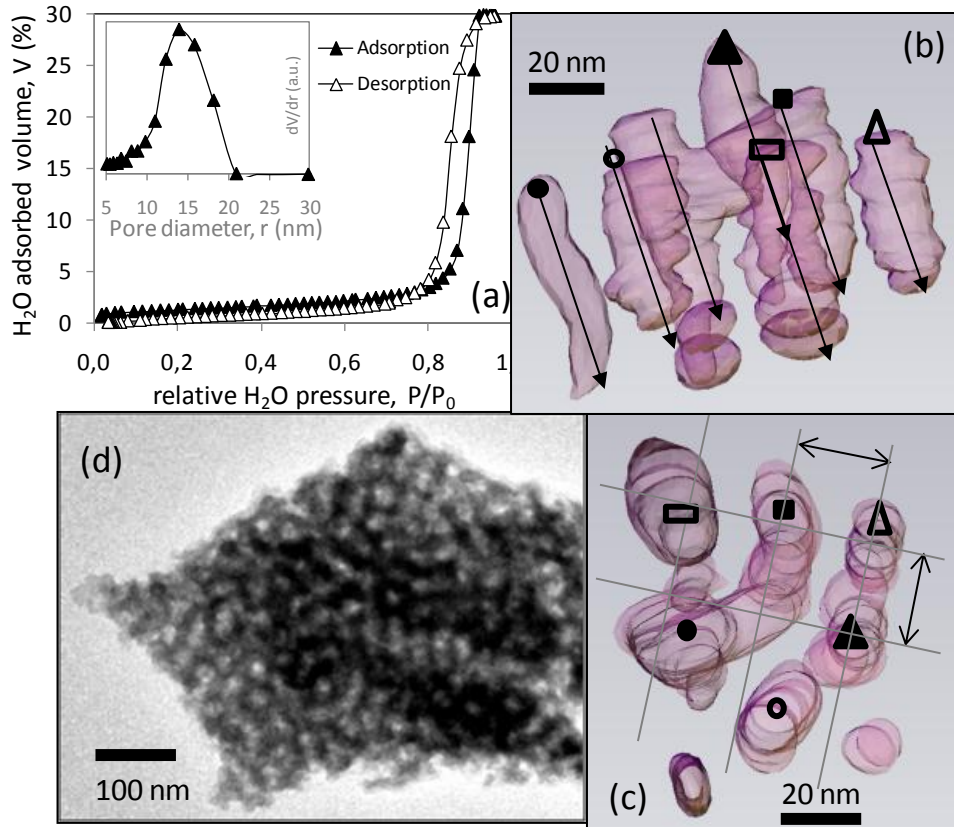
Fig. 1.4: (a) Ellipsometric porosimetry: water adsorption-desorption isotherm (main figure) and the corresponding pore-size distribution (inset) of a PSA-based NbVO₅ film treated at 500°C for 1 min; (b) and (c) Views of pores of a fraction of the samples rebuilt from electronic tomography analysis, the void part is delimited by a translucid veil (c) perpendicularly to the substrate (c) top view; (d) The corresponding TEM image at 0° tilt

The mesoporous character is supported by 30% water-accessible porous volume deduced from the adsorption-desorption isotherm obtained for PSA-based film. The 14 nm-diameter pore obtained from the derivative of the adsorption curve (inset of figure 1.4(a)) is consistent with the size provided by TEM micrograph analysis. The shape of the isotherm, characterized by the absence of hysteresis, suggests that the pores are shaped as closed cylinders (41). In order to support this hypothesis, the film architecture has been visualized by electronic tomography. The volume reconstructed from TEM images of the sample tilted around an axe is not presented here but one of these TEM image is presented figure 1.4(b). It shows the tri-dimensional mesoporous architecture. A portion of the reconstructed volume is presented in figure 1.4(b) and 1.4(c). It appears that pores have merged to form parallel tubes as predicted by the porosimetry measurement. The center to center distance was evaluated to about 20 nm (figure 1.4(c)). Two of these tubes are locally connected through perpendicular channel which displays the tri-dimensionality of the mesoporous framework.

Mesoporous networks containing vanadium species were thus successfully achieved. In our Nb-V mixed oxide system, V^{4+} was detected by Electronic Paramagnetic Resonance and its surface content was evaluated by X-ray photoelectron spectroscopy. It appears that 95% of the vanadium species are present as V^{5+}, while only 5% as V^{4+}. The content of V^{4+} is small compared to what was reported in literature for hybrid mesostructured thin films of pure vanadium oxide prepared by EISA (27). The latter study highlights that a 50% of V^{4+} is needed as it acts as both a condensation activator and a 3D-orientator of the inorganic network molding properly the curved design of the pores (27). This V^{4+} property is actually widely used in the synthesis of vanadium oxide nanotubes (42). In our case, the Nb^{5+} specie appears to stabilize the vanadium specie in three dimensional structure. As Nb^{5+} preferentially adopts an isotropic octahedral configuration, it takes the role V^{4+} as a 3D-orientator.

At this stage, the mesoporous Nb-V mixed oxide is amorphous. The achievement of crystalline mesoporous film appears challenging, regarding the fact that the diffusive sintering upon $NbVO_5$ crystalline growth is strongly detrimental to the mesostructure. In order to take up this challenge, films presenting thick inorganic walls which are able to better accommodate sintering are investigated, and a careful thermal post-treatment allowing to increase the number of nucleation centers while limiting crystal growth was selected. The latter consist in a succession of very short quenches at high temperature, typically 500°C (60 s) - 510°C (30 s) - 520°C (30 s) - 530°C (30 s) which was applied after the 350°C (10 min) step on a PSB-based film. TEM and the corresponding diffraction pattern attest respectively of the preservation of the mesostructure and of the presence of $NbVO_5$ crystallites inside the walls (figure 1.2(f)). In the light of these results, it appears the synthesis of crystalline $NbVO_5$ MTF remains challenging, especially when the walls are thin (15 nm). However, amorphous $NbVO_5$ mesoporous network can be achieved relatively easily using the here-presented EIMP synthesis. To remain a suitable candidate for the present study, the amorphous $NbVO_5$ have to be affected by lithium insertion. As V^{4+} species obtained after Li^+ insertion in $NbVO_5$ cannot fit in a tetrahedral site, the presence of vanadium in VO_4 coordination becomes a condition to affect the capacity during cycling and hence to be a good candidate to test the mechanical stability of MTF. ^{51}V Solid State NMR experiments have been performed on scratched amorphous $NbVO_5$ MTF obtained after the above described thermal treatment (350°C (10min) - 500°C (1min)) (22), and highlight the presence of V in VO_4. It appeared thus interesting to study the electrochemical behavior of amorphous $NbVO_5$ MTF among lithium insertion.
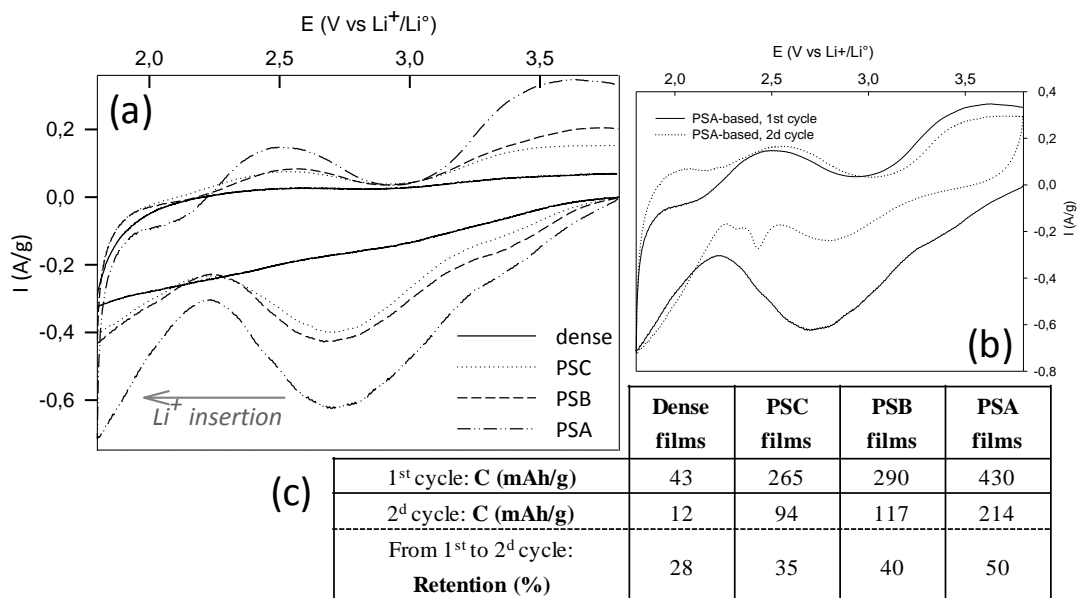
V.1.4.3 Electrochemical characterizations

In order to evaluate the potentiality of MTF as electrode in lithium battery, and in particular to test their ability to support stresses resulting from important structural distorsions

occurring during cycling, cyclic voltammograms of PSA, PSB and PSC- NbVO5 amorphous MTF are presented in figure 1.5(a). These curves are compared to the electrochemical response of a non porous film as a reference.

Regarding the capacity of the material in inserting lithium during the first cycle, it appears that the current densities are larger for mesoporous films compared to dense. This first observation shows a first positive role played by the nanostructured architecture on electrochemical performance. Among the three types of mesoporous films investigated here, the PSA-film, presenting the smallest pore size (~ 15 nm), appears as the most promising high capacity candidate, which is mainly related to the contact surface between the electrode and the electrolyte (39).

It is also observed that the Li^+ inserted upon the first reduction process is not fully extracted during the first oxidation step (figure 1.5(a)). In the case of PSA-film, for example, 1.3 Li^+ per $NbVO_5$ are inserted while only 0.5 Li^+ are effectively extracted (figure 1.5(b, c)), neglecting the capacitive contribution and thus assuming that the totality of the current is assigned to the lithium insertion process. For the subsequent cycle, the system presents more reversible lithium insertion/extraction (+0.8 Li^+/-0.5 Li^+).

	Dense films	PSC films	PSB films	PSA films
1st cycle: **C (mAh/g)**	43	265	290	430
2d cycle: **C (mAh/g)**	12	94	117	214
From 1st to 2d cycle: **Retention (%)**	28	35	40	50

Fig. 1.5: (a, b) Cyclic voltammograms of thin films obtained at a scan rate of 0.5 mV/s; (a) First cycles of PSA-, PSB-, PSC-based and dense thin films of amorphous NbVO₅ heated at 500°C; (b) First and second cycles of PSA-based thin films of amorphous NbVO₅ (heated at 500°C); (c) Table reporting Li⁺ insertion capacities of the first and second cycles for PSA-, PSB-, PSC-based and dense thin films

Poor reversibility in the first cycle is often attributed to the formation of a Solid Electrolyte Interface (SEI) layer (43). However, for V_2O_5 and Nb_2O_5 thin films prepared under similar

conditions, this irreversibility is not observed. SEI layer formation is therefore probably not the only relevant phenomenon. Furthermore, it has been shown that, after the first Li insertion, bulk crystalline $NbVO_5$ lost 80% of its initial capacity (23)(24). This value is close to what is obtained for the non porous (dense) film.

The table, in figure 1.5(c), illustrates the percentage of retained capacity from the first to the second cycle which has been directly related to the ability of accommodating stresses. It appears that the smaller the pore size, the better the accommodation of the mechanical stresses. Furthermore a TEM image of a 20 times cycled amorphous PSA-film proves that the mesoporous network does not look to have suffered from cycling.

These observations consist in another proof of the advantage in integrating a mesostructure in a lithium battery, as comforted by a recent studies performed on MnO_2 cathode material (44).

In order to approach the kinetic of the electrochemical processes in these mesoporous thin films, focusing of PSA-MTF presenting the smallest pore size, cyclic voltammograms were conducted at varying scan rates (from 0.007 mV/s to 100 mV/s) and are shown in figure 1.6. It has to be noted that in order to be able to compare the different time dependent experiments, differential capacities (*Cdiff = dQ/dE = Iv^{-1}*) were considered (45). Because both the redox active potential of the transition metal (TM) cation and the diffusion of the lithium into the solid inorganic matrix are time dependent, changing the scan rate is expected to drastically affect the performance of the material and, consequently, the shape of the voltammogram. A more detailed depiction of the voltammogram shape is given in figure 1.7, which shows a voltammogram of a $NbVO_5$ thin film at moderate scan rate (0.5 mV/s).

This curve can be divided into three large cathodic peaks (reduction of TM – insertion of Li$^+$), designated by C1, C2 and C3 and the corresponding anodic peaks (oxidation of TM - extraction of Li$^+$), named A3, A2 and A1, respectively. In order to discriminate the contributions of the vanadium and the niobium species in these three regions, electrochemical responses of V_2O_5 and Nb_2O_5 are shown in figure 1.7. Comparison with $NbVO_5$ curves suggests that the reduction of V^{5+} to V^{4+} mainly takes place in the C1 and C2 domains while the reduction of Nb^{5+} to Nb^{4+} essentially occurs in the C3 region in agreement with the expected sequence of the reduction potential of the two metallic cations.
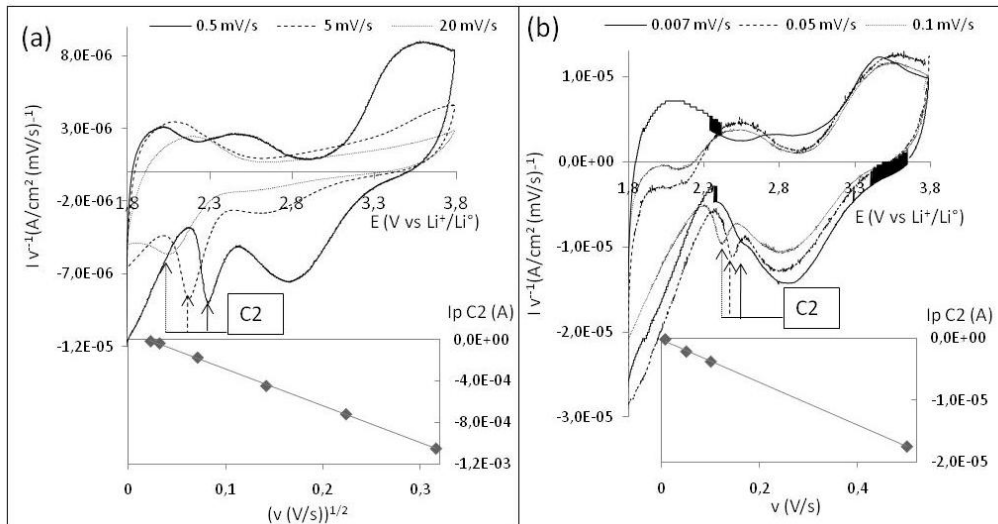
Fig. 1.6: Cyclic voltammograms of PSA- thin films of amorphous NbVO$_5$ heated at 500°C at various scan rates; (a) High scan rates (from 0.5 to 20 mV/s); (b) Low scan rates (from 0.1 to 0.007 mV/s); (Below) Evolution of C2 peak intensity with the scan rate

Increasing the scan rate (figure 1.6) shifts the reduction peak to lower potentials and the oxidation peak to higher potentials. The resulting potential interval between the reduction and the corresponding oxidation peak (E_{A2}-E_{C2}) thus increases meaning that the redox processes become less reversible. For the third Li insertion-extraction process, (see arrows in figure 1.6(a) and 1.6(b)) the potential intervals increases from 0.18, to 0.2 and 1.05 V for scan rates of 0.007, 0.5 and 5 mV/s. The larger polarization of the electrode material as the scan rate increases limits the cell to low rate performance applications.
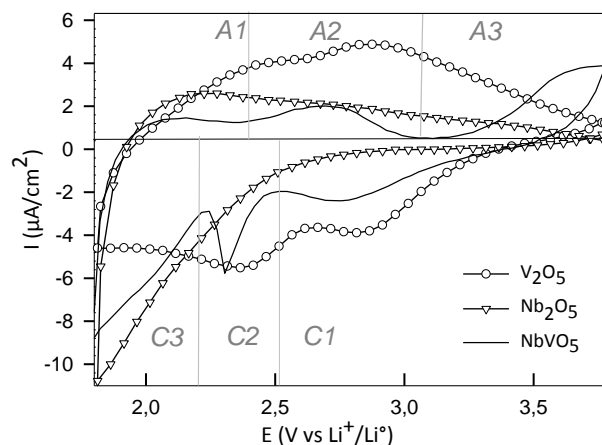
Fig. 1.7: Cyclic voltammograms (2^d cycle, 0.5 mV/s) of PSA-amorphous thin films of different composition V$_2$O$_5$, NbVO$_5$ and Nb$_2$O$_5$

The scan-rate vs. peak intensity dependence gives also information about the solid state diffusion of lithium ions in the inorganic walls. The evolution of the peak current I_p of the C2 reduction process was studied as a function of the scan rates. In the studied range of scan rates, two different kinetic behaviors were revealed: a linear $I_p(v)$ for low scan rates from 0.5 to 0.007 mV/s (figure 1.6(b)) and a linear I_p vs $v^{1/2}$ for high scan rates from 0.5 to 100 mV/s figure 1.6(a)). A linear I_p vs v relation is assigned to a redox process which is not limited by lithium diffusion (46). On the other hand, a linear I_p vs $v^{1/2}$ relation reveals a diffusion-controlled Li intercalation. Assuming a semi-infinite or finite diffusion of Li$^+$ into a solid thin film (47): $I_p = 0.446\ n^{3/2}\ F^{3/2}\ C_{Li}\ SR^{-1/2}\ T^{-1/2}\ D_{Li}\ v^{1/2}$ where I_p is the peak current (A), n is the charge transfer number (1 for Li$^+$), F is Faraday's constant (96486 Cmol^{-1}), C_{Li} is the maximal Li-ion concentration (0.009 mol/cm^3 for C2 at the lowest scan-rate), S is the surface area of the electrode (4 cm^2), R is the gas constant (8.314 J mol^{-1}K^{-1}), T is the temperature (298K), D_{Li} is the Li diffusion coefficient and v is the scanning rate (Vs^{-1}). The chemical diffusion coefficient D_{Li} evaluated from the slope of the linear regression for high scan rate curve (fig. 1.6) and is found to be ~10^{-8} cm^2/s for the second intercalation and deintercalation processes, which is characteristic of Li$^+$ diffusion in solid materials and within the same order of magnitude as V_2O_5 nanotube materials (48). The capacity of the material appears to be affected by the scan rate, the number of lithium reversibly inserted and extracted is higher at slow scan rates: 0.9 Li$^+$ at 0.007 mV/s compared to 0.5 Li$^+$ at 0.5 mV/s.

Increasing the capacity of the material may also be achieved by increasing the thickness of the film, however a maximal thickness will be exist due the poor electron conducting character, which can become a problem when the active matrix is far from the current collector. Experimental considerations such as, for example, the accessibility of the 3D porous network in thick films might also become an issue at that point. In this respect, encouraging results have been obtained for a 1.3 µm-thick PSA-based NbVO$_5$ film (figure 8) prepared by multi-dipping (9 layers): ellipsometric porosimetry suggests that the accessible porosity represents 17% of the bulk volume, compared to the 30% obtained for the 100 nm-thick one-layer film.
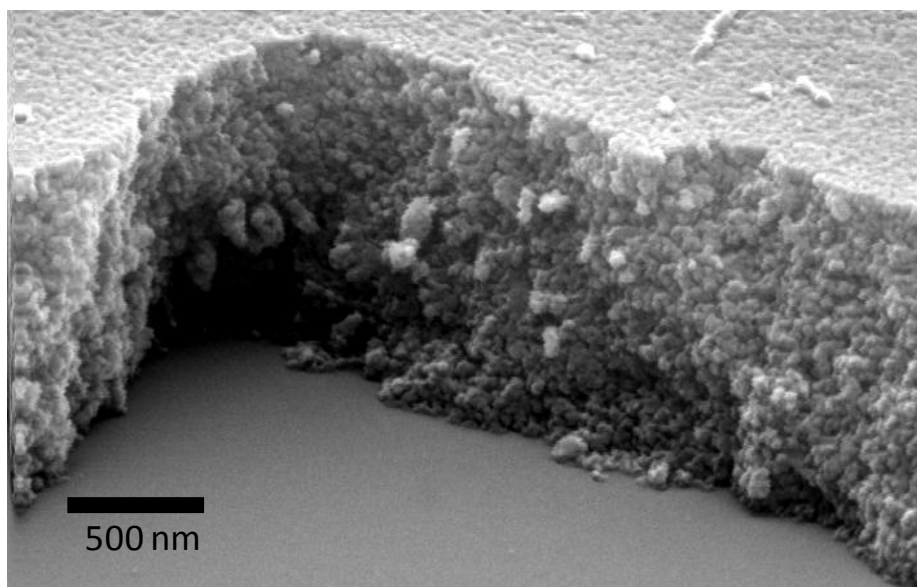
Fig. 1.8: SEM-FEG micrograph of a section of a PSA-templated amorphous NbVO$_5$ film resulting from a multi-dipping process. The 1.3 µm thick film on silicium consists of 9 layers, stabilized at 180°C after each layer deposition, and finally heated at 350°C for 5h.

V.1.5 Conclusions and outputs

This work aimed at evaluating the potential of MTF as a positive electrode architecture in Li battery, in particular, testing its ability to support mechanical stresses occurring during cycling because it is at the origin of the low battery cyclability. The approach consists in comparing the electrochemical behavior of non porous film and MTF (with three different pores sizes) of a material that presents large structural distortion upon the first lithium insertion. **NbVO$_5$ was selected as a suitable candidate.**

Amorphous NbVO$_5$ mesoporous thin films (MTF) presenting wormlike mesoporous structures are successfully obtained via the EIMP method from ethoxy-chloride precursor solutions containing PS-PEO as a structuring agent. Tunable pore and inorganic wall sizes (from 15 to 100 nm), with quite narrow size distributions, are achieved by varying the length of the hydrophobic (PS) and the hydrophilic (PEO) part of the amphiphilic block copolymer surfactants. In situ thermo ellipsometric measurements performed on the stabilized films highlight the behavior of the mesoporous layer upon heating in terms of surfactant removal and crystallization. As the calcination of the structuring agent begins at about 220°C with the PEO elimination and ends at around 380°C with the PS micelle core removal, the PS-*b*-PEO copolymer shows greater thermally stability compared with pluronic surfactants. Condensation reactions occurring at elevated temperatures can consequently take place in the presence of the template. This mechanically stabilized framework can then support the complete removal of surfactant leading to the mesoporous amorphous thin films shown here by AFM and TEM. Upon crystallization, however, in situ thermo ellipsometry

characterization shows that this architecture undergoes an abrupt collapse as a result of the rapid diffusive sintering of the $NbVO_5$ crystallites. A fine control of the heat treatment together with thick inorganic walls ($\geq$ 50 nm) allows preserving the mesostructure while partially crystallizing the $NbVO_5$ phase.

Amorphous $NbVO_5$ MTF can nevertheless be used to efficiently test the ability of the network to accommodate mechanical stresses, as V species possess the tetrahedral coordination requested to induce the important structural distortion after the first lithium insertion. The electrochemical behaviors of amorphous $NbVO_5$ MTF with three different pore sizes were tested by cyclic voltammetry and compared to non porous films. It turns out that the drastic structural modification affected less the mesoporous network than the non porous one. Furthermore, the smaller the pore sizes, the higher the ability to accommodate stresses. In addition, the electrochemical characterizations confirm the capacity gains offered by MTF architectures compared to non porous thin films, due to decreasing the diffusion path. In agreement with the quite slow kinetics of solid state lithium diffusion (10^{-8} cm^2/s for PSA-based film), larger reversible capacities are obtained at slow scan rate (7μV/s). Increasing the capacity of the material might also be achieved by increasing the film thickness. **These materials have thus a great potential for the next generation of Li-ion battery components with regard to the cyclability and operationability (charging time).**

V.1.6 Notes and references

(1)   Aricò A. S., Bruce P., Scrosati B., Tarascon J., van Schalkwijk W., Nature materials 4 (2005) 366-77.

(2)   Bruce P., Scrosati B., Tarascon J., Angewandte Chimie-International Edition 47 (2008) 2930-2946.

(3)   Liu D., Cao G., Energy & Environmental Science 3 (2010) 1218.

(4)   Baggetto L., Knoops H. C., Niessen R. A., Kessels W. M., Notten P. H., Journal of Materials Chemistry 20 (2010) 3703.

(5)   Centi G., Perathoner S., European Journal of Inorganic Chemistry 26 (2009) 3851-3878.

(6)   Aurbach D., Levi M. D., Levi E., Solid State Ionics 179 (2008) 742-751.

(7)   Cheng F., Tao Z., Liang J., Chen J., Chemistry of Materials 20 (2008) 667-681.

(8)   Bruce P. G., Scrosati B., Tarascon J., Angewandte Chemie 47 (2008) 2930-2946.

(9)   Hart R. W., White H. S., Bruce D., Rolison D. R., Electrochemistry Communications 5 (2003) 120-123.

(10)   Rhodes C. P., Mcevoy T. M., Bourg E., Lubers A. M., Scientist (2009).

(11)   Xie Y., Wu C., Dalton Transactions (2007) 5235-5240.

(12) Brezesinski T., Wang J., Polleux J., Dunn B., Tolbert S. H., Journal of the American Chemical Society 131 (2009) 1802-1809.

(13) Szeifert J. M., Feckl J. M., Fattakhova-Rohlfing D., Liu Y., Kalousek V., Rathousky J., Bein T. Journal of the American Chemical Society 132 (2010) 12605-12611.

(14) Yasushi S., Keita I., Makoto O., Masakazu A., Applied Catalysis A: General 254 (2003) 251-259.

(15) Procházka J., Kavan L., Zukalová M., Frank O., Kalbáč M., Zukal A., Klementová M., Carbone D., Graetzel M., Chemistry of Materials 21 (2009) 1457-1464.

(16) Fattakhova-Rohlfing D., Wark M., Brezesinski T., Smarsly B., Rathouský J., Advanced Functional Materials 17 (2007) 123-132.

(17) Zhi-mei Q., Itaru H., Haoshen Z., Applied Physics Letters 88 (2006) 053503-053506.

(18) Sallard S., Brezesinski T., Smarsly B., Journal of Physical Chemistry C 111 (2007) 7200-7206.

(19) Sanchez C., Boissière C., Grosso D., Laberty C., Nicole L., Chemistry of Materials 20 (2008) 682-737.

(20) Ren Y., Armstrong A. R., Jiao F., Bruce P. G., Journal of the American Chemical Society 132 (2010) 996-1004.

(21) Sayle T. X., Maphanga R. R., Ngoepe P. E., Sayle D. C., J. Am. Chem. Soc. 131 (2009) 6161-6173.

(22) Amarilla J. M., Casal B., Ruiz-Hitzky E., Journal of Materials Chemistry 6 (1996) 1005-1011.

(23) Amarilla J. M., Perez-Revenga M., Casal B., Ruiz-Hitzky E., Catalysis Today 78 (2003) 571-579.

(24) Brown J., Altermatt D., Acta Crystallographica Section B 41 (1985) 244-247.

(25) Yang P., Zhao D., Margolese D. I., Chmelka B. F., Stucky G. D., Chemistry of Materials 11 (1999) 2813-2826.

(26) Brezesinski T., Groenewolt M., Pinna N., Amenitsch H., Antonietti M., Smarsly B., Advanced Materials 2006, 18, 1827-1831.

(27) Crepaldi E. L., Grosso D., de A. A. Soler-illia G. J., Albouy P., Amenitsch H., Curie M., Chemistry of Materials (2002) 3316-3325.

(28) Wu C., Wei H., Ning B., Xie Y., Advanced Materials 22 (2010) 1972–1976.

(29) Yuan L., Bhatt S., Beaucage G., Guliants V. V., Mamedov S., Soman R. S., The journal of physical chemistry B 109 (2005) 23250-23254.

(30) Yu K., Hurd A., Eisenberg A., Brinker C., Langmuir 17 (2001) 7961-7965.

(31) Kuemmel M., Allouche J., Nicole L., Boissière C., Laberty C., Amenitsch H., Sanchez C., Grosso D., Chemistry of Materials 19 (2007) 3717-3725.

(32) Sassoye C., Laberty C., Le Khanh H., Cassaignon S., Boissière C., Antonietti M., Sanchez C., Advanced Functional Materials 19 (2009) 1922-1929.

(33) Boissiere C., Grosso D., Lepoutre S., Nicole L., Bruneau A. B., Sanchez C., Langmuir : the ACS journal of surfaces and colloids 21 (2005) 12362-12371.

(34) Bass J. D., Grosso D., Boissiere C., Sanchez C., Journal of the American Chemical Society 130 (2008) 7882-7897.
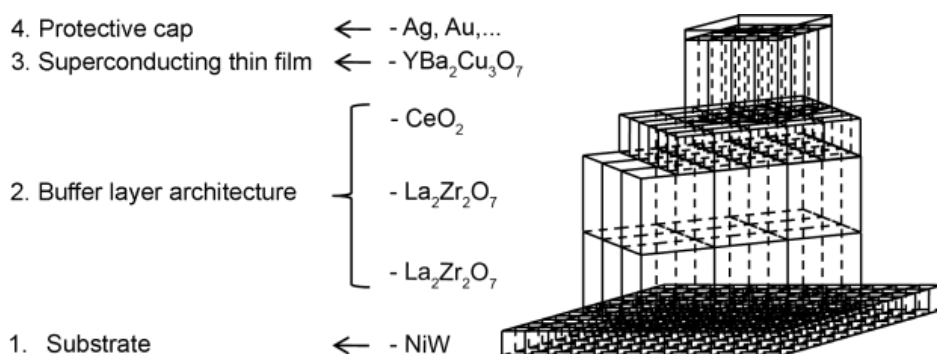
(35)   Stoll S., Schweiger A., Journal of magnetic resonance (San Diego, Calif. : 1997) 178 (2006) 42-55.

(36)   Benayad A., Martinez H., Gies A., Pecquenard B., Levasseur A., Gonbeau D., Journal of Electron Spectroscopy and Related Phenomena 150 (2006) 1-10.

(37)   Crepaldi E. L., De A. A. Soler-Illia G. J., Grosso D., Cagnol F., Ribot F., Sanchez C., Journal of the American Chemical Society 125 (2003) 9770-9786.

(38)   Bass J. D., Grosso D., Boissiere C., Sanchez C., Journal of the American Chemical Society 130 (2008) 7882-7897.

(39)   Brezesinski T., Rohlfing D. F., Sallard S., Antonietti M., Smarsly B. M., Small 10 (2006) 1203-1211.

(40)   Huguenin F., Torresi R., Buttry D., Pereira Da Silva J., Cordoba de Toresi S., Electrochimica Acta 46 (2001) 3555-3562.

(41)   Rouquerol F., Rouquerol J., Sing K., Adsorption by Powders and Porous Solids - Principles, Methodology and Applications, Academic Press, London (1998).

(42)   Nordlinder S., Nyholm L., Gustafsson T., Edström K., Chemistry of Materials 18 (2006) 495-503.

(43)   Swiatowskamrowiecka J., Maurice V., Zanna S., Klein L., Briand, E., Vickridge I., Marcus P., Journal of Power Sources 170 (2007) 160-172.

(44)   Sayle T. X., Ngoepe P. E., Sayle D. C., ACS nano 3 (2009) 3308-3314.

(45)   Scarminio J., Catarini P. R., Urbano A., Gelamo R. V., Rouxinol F. P., Moraes M. A., Journal of the Brazilian Chemical Society 19 (2008) 788-794.

(46)   Desportes C., Duclot M., Fabry P., Fouletier J., Hammou A., Kleitz M., Siebert E., Electrochimie des solides, Science, Collection Grenoble (2000) p. 440.

(47)   Xie J., Imanishi N., Hirano A., Matsumura M., Takeda Y., Yamamoto O., Solid State Ionics 178 (2007) 1218-1224.

(48)   Malta M., Louarn G., Errien N., Torresi R., Journal of Power Sources 156 (2006) 533-540.

V.2 Coated conductors using superconducting materials

V.2.1 Introduction

Superconductors in earlier days of invention were based on Lanthanum (LBCO), Yttrium (YBCO) and Bismuth (BSSCO) compound oxides and were primarily studied and used as bulk samples. In recent years however, thin film technology using YBCO has replaced the older version of preparation, envisaging the idea of easy transport of these materials over long lengths for energy transportation which is the basic idea behind their manufacture. The ceramic material YBCO is universally acknowledged as the material with the highest technological qualities, in particular, its capacity to carry very large electrical currents without resistive losses. However, one of the biggest hurdles to widespread application of YBCO coated conductor tape is developing a manufacturing process that will produce long lengths of tape at prices competitive to the ubiquitous copper for applications such as motors, generators, transmission cables and other power systems. The coated conductors potentially exhibit superior performance in comparison to the available first generation bismuth based HTS compounds (BSCCO), in that they can have a higher irreversibility field-temperature envelope and therefore can operate effectively at higher critical fields in the temperature range of 30-77K. The extraordinary performances of YBCO under very high magnetic fields gave rise to high expectations in view of future technological developments of paramount importance to mankind where extreme qualities are indispensable such as the production and transport of electrical energy.

In the coated conductor architecture (fig. 2.1), YBCO is deposited on a flexible Ni-W substrate for strength and for practically easy transportation purposes. A number of buffer layers are deposited in between the superconducting layer and the metal substrate to avoid oxidation of the metal tape, penetration of Ni ions into the YBCO layers and to enhance epitaxial growth of the superconducting material.

4. Protective cap   ← - Ag, Au,...
3. Superconducting thin film   ← - $YBa_2Cu_3O_7$

2. Buffer layer architecture ⎧ - CeO_2
                             ⎨ - $La_2Zr_2O_7$
                             ⎩ - $La_2Zr_2O_7$

1. Substrate   ← - NiW

Fig. 2.1: Basic coated conductor – architecture

The YBCO material has a characteristic critical current of the order of 1.0×10^6 A/cm^2 when observed on single crystals of the parent material. In a multi-crystalline structure, the critical current density is drastically reduced by the presence of crystalline boundaries and is termed the "weak link" behavior. In thin films, it is desired to grow the films maintaining a high order or texture in the film such that a highly aligned crystalline matrix having low angle grain boundaries results. When this is successfully accomplished the film intragranular *critical* current density approaches the film intragranular current density.

At present, there is no infrastructure for making long length coated conductors in our laboratory or in Belgium. Coated conductors have only been produced in a laboratory environment with a characteristic area of a few square centimetres. In the present study of coated conductor manufacturing, only YBCO is considered in recognition of its extensive study to date. In the case of producing a coated conductor in long lengths, there are two figures of merit: current capacity and cost. Any conductor will have to meet some minimal value of engineering current density where the minimum value is application specific.

The development of high-T_c superconducting thin films on metallic substrates is of great importance from the point of view of their applications in preparing superconducting magnets, cables, electromagnetic shields, etc. For applying suitable coatings of buffer and high temperature superconductor (HTS) materials on textured substrates (1), several preparation methods exist, each with their own advantages and disadvantages. Chemical solution deposition (CSD) methods can be used in non-vacuum based procedures and allow universal, straightforward deposition of ceramic coatings.

Under the Belspo project, the development of a sol-gel based flexible coated superconductor is the main goal of UGent. The research includes the preparation and analysis of novel oxides and their use as potential candidates for the design of efficient energy storage or conversion systems by ecologically acceptable new chemistries.

Dip-coating and ink-jet printing have been selected as part of the water-based chemical solution deposition approach in the work carried out in the Department of Inorganic and Physical Chemistry, UGent. The research can be divided in 3 major topics.

- Part 1: Development and characterisation of LZO and LCO buffer layers for coated conductor design
- Part 2: Study of the roughness of CeO$_2$ buffer layers
- Part 3: Ink-jet printing of YBCO superconducting layers.

V.2.2 Experimental results

V.2.2.1 Part 1: Development of $La_2Zr_2O_7$ and $La_2Ce_2O_7$ buffer layers for coated conductor design

In this part of the project, the focus is on CeO_2 and LZO buffer layers. In recent years, LZO and CeO_2 have been found to have a comparable lattice match with the NiW substrate. CeO_2 has a slightly better compatibility and lattice match with YBCO. Hence, a two-buffer layered architecture of CeO_2/LZO/Ni-5at%W has been widely accepted (2-5). But, the famous three-buffer layered architecture of CeO_2/YSZ/CeO_2/Ni-5at%W has not been tested with the replacement of LZO in place of YSZ. This could reduce the number of coated layers and hence the cost of production. All the above mentioned combinations of buffer layers described in literature employ LZO prepared from non-aqueous solution system. In contrast, the work in this paper is carried out on an environmentally friendly aqueous LZO buffer system.

As mentioned in the introduction, a good quality YBCO thin film can be obtained after deposition of smooth, dense, crack-free and highly aligned oxide buffer layers on textured metal substrates to protect the superconductors from metal contamination and, to provide an appropriate biaxially oriented, lattice matched substrate for the subsequent epitaxial growth of YBCO on top of it. XPS, XRD and AFM characterizations have been done to analyse the samples. Before a buffer layer can be deposited, the substrates must be prepared for coating by an optimized clean procedure. Subsequently, an optimized buffer layer architecture must be designed in order to have a biaxially textured, smooth and dense thin film that meets all the requirements.

V.2.2.1.1 Influence of the cleaning method on the thin film quality

The first focus was on elucidation of the action of the presently used cleaning technique for the Ni- 5at%W substrates. These 35 µm thick and polished substrates are used as flexible base substrates, on top of which buffer layers, superconductor layers and buffer layers are coated. The study is based on testing the homogeneous nucleation of buffer layers of CeO_2, which are deposited by dip coating of a sol-gel precursor that is subsequently thermally treated to obtain a ceramic layer of CeO_2. The dip-coating process coats the substrate at a specific speed to control the thickness of the layer. The wettability of the substrate is of the utmost importance in the whole process. Two different cleaning sequences have been tested to carry out this cleanliness: method 1: thermal cleaning followed by chemical cleaning and method 2: chemical cleaning followed by thermal cleaning. The main purpose of the chemical process is the dissolution of the lubricating oils whereas the thermal

treatment ensures the pyrolysis of impurities (6). The details of the different cleaning methods are given here.

Chemical cleaning process: The substrates were dipped consecutively in trichloroethylene 99% (ACROS Organics), in acetone 99.5% (Fiers) and in methanol 99.85% (Fiers) where each dipping step lasted for 5 minutes for removing organic traces of oil, grease and also dirt. This degreasing procedure was followed by a 5 minutes rinse in MiliQ water obtained from MILLIPORE 00A/040 MiliQ water purification system. In this step, residual solvents and ionic salts were removed. Subsequently, the substrates were introduced in a hot mixture (50-55°C) of hydrogen peroxide (H_2O_2) 35% in weight (Sigma ALDRICH) : formic acid (HCOOH) 99% (Chem-Lab) for 15 minutes. By this etching step, the grain boundaries are mainly attacked by the mixture of hydrogen peroxide and formic acid. Substrates were rinsed twice for 10 minutes again with MiliQ water.

Thermal cleaning process: Substrates were exposed to high temperatures (800°C) for 1 hour in a quartz tubular furnace (CARBOLITE, Three zone furnace) and in a reducing atmosphere provided by Ar-5%H_2. Heating and cooling rate was set at 10°C/min. After this thermal treatment the substrates are stored in methanol to avoid contamination to air and particulates in the atmosphere. NiW substrates cleaned by both methods are covered with a CeO_2 layer (preparation route described below) by sol-gel dip coating. The effect of the cleaning procedure is quantified by contact angle measurements. A low contact angle represents a good wettability of the substrate and a successful cleaning procedure.

These two cleaning methods were tested for a CeO_2 thin film on NiW. The precursor solution for dip coating was prepared by dissolving Cerium(III) Acetate Hydrate 99.9% (Sigma-ALDRICH) and nitrilotriacetic acid 99% (Sigma-ALDRICH) in water with a final concentration of 0.25 mol/L, pH 6.3 and viscosity 2.628 mPa s. pH was measured with pH-meter "conser P901" (Fischer Biobloc Scientific) and viscosity with viscometer "DV-E" (Brookfield engineering). The cleaned NiW (according to method 1 or 2) substrates were dip-coated in a class 10,000 clean room with a dip coater (KSV Instruments) at the speed of dipping and withdrawal of 20 mm/min, and preliminarily dried in the oven in the horizontal position at 60°C for one hour. Dip-coated and dried substrates were annealed in the tube furnace heated at a ramp of 2°C/min to 900°C and dwelled for 60 minutes. Secondly, they were heated to 1050°C with a ramp of 10°C/min and dwelled for 20 minutes. Finally, they were cooled down until the room temperature. The samples were fully characterized by XRD and XPS.

The XRD pattern in figure 2.2 is the result of a CeO_2 film deposited on a substrate that is first thermally and then chemically cleaned. A crystalline high intense cerium oxide along (002) plane was formed. There was no indication of the undesired (111) peak. A crystalline cerium oxide along (002) plane was also formed on a first chemically cleaned and then thermally treated sample. The intensity is a slightly lower and the peak is relatively broad. It can be concluded that the use of the thermal-chemical cleaning sequence results in a slightly better texture of the buffer layer.
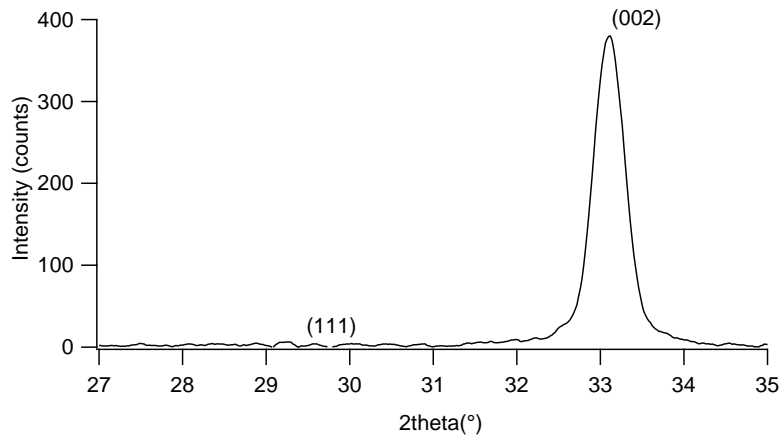
Fig. 2.2: X-Ray diffraction pattern of CeO₂ on thermal-chemical treated Ni-5at%W

XPS sputter experiments were performed for both cleaning sequences. It is inferred that, Ni diffused throughout the complete 30 nm thick CeO_2 buffer layer for the thermal-chemical treated Ni-5at%W. In contrast, if the substrate is first chemically cleaned, the surface of the CeO_2 coated sample is free of nickel contamination on the surface (fig. 2.3). It can be observed that diffusion exists between the nickel and CeO_2 layers in both samples. When the sputtering goes deeper, the cerium oxide layer is reduced and nickel concentration increased, with an inflexion point at about 20% on atom percentage. In CSD, the processes are carried out at very high temperatures in the order of 1000°C and penetration of nickel during repeated heat treatments is a concern. Henceforth, chemical-thermal cleaning treatment has been followed for the sample preparations.
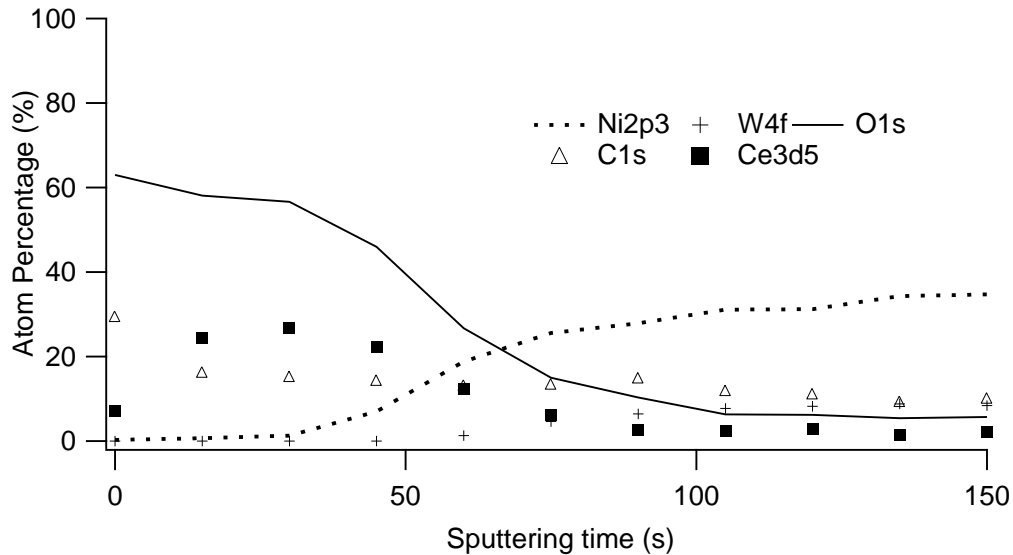
Fig. 2.3: XPS depth profile graph for CeO₂ on a chemical–thermal treated Ni-5at%W substrate

V.2.2.1.2 Multiple layered CeO₂ and LZO buffer coatings

A single-aqueous LZO buffer layer of 70 nm was obtained by dip-coating and published by our group (3). To obtain thicker buffer layer and hence to protect Ni penetration, two different combinations of CeO₂ and LZO buffer layer architecture systems have been employed. System 1 employs a combination of CeO₂/LZO/NiW. System 2 is analogous to the classical buffer layer architecture of CeO₂/YSZ/CeO₂/NiW.

The two-buffer layered substrate in system 1 is based on the combination of cerium oxide (CeO₂) on top of lanthanum zirconate (LZO) coated on NiW substrate. First, a LZO layer is initially dip-coated on a Ni-5at%W. It is annealed at optimised conditions. In the second step, a layer of CeO₂ is dip-coated on top of the LZO coated NiW and is heat treated to obtain a ceramic thin film.

The three-buffer layered substrate in system 2 is based on sandwiching LZO between two CeO₂ layers on top of NiW substrate. Initially, CeO₂ is coated on top of NiW and is annealed at optimised conditions. The second step involves depositing LZO on top of CeO₂ coated NiW with again an appropriate annealing step. The final CeO₂ layer is deposited followed by a subsequent heat treatment at optimised conditions. Studies are done on this multiple buffer layer coated substrates. The chemistry of these precursor solutions are given below. The NiW tape (Evico GmbH, Germany) (80 µm thick) was cut into strips of approximately 3 cm. The tapes were chemical cleaned followed by a thermal treatment.

The LZO solution is prepared by using 1:1 molar ratio of lanthanum acetate and zirconium acetate metal precursors; 1:2 ratios of metal ions:TEA; 1:10 ratio of metal ions:acetic acid and 1:10 ratio of acetic acid:water. The CeO_2 solution is prepared by using 0.2M cerium acetate; 1:1 ratio of metal ions:NTA; 1:10 ratio of metal ions:acetic acid and 1:150 ratio of metal ions:water.

A system 1 – buffer layer architecture was prepared by using a solution with a total metal concentration of 0.4M for dip-coating LZO. Dip-coating was carried out at room temperature with varying dip-coat velocity and the substrates were withdrawn from the solution under an angle of 90°. The substrates were immersed in the solution for 30 s before they were withdrawn. Initially, the cleaned metal strips were coated with LZO at a dip coating speed of 40 mm/min. Subsequently, it was dried in an oven at 60°C for one hour to evaporate water on the surface. Later, the layer was annealed between 900°C and 1000°C to obtain better crystallinity of the deposited LZO buffer layer. The CeO_2 layer was successively deposited on top of the previously annealed buffer layer of LZO. A dip coating speed of 20 mm/min was employed. It is followed by drying in the oven at 60°C to remove most of the water. Finally the layers were annealed between 900°C-1050°C to obtain a ceramic thin film. This completes the architecture of double buffer layered system of CeO_2/LZO/Ni-5at%W. The deposition and annealing methods are the same for a system 2 architecture, but with an extra CeO_2 layer directly on top of Ni-5at%W.

The double buffered layer of CeO_2/LZO/Ni-5at%W and triple buffered layer of CeO_2/LZO/CeO_2/Ni-5at%W are characterized using XRD technique (fig. 2.4) to study the crystallinity and orientation of the (002) cubic peaks of the thin films. The desired cubic (002) peak of CeO_2/LZO/Ni-5at%W is marked. Also, the undesirable growth of (111) peak is as well indicated. For the CeO_2/LZO/CeO_2/Ni-5at%W system, the desired crystalline growth along (002) plane is obtained with negligible growth along the undesired (111) plane. The poor growth of (002) in the double buffer layered system can be attributed to the absence of better coordination of thicker LZO (LZO-LZO instead of CeO_2-LZO) system with the underlying Ni-5at%W. The LZO system, being a novel water based system has quite few problems in adapting the texture of the substrate. In contrast, system 2 containing double CeO_2 layers, sandwiching LZO in between shows prominent growth of (002) peak. The individual layers of LZO and CeO_2 are 70 nm and 20 nm thick respectively.
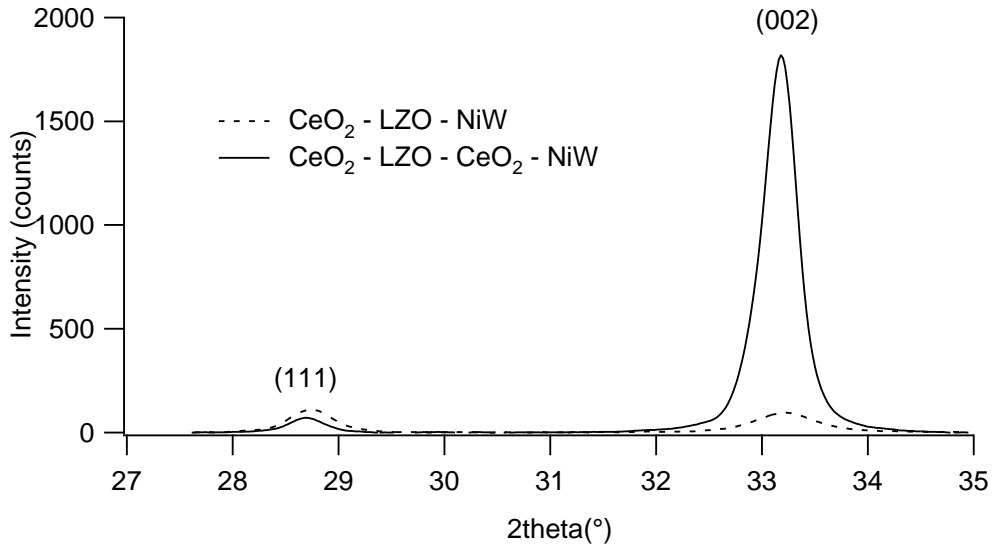
Fig. 2.4: XRD diffractogram of CeO$_2$-LZO-Ni-5at%W (system 1) and CeO$_2$-LZO-CeO$_2$-Ni-5at%W (system 2)

An XPS analysis (figs 2.5 and 2.6) on these multiple layers was performed to study the in-depth distribution of various elements at different depths of the deposited thin films. The appearance of La and Zr atoms in the first couple of layers indicate a probability of diffusion of Ce and La ions during annealing at high temperatures. The presence of carbon and oxygen at the surface is well indicated in the graph. Starting from 150 s of sputtering on, Ni is observed in the measurements. According to the calibration of the sputter rate with Ta$_2$O$_5$ this would refer to a depth of 20 nm. Ni-peaks were not expected to appear until a later stage in the experiment. Figure 2.6 shows the depth profile measurement showing the presence of various elements at different depths of the thin film in system 2.

Two distinct CeO$_2$ layers sandwiching the LZO layer can be observed. There is a clear overlap of CeO$_2$- LZO- CeO$_2$ regions indicating diffusion of Zr, Ce and La ions. The Ni ions are seen as few as 8-10 nm (according to Ta$_2$O$_3$ calibration) depth from the top surface. This indicates Ni penetration through the buffer layers. There is higher nickel diffusion in CeO$_2$-Ni region (fig. 2.6) compared to LZO-Ni region (fig. 2.5). This indicates LZO is a better Ni diffusion barrier compared to CeO$_2$. It needs to be taken into account that in system 2 the total buffer layer architecture undergoes 1 heat treatment more in comparison with system 1. As can be seen from the XRD results, system 2 has better lattice-matching with the substrate compared to system 1. This helps in better transfer of texture from the substrate to the to-be deposited YBCO layer. In contrast, Ni penetration occurs drastically in system 2 compared to system 1. This is undesired. Ni penetration will poison the YBCO layer and the superconducting current will be reduced. From the results obtained, we can conclude that system 1 suits more as a Ni

penetration barrier but the low texture is not desired. There is a need for thicker LZO to solve this problem.
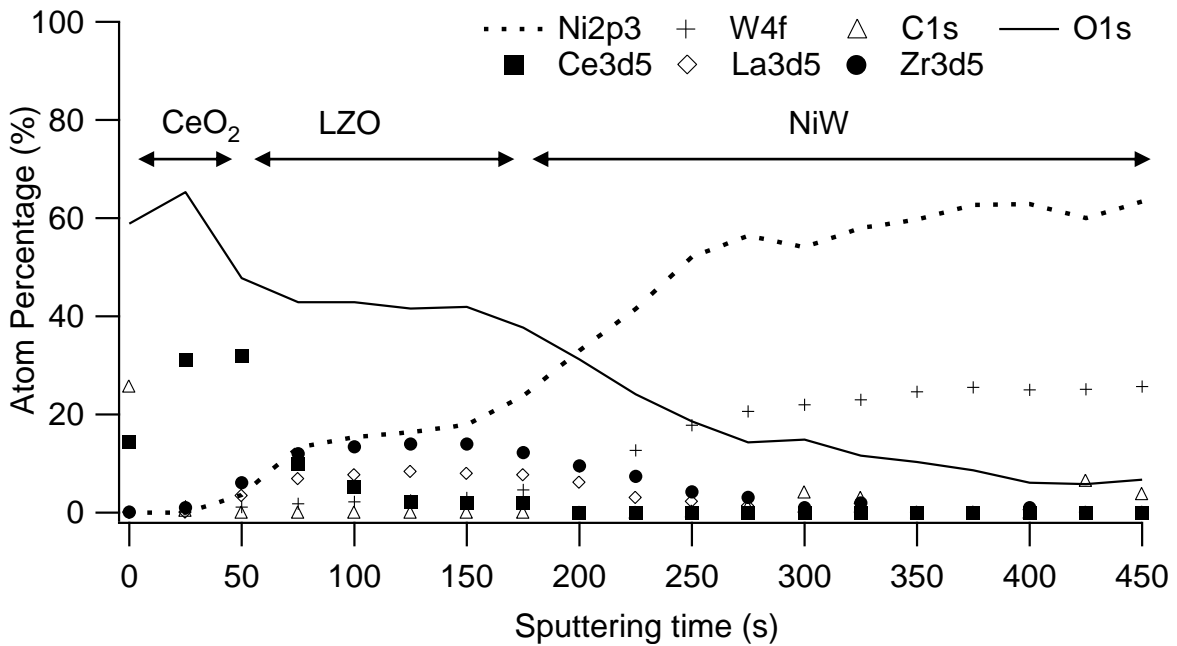
Fig. 2.5: XPS analysis of CeO$_2$-LZO-Ni-5at%W (system 1) substrate
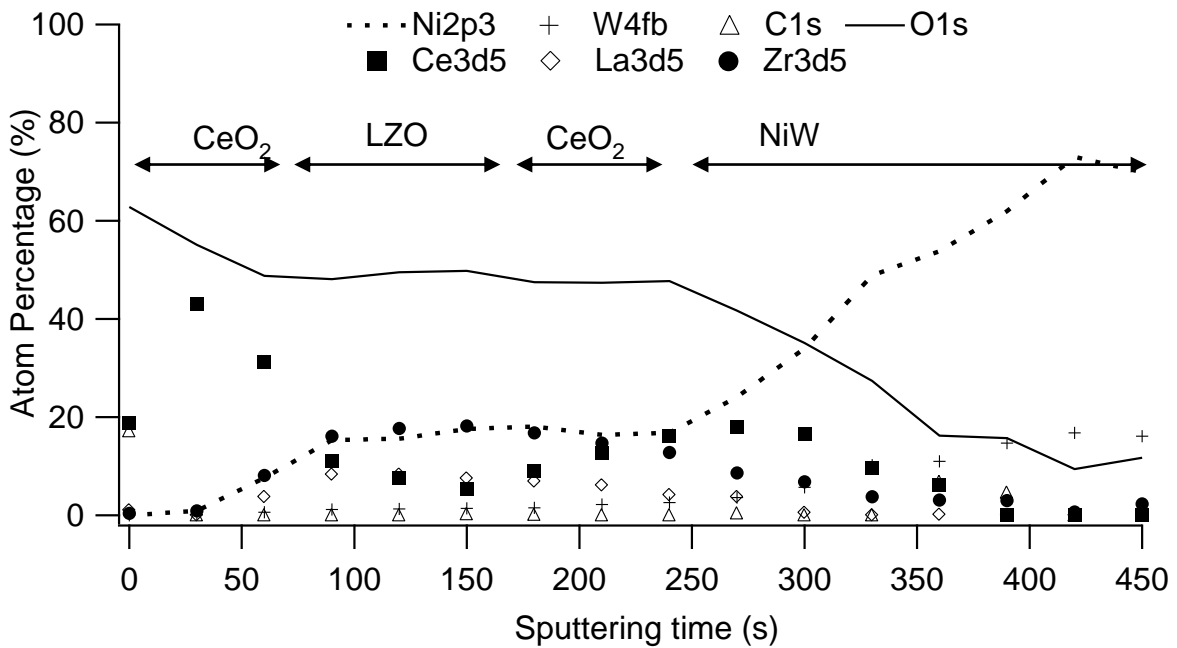
**Fig. 2.6: XPS analysis of CeO-LZO-CeO-Ni-5at%W (system 2) substrate**

V.2.2.1.3 Novel water based thick LZO buffer layers

Thicker LZO of more than 150 nm are desired as buffer layers. These thick LZO layers control the defects that are being transferred from substrate and buffer layers to the YBCO. Various solutions were prepared for sol-gel dip coating of single coating LZO layers. The most promising ones are given here.

	LZO precursor 1	LZO precursor 2	LZO precursor 3
Metal precursors	lanthanum acetate : zirconium propoxide	lanthanum acetate : zirconium propoxide	lanthanum acetate : **zirconium acetate**
Metal ions : EDTA	1 : 0.5	1 : 0.5	1 : 0.5
Metal ions : acetic acid	1 : 10	1 : 10	1 : 10
Metal ions : water	1 : 150	1 : 150	1 : 150
EDTA : PVP	1 : 1	1 : 1	1 : 1
EDTA : EG	-	**1 : 3**	1 : 3

Table 2.1: Overview of the different novel LZO precursor solutions

Here, EDTA has been used as a chelating agent as it is a stronger ligand and is expected to give better distribution of metal ions in the gel state and hence uniform and homogeneous thin films**.** The three different LZO precursors with each a total metal concentration of 0.4M was used for dip-coating. Cleaned metal strips were coated with the LZO precursors at a dip coating speed of 60 mm/min. Subsequently, the wet coatings were dried in an oven at 60°C. Later, they are annealed under various conditions and studied for their properties using XRD. The XRD results for LZO precursor 1 are given in figure 2.7. The thickness of the films is 100-110 nm. Intense reflections of (00l) orientation can be found although the presence of (111) orientation cannot be ignored. High temperatures give better results in this case. An overview of the XRD analysis and the thicknesses of the annealed LZO layers are given in table 2.2. High gas flow and high temperature annealing gives high intensity peaks oriented along (00l) plane. But, the presence of (111) peaks cannot be completely ruled out. It is clear from these experiments that further improvement is required. Also, the layers need to be pore-free, dense and homogeneous.
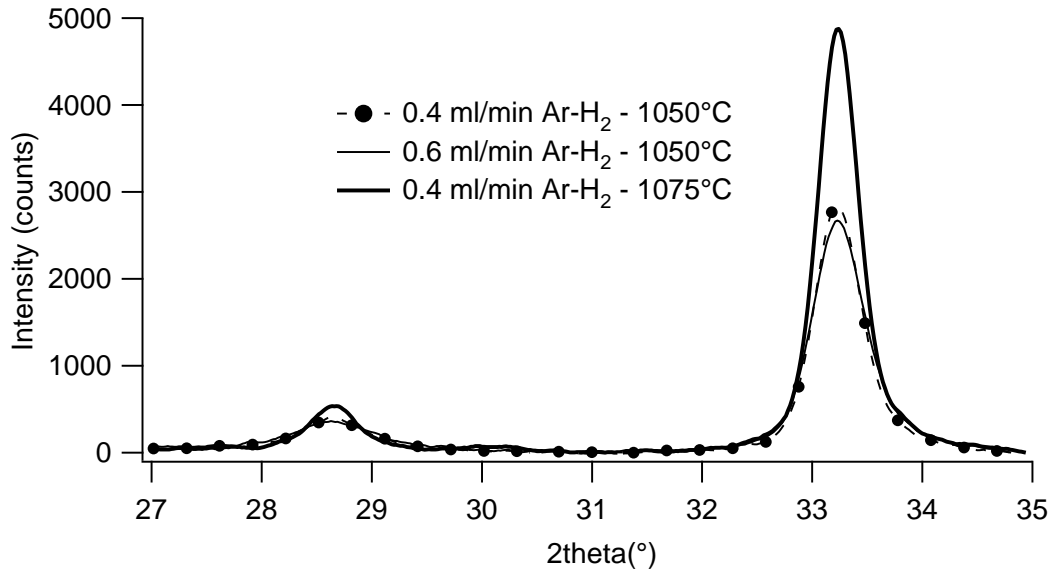
Fig. 2.7: XRD results of LZO precursor 1

Annealing condition	LZO precursor 1		LZO precursor 2		LZO precursor 3	
	(111 : 00l)	Thickness (nm)	(111 : 00l)	Thickness (nm)	(111 : 00l)	Thickness (nm)
(1) 1050°C 0.4ml/min Ar-H$_2$	14.6%		13.7%		11.5%	
(2) 1050°C 0.6ml/min Ar-H$_2$	14.4%	100 – 110	10.2%	130 – 140	9.72%	80 – 90
(3) 1075°C 0.4ml/min Ar-H$_2$	10%		11.6%		7.5%	

Table 2.2: Overview of the annealing experiments for LZO precursors 1-3

V.2.2.1.4 Development of La$_2$Ce$_2$O$_7$ buffer layers

Besides the development of thick LZO layers, lattice matched LCO layers with different ratios of La and Ce metal ions have been prepared and tested for their ability to act as buffer layers. There has been a report of lattice matched lanthanum doped cerium oxide buffer layers by pulsed laser deposition as a buffer layer on STO substrates (7). Different percentages of the La and Ce precursors were mixed to obtain homogeneous LCO solutions, which were used for film deposition. A 50% combination of La and Ce was analogous to the preparation of a composition similar to La$_2$Ce$_2$O$_7$ (8-9). Here, Ce replaces Zr to form La$_2$Ce$_2$O$_7$. A general 0.4M LCO solutions were prepared by dissolving stoichiometric cerium acetate in a water-acetic acid mixture (molar ratio (Ce^{3+}+La^{3+}):acetic acid:water = 1:10:90) at 80°C until a clear solution was obtained. Lanthanum acetate (La (CH$_3$COO)$_3$.1.5H$_2$O, Alfa-Aesar, 99.9%) was used as the lanthanum precursor. The stoichiometric lanthanum acetate was added to the cerium precursor solution at 80°C. To keep the metals in solution, ethylene-diamine tetra acetic acid was used as a complexant. An EDTA solution was prepared by dissolving

EDTA in a water and ethylene diamine (EDA, Fluka, 100%) mixture (molar ratio EDTA: Water: EDA = 1:60:4) at room temperature. The molar ratio of EDTA:(Ce^{3+}+ La^{3+}) was fixed at 0.5:1.5. Then, the metal solution (Ce^{3+}+ La^{3+}) was slowly added to the EDTA solution at room temperature and stirred for 10 minutes. The pH of the mixed solution was adjusted to 6 by adding ammonia and this mixture was heated to 60°C. A fixed amount of ethylene glycol was added to the above solution at 60°C (molar ratio EDTA:EG = 1:8)). This solution was stirred and the excess solvent evaporated until the desired concentration of 0.4 mol/L was obtained. The final solution of 0.4 mol/L concentration was found to have a pH of 6 and a viscosity of 4.60 mPa s.

The dip-coat speed was maintained at 60 mm/min. The as-deposited layers were transformed into a gel by placing them in a drying furnace at 60°C for one hour. The amorphous layers were transformed into crystalline layers by a suitable heat treatment. The as-deposited layers were first heated from room temperature to 450°C (ramp rate of 1°C/min) and let to dwell for 30 minutes. Secondly, a 3°C/min heating rate was applied from 450°C until 900°C (dwell time = 1h). Finally, the films were heated to 1050°C at a 10°C/min ramp with a dwell time of one hour. After the heat treatment, the furnace was switched off and the samples were left to cool inside the furnace. The entire heating process was carried out in an Ar-5%H_2 atmosphere (constant gas flow of 0.55 L/min).

Figure 2.8 shows the XRD pattern of different LCO buffer layers. A clear (002) oriented growth in all the three LCO layers. $L_{0.25}C_{0.75}O_{1.875}$ – LCO1 shows the maximum (002) orientation with no unwanted (111) growth. $L_{0.4}C_{0.6}O_{1.8}$ – LCO2 shows 20% (111) growth in comparison to 35% (111) orientation seen in $L_{0.5}C_{0.5}O_{1.75}$ - LCO3. The exact reasoning for the diminishing growth of (002) orientation, with increasing La content in the solutions is not clear. But the XRD pattern shows that, LCO can adapt the (002) orientation from the substrate.

The buffer layer capability of the LCO layers can be measured by monitoring the depth of Ni penetration throughout the buffer layers (XPS). The XPS analysis of a LCO 1 layer is given in fig. 2.9. LCO 1-3 layers with thicknesses of 85 nm were considered for analysis. In all samples (LCO 1-3) Ni is detected after a sputtering time of 320-400 s. This correlated with a Ni-free LCO layer of 60-70 nm. LCO proved to be a good barrier for Ni diffusions. No Ni is seen at the top of the buffer layers. The YBCO layers can be safely deposited on top of these improved buffer layers.
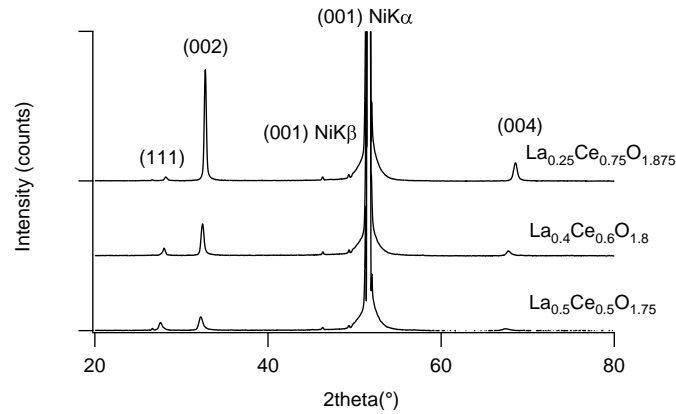
Fig. 2.8: XRD patterns of different LCO buffer layers
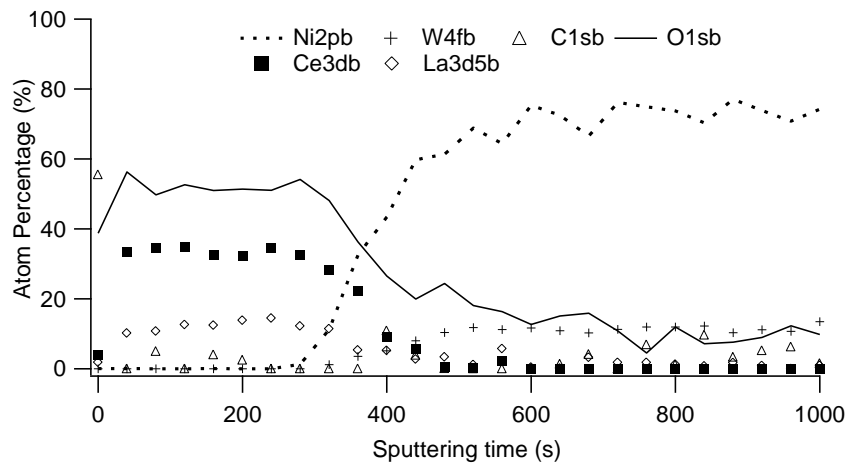
Fig. 2.9: XPS analysis of a La$_{0.25}$Ce$_{0.75}$O$_{1.875}$ layer

V.2.2.2 Part 2: Surface roughness of CeO$_2$ buffer layers

As mentioned before, the architecture chosen by UGent exists of a combination of CeO$_2$ (a=5.411 Å) and La$_2$Zr$_2$O$_7$ (a=10.804 Å), based on their good lattice mismatch, low oxygen diffusion and relatively easy synthesis chemistry. One of the main difficulties remains in the insufficient chemical stability of the CeO$_2$ layer during the YBCO process when working in solution deposition conditions, resulting in the formation of BaCeO$_3$. At the moment there is still an ongoing discussion about the reaction mechanism and especially when this formation takes place. According to Goswami et al. the BaCeO$_3$ is formed after the YBCO synthesis on top of the CeO$_2$ and should have no detrimental effect on the epitaxial growth of the YBCO (10). Nevertheless, the formation of BaCeO$_3$ will result in an excess of Y^{3+} and Cu^{3+} and into the formation of Y- and Cu-oxide phases. These sites are likely to cause internal stresses into the superconducting material, which is expected to result in a decrease in superconductivity. Therefore, neglecting when the reaction actually takes place, it is necessary to minimize the formation of BaCeO$_3$ as much as possible. This can be achieved by minimizing the surface

roughness of the CeO$_2$ buffer layer, by increasing the chemical stability through metal substitution (11) or by a combination of both.

In order to understand why a decrease in surface roughness will be beneficial to avoid BaCeO$_3$, it is necessary to know some fundamentals about the formation of a solid (12). After the deposition of a liquid film (e.g. by dip coating), a thermal process is started. At a certain temperature the metals in this film will start nucleating at the surface of the substrate. At these sites grains will start growing by diffusion of nearby atoms. This will continue until 2 of those grains come together and form a grain boundary. This abrupt growth cutoff will cause the atoms on these spots to be less regularly bonded than the center atoms in the grain, which will lead to a higher energy state. According to the laws of thermodynamics, this induces a strong behavior towards energy relaxation mechanisms. In reality this means that the atoms at grain boundaries will have a tendency to form bigger grains or to react with other present elements, i.e. Y^{3+}, Ba^{3+} and Cu^{3+} during the formation of the YBCO layer. Overlooking the complete process from sol to ceramic oxide thin film, we can distinguish several steps that are prone to have an effect on the surface roughness.

V.2.2.2.1 Precursor chemistry

The precursor solutions were prepared by dissolving stable, cost-effective and widely available inorganic salts in an aqueous solution of coordinating ligands. In this experimental work we used citric acid (13) or iminodiacetic acid (IDA) as ligands. These organic ligands form the major part of the species that need to be combusted during the process. Therefore it was necessary to take a look into the thermal decomposition of our systems (figs 2.10-2.11) and the resulting effect on the surface roughness (fig. 2.12).
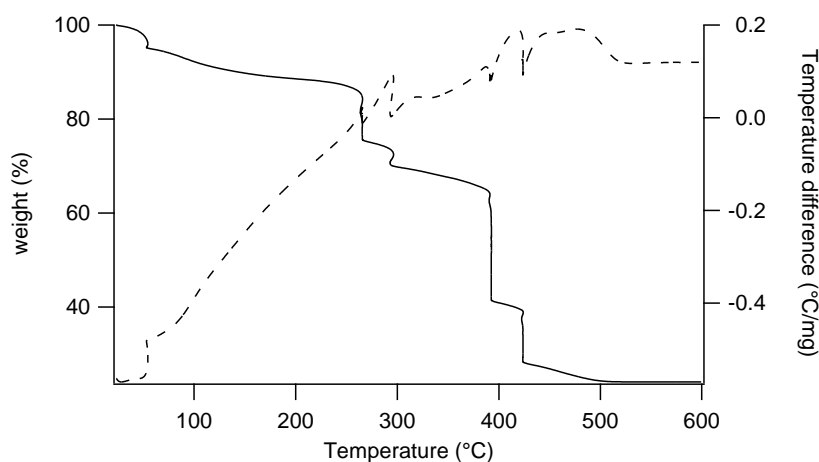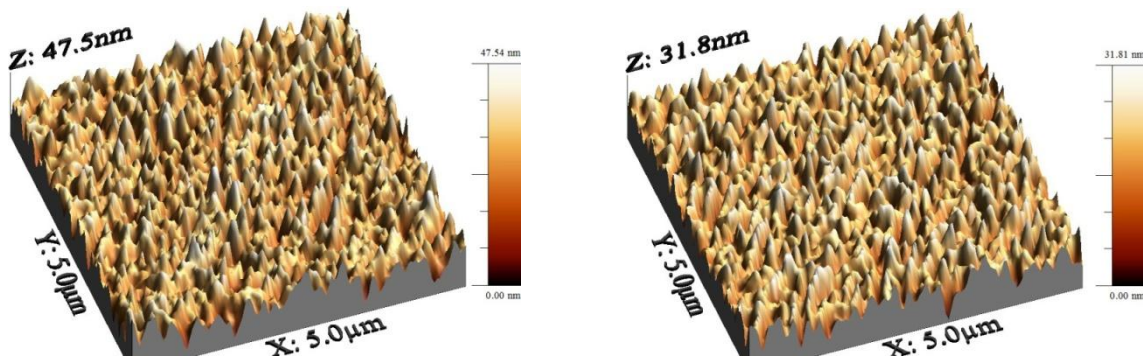

Fig. 2.10: Thermal analysis of the citric acid based system
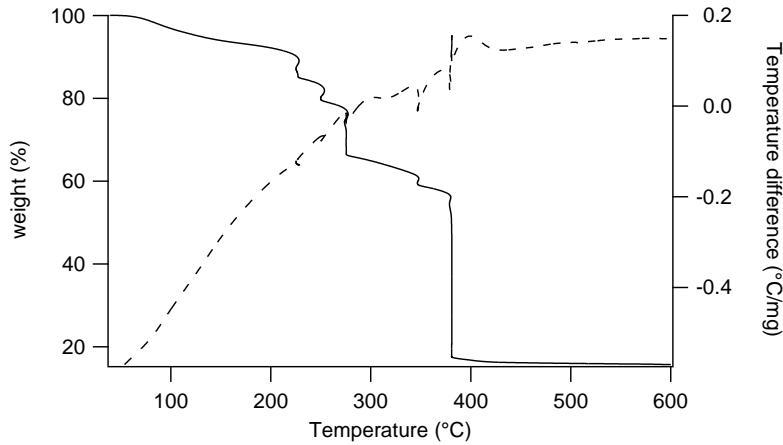
*Fig. 2.11: Thermal analysis of the IDA based system*

Experiments showed that the IDA based system was more favorable to synthesize low surface roughness buffer layers in comparison to the citric acid based system. For an optimized synthesis process we achieved an optimal surface roughness of approximately 7 nm RMS for the citric acid based system and 4 nm RMS for the IDA based system. A good choice of the precursor chemistry thus leads to a substantial decrease of the surface roughness.

Fig: 2.12: Optimized surface roughness for the citric acid (left) and IDA (right) based system

V.2.2.2.2 The thermal synthesis process

Taking a look at the thermal analysis of the precursors in figures 2.10 and 2.11 we see that the thermal decomposition is completed well before 500°C. This step is generally called calcination. At higher temperatures the diffusion kinetics of the metals will increase and grain growth and crystallization will occur during the sintering step.
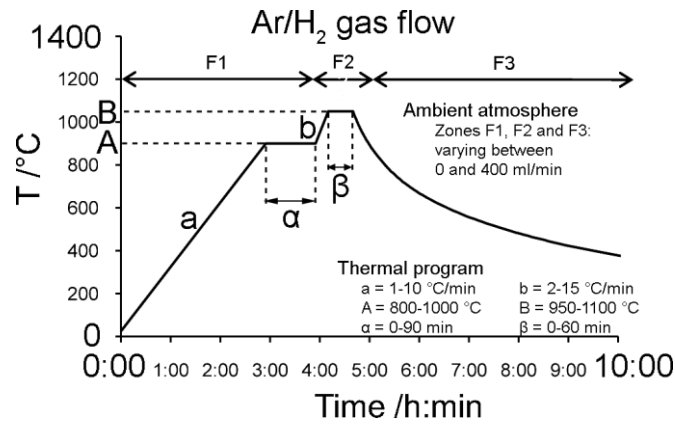
*Fig. 2.13: Thermal synthesis process of CeO$_2$ buffer layers*

	a Calcination ramp	b Sintering ramp	B Sintering level	β Sintering dwell	F atmosphere
RMS$_{max}$/RMS$_{min}$	2.8	2.0	1.5	1.9	2.0

Table 2.3: Effect of optimized parameter on surface roughness

Above table clearly shows that the calcination ramp has the biggest effect on the surface roughness. A variation of the calcination ramp between 1 and 10°C/min resulted in a variation of the RMS roughness with a factor 2.8.

V.2.2.2.3 Metal substitution

After choosing the most favorable precursor system and optimizing the thermal process, we could achieve a surface roughness of 4 nm RMS, whereas the objective was to synthesize film with a surface roughness below 3 nm RMS. One of the options to realize a further decrease in surface roughness is to add doping elements such as Gd^{3+} into the precursor system. This metal substitution is known to exhibit a positive effect on the metal diffusion along the grain boundaries, what results in an optimized surface morphology. An extra decrease in surface roughness up to 20% is shown for these 2 samples. Combining this with the optimized process in table 2.3, allows to get very close to our objective of a surface roughness of 3 nm RMS.
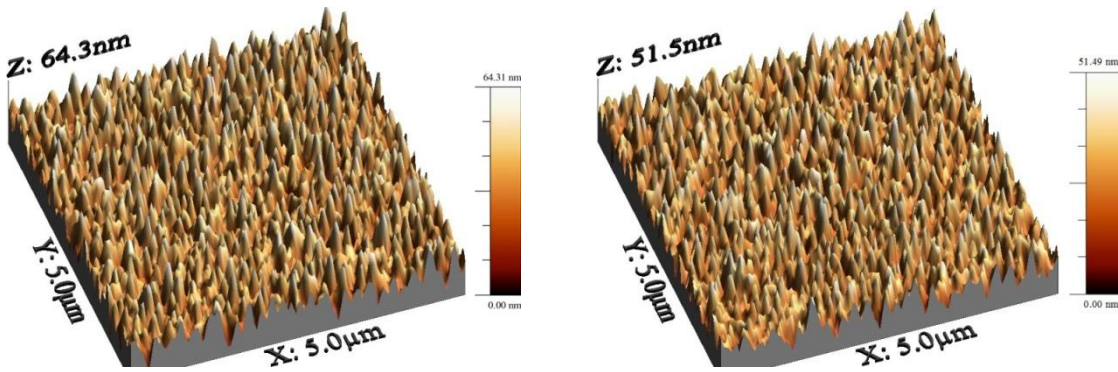
Fig. 2.14: Surface roughness of non-doped CeO₂ versus 3% Gd³⁺ doped CeO₂

V.2.2.3 Part 3: Ink-jet printing of YBCO superconducting layers

In this third part of the project, the focus is on the development of a precursor solution which will be ink-jet printed onto an appropriate substrate. In the field of ink-jet printing of high temperature superconducting materials, an intense cooperation was started with the University of Cambridge. They provided us with the ink-jet printing system (electromagnetic print head and XY positioning system). A semi-clean environment has been created to minimize the incorporation of dust. Many parameters (opening time and diameter of the nozzle, applied pressure, viscosity, density, surface tension of the solution) can be tuned for ink printing. Some of the most important results are given here.

V.2.2.3.1 Ink properties

This goal was investigate not only the properties of the YBCO ink itself, but also the changes which take place during the heat treatment and to conclude if hydrolysis and condensation reactions occurred. Due to the wide variety of these chemical changes, different techniques are used for this investigation. Measurements were done at the University of Louvain-La-Neuve (UCL, Raman), at the University of Brussels (VUB, ATR and rheology) and in-house. The examined samples are given in table 2.4 and are based on the AWAT precursor solution (24). The influence of metal ions and metal ion concentration was tested. None of the used techniques show strong evidence for the existence of a macroscopic network. It is more appropriate to describe the condensed solutions as a highly viscous, viscoelastic liquid instead of a gel. The increase of the viscosity with the metal concentration may then be attributed only to electrostatic forces (14-23).

	Water: acetic acid	TEA (ml)	NH$_4$OH (ml)	Metal ions	10 ml dried at 60°C (hours)	η gels (mPa s)
Blank	4:1	5	5.6	-	18	1593
0.6 M	4:1	5	5.6	0.1 M Y(Ac)$_3$ 0.2 M Ba(Ac)$_2$ 0.3 M Cu(Ac)$_2$	16	1408
1 M	4:1	8.3	4.6	0.167 M Y(Ac)$_3$ 0.333 M Ba(Ac)$_2$ 0.5 M Cu(Ac)$_2$	16	1747

Table 2.4: Composition of the rheology samples

V.2.2.3.2 Ink-jet printing of YBCO inks

- Cleaning of the surface

The first approach for immerging of the individual drops into a coating was by modifying the substrate surface by a soft cleaning procedure. Just before printing, the substrate is pulled out of the acetone and dried on a hot plate. This is to assure that no dirt would remain on the surface.

- Modification of inks

The next strategy was to modify the surface tension and/or the viscosity of the AWAT precursor by addition of alcohols, lowering the concentration of the inks, addition of surfactants. None of these modification resulted in a dense, epitaxial YBCO layer. The layers peeled off or showed a lot of secondary phases. A new ink formulation was needed to be developed.

By changing its composition, an adaptation of properties of the ink to the properties of the substrate and to the heat treatment was done. In this bottom down approach, the new solution is composed of metal acetates dissolved in water. To have a good complexing agent that gives (even at higher temperatures) soft gels, triethanolamine (1:5; [Cu]:TEA) remains in the solution. To lower the pH without adding more solvents, EDTA was added. This not only lowers the pH but acts as a good complexing agent for the three metal ions. After the metal ions are dissolved, the pH was brought to 6-7 by adding a small volume of acetic acid. This composition is stable for weeks and after drying in a drying furnace it gives clear gels (fig. 2.15).
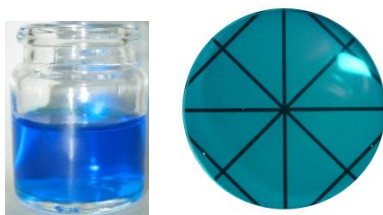

Fig. 2.15: (Left) precursor solution (right) clear gel

For printing these solutions with an piezoelectric (DMP) ink-jet set-up, a 1.2 M total metal concentration ink was injected into 10 pl cartridges. For the experiments done up to now, a drop spacing of 20 µm and a voltage of 17-18 V were used. After small changes of the precursor solution, a fully covered substrate could be obtained starting from a non filtered solution. After a burn-out step to 400°C in air, a final heat treatment was applied. Unfortunately, the sample had almost no preferential YBCO orientation and a significant amount of $BaCeO_3$ side phases.

Fig. 2.16: Droplet formation, coated substrate from liquid to 200°C (+ optical microscopy) and after 400°C

Further optimization of the ink composition (different metal salts, complexing agents, ratio of complexing agent) made it was possible to improve the spreading of the ink on the buffered substrate. This gave excellent coatings with no contraction upon heating. The layers were subjected to a fast drying step on a hot plate (~240°C). It was possible to obtain almost dry layers without cracks in 15 minutes (fig. 2.17).
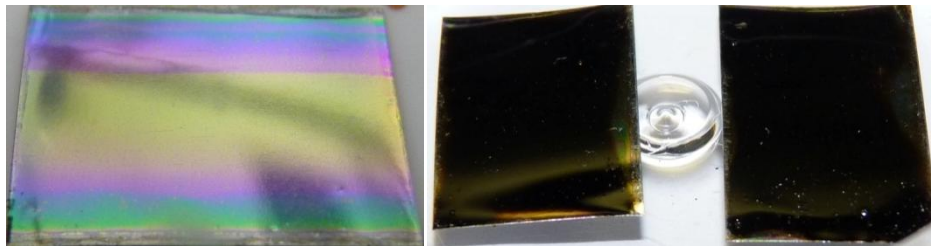

Fig. 2.17: Printed layer on tape before and after hot plate treatment

New samples pretreated on the hotplate were further calcined in the tube furnace under controlled atmosphere. These calcined layers were further processed and sintered at higher temperatures in 100 ppm O_2 atmosphere. The new solution results after sintering, both for tape and single crystal, in c-axis oriented YBCO. There are some unidentified reflections present, so further optimization of the heat treatment is still necessary. Because of this promising XRD measurement, the superconducting properties of these two samples were tested.
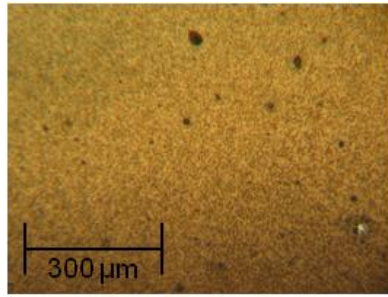
Fig. 2.18: Optical microscopy picture of the sintered YBCO layer on SrTiO₃

The measurement of the resistivity in function of the temperature resulted in a drop of the curve (T_c) at 92 K for the YBCO printed on tape and 90 K for the YBCO printed on SrTiO$_3$. Both samples still have a broad drop of the resistivity and they do not fall completely to zero. This could be due to the unidentified phases visible in XRD. Nevertheless, these last measurements give us hope for the further research on this subject.
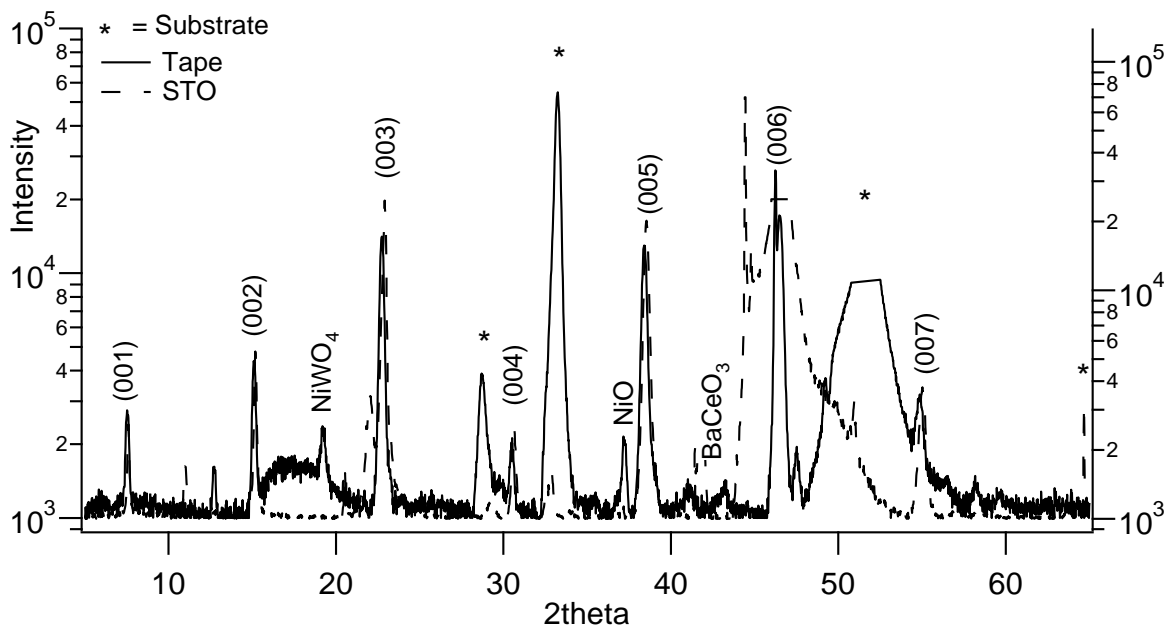
Fig. 2.19: XRD measurement of the sintered layers on buffered tape and on SrTiO₃
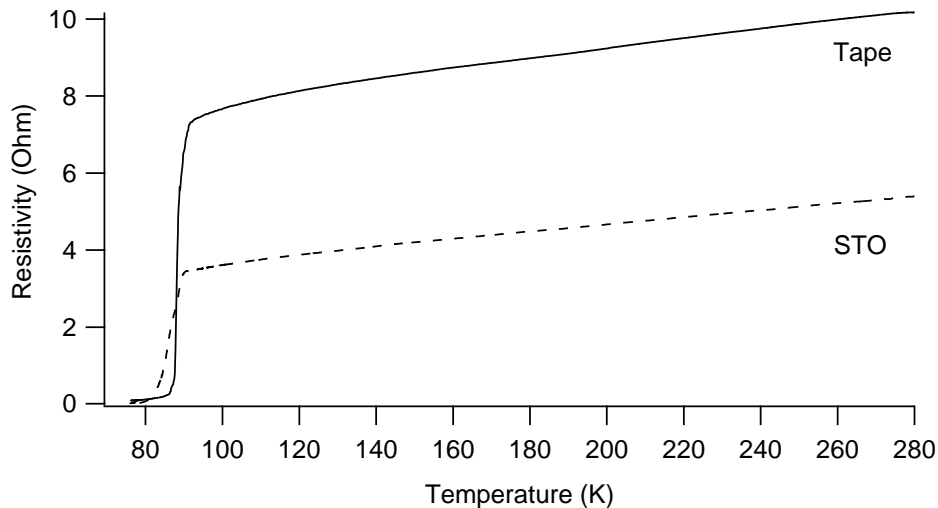
Fig. 2.20: Resistivity measurement of the YBCO layer processed on buffered tape and on single crystal

<u>V.2.3 Conclusions and outputs</u>

V.2.3.1 Part 1: Development of $La_2Zr_2O_7$ and $La_2Ce_2O_7$ buffer layers for coated conductor design

Two sequences of cleaning were tested: chemical followed by thermal processing and thermal followed by chemical processing. It is found that chemical - thermal treatment of Ni-5at%W is better suited compared to thermal-chemical treatment. The buffer architecture system CeO_2/LZO/NiW with less heat treatment cycle shows higher Ni free region compared to the system CeO_2/LZO/CeO_2/NiW with more heat treatment cycles. Both systems are unable to stop the penetration of Ni ions totally, as seen from the XPS data. Therefore we shifted towards another buffer layer architecture: a thick (min 150 µm) LZO layer.

Lattice matched lanthanum-cerium oxide (LCO) films on Ni-5%W substrates were deposited by chemical solution deposition (CSD). Three different ratios of lanthanum and cerium based precursor solutions were prepared. The ratios of the metal ions of these layers were optimized to have minimal lattice mismatch with that of the b-axis of YBCO superconducting layer. Single, crack-free LCO layers with a thickness of up to 120 nm that could prevent Ni penetration were obtained.

V.2.3.2 Part 2: Surface roughness of CeO_2 buffer layers

In this part 3 different approaches were tested to decrease the roughness of the surface: 1) precursor chemistry, 2) optimized thermal treatment and 3) metal doping of CeO_2. It was proven that the use of iminodiacetic acid induces a decrease of the surface roughness whereas the calcination ramp is the most important parameter in the temperature program.

As last conclusion it can be stated that the doping of CeO$_2$ by Gd^{3+} has a positive influence on the roughness of the buffer layer.

V.2.3.3 Part 3: Ink-jet printing of YBCO superconducting layers

The characterization of the solution properties was done by rheology, Raman and ATR-IR. For the moment there is no proof of that "macroscopic" reorganization or condensation reactions are happening when the temperature is raised to 100°C.

The AWAT ink as such was not suitable for ink-jet printing of YBCO layers. More extensive research on the calcinations behavior of the precursor solution gave insight on the problem during the different steps of the heat treatment. A new ink formulation resulted in a gradual weight loss between 250 and 450°C. This less exothermic decomposition of the ink is necessary in order to obtain reproducible coatings with a thickness around 500 nm. With this new ink formulation, it was finally possible to produce YBCO films with some superconductive behavior. Further optimization of the heat treatment is still necessary in order to improve the superconductive properties: narrow T_c drop, resistivity = 0 Ohm at 77K and the possibility to measure J_c values.

We are still far away from a production of YBCO tapes with attractive physical properties. YBCO tapes are of great interest for current transport applications but also for energy storage through SMES (superconducting magnetic energy storage) systems.

V.2.4 References

(1)   A. Goyal, D.P. Norton, D.K. Christen, D. Specht, M. Paranthaman, M. Kroeger, M. Budai, Q. He, A. List, R. Feenstra, H.R. Kercher, D.F. Lee, E. Hatfield, P.M. Martin, J. Matthias, IEEE. Trans. Appl. Supercond. 69 (1996) 403.

(2)   M. Steffens, M. Falter, M. Bäcker, C. Oligschleger, Journal of Physics: Conference Series 97 (2008) 012165.

(3)   V. Cloet, J. Feys, R. Hùhne, S. Hoste, I. Van Driessche, Journal of Solid State Chemistry 182 (2009) 37–42.

(4)   G. Kotzyba, B. Obst, R. Nast, W. Goldacker, B. Holzapfel, Journal of Physics: Conference Series 43 (2006) 345-348.

(5)   T. Caroff, L. Porcar, P. Chaudouët, A. Abrutis, C. Jiménez, P.Odier, F. Weiss, IEEE transactions 19 (2009) 3184-3187.

(6)   S. Sathyamurthy and K. Salama, Supercond. Sci. Technol. 14 (2001) 643– 645.

(7)   D. Chambonnet, D. Keller, C. Belouet, Physica C 302 (1998) 198-206.

(8)   J.S. Bae, W.K. Choo, C.H. Lee, Journal of the European Ceramic Society 24 (2004) 1291–1294.

(9)   K. Knoth, B. Schlobach, et al., Physica C: Superconductivity (2005) 426-431 (Part 2): 979-984.

(10) R. Goswami, R.L. Holtz, G. Spanos, IEEE Transactions on Applied Superconductivity 17 (2007) 3294-3297.

(11) Y. Takahashi et al. Physica C-Superconductivity and Its Applications 412 (2004) 905-909.

(12) W.D. Callister, Materials Science and Engineering: An Introduction. John Wiley & Sons, Inc. 869 (1999).

(13) N. Van de Velde, et al., European Journal of Inorganic Chemistry (2010) 233-241.

(14) J.D. Ferry, "Viscoelastic properties of polymers", New York (N.Y.): Wiley (1970).

(15) F. Dollish, W. Fateley, F. Bentley, "Characteristic Raman frequencies of organic compounds", John Wiley & Sons, New York (1974).

(16) K. Nakamoto, "Infrared and Raman spectra of inorganic and coordination compounds, Part B", John Wiley & Sons, New York (1997).

(17) M. Flett, "Characteristic frequencies of chemical groups in the infra-red", Elsevier Publishing Company (1963).

(18) D. Simonelli, M.J. Shultz, Journal of Molecular Spectroscopy 205 (2001) 221-226.

(19) S. Ben Yahia, L. Znaidi, Spectrochimica Acta Part A 71 (2008) 1234-1238.

(20) F. Quilès, A. Burneau, Vibrational Spectroscopy 16 (1998) 105-117.

(21) S. Sakohara, M.A. Anderson, Journal of Physical Chemistry B 102 (1998) 10169-10175.

(22) A. Ghauch, P.A. Deveau, Talanta 68 (2006) 1294-1302.

(23) A. Baranauskas, D. Jasaitis, Vibrational Spectroscopy 28 (2002) 263-275.

(24) P. Vermeir, I. Cardinael, M. Backer, J. Schaubroeck, E. Schacht, S. Hoste, I. Van Driessche, Superconductor Science & Technology (2009) 075009.

V.3 Oxides for Heat-to-Electricity converter

V.3.1 Introduction

In the previous reports, we tried various synthesis routes to produce cobaltite and manganite powders. The first deliverable, which consists in the synthesis of thermoelectric powders through "chimie douce" processes, was finally focused on the development of hydrothermal route for the synthesis of strontium manganite, and the citrate route for the synthesis of calcium cobaltite. The most efficient processes being selected, the next step of this work was to optimize the sintering step and determine the ceramics properties. In the frame of the WP3-D4 deliverable, an equipment that measures the Seebeck coefficient and the electric conductivity (RZ-2001-I from Ozawa Science, Nagoya, Japan) was purchased and used to characterize thermoelectric properties of P-type and N-type ceramics. The final goal of this work was to prepare 2-legs thermoelectric modules and to develop a testing bench for their characterization.

Deliverables were successfully achieved and are described in the following sections.

V.3.2 Manganite systems

V.3.2.1 Hydrothermal synthesis of manganite powders

Synthesis conditions were assessed from Pourbaix diagrams (1), and from papers of Spooren et al. (2) and Hashimoto et al. (3).

$KMnO_4$, $Mn(NO_3)_2.6H_2O$ and $Sr(NO_3)_2.6H_2O$ (Aldrich) were used as precursors. After weighing, precursors are either directly poured in the mineralizer solution (0.9 mol/l KOH solution) or dissolved in water before mixing with KOH solution. The precursor mixture is placed in a teflon lined digestion bombs for a hydrothermal treatment of 12 hours at 240°C. The powder is then washed until neutral pH. If only washed with water, powders exhibit minor amounts of $SrCO_3$ and $K_{0.5}Mn_2O_4$ which has been reported as a possible intermediate specie in the hydrothermal crystallization mechanism of perovskite manganites (5). Carbonate ions are mainly brought by the KOH pellets. To fully remove $SrCO_3$, two successive acidic washings in a diluted HCl solution are necessary. Because of powder loss during the acidic and neutral washings, the total reaction yield of the whole synthesis process lies between 70 and 76 wt%.

Powder density, measured by He pycnometry, varies from 5.3 to 5.8. Particles morphology is needle like (figure 3.1).
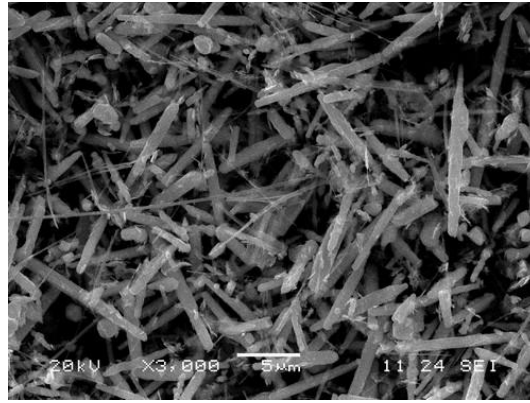
Fig. 3.1: SEM micrographs of the needle-like SrMnO₃ particles

The chemical composition was assessed through ICP spectrometry and iodometric titration: depending on the sample, the amount of potassium is between 200 and 600 ppm, the amount of strontium is between 42.0 and 44.8 x10^4 ppm, and the amount of total manganese is between 30.5 and 31.5 x10^4 ppm. Manganese valency is quite constant (3.8 to 3.9) but is lower than the theoretical value. This suggests that some reduction occurs in the reaction media, transforming part of the MnO_2 into Mn_2O_3 species. Potassium ion is present in the manganite crystalline network: either as an impurity (interstitial) or as a doping element (on Sr or Mn sites).

V.3.2.2 Thermoelectric properties of strontium manganites

In the dilatometric recordings, a linear shrinkage of about 18% is observed when T reaches 1377°C. Above that temperature, the sample melts. As there was a very little amount of available powder, compacting and sintering conditions could not be optimized.

Two samples were prepared. They were compacted at 75 MPa and 150 MPa respectively, and sintered for 1 hour at 1370°C. Both were porous (20.9 and 10.1 vol% respectively). Their thermoelectric properties are presented on figure 3.2. They were measured under air with the RZ-2001-I equipment (figure 3.3) manufactured by Ozawa Science (Nagoya – Japan).
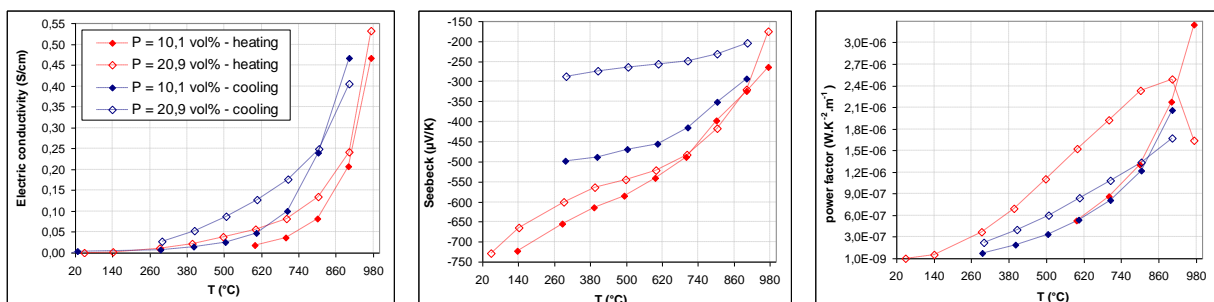
Fig. 3.2: Thermoelectric properties of SrMnO₃ porous ceramics

Fig. 3.3: RZ-2001-i equipment (left) and sample positioning (right)

As expected, strontium manganite is a N-type semiconductor (negative Seebeck coefficient). According to Hashimoto datas (3, 4), the electric conductivity of undoped $SrMnO_3$ rises sharply with temperature reaching values of 0.05 S/cm at 600°C and 0.4 S/cm at 800°C. According to Kolesnik et al. (5), the Seebeck coefficient and power factor at room temperature should be equal to -400 µV/K and 7×10^{-4} W K^{-2} m^{-1} respectively. In this study, the Seebeck coefficient of the as-prepared porous manganites is far from the values reported by Kolesnik, but gets closer after a heat treatment at 970°C. However, because of the large porosity and maybe because of the presence of K^+ ions, the ceramics remain too resistive leading to poor values of the power factor.

V.3.3 Cobaltite systems

V.3.3.1 Properties of cobaltite powders

The starting $Ca_3Co_4O_9$ powders were prepared from the citrate route, from the solid state route and from the flux-growing process described in the previous CHEMAT report (6). The powders processing conditions, properties and morphology are presented in table 3.1 and in figure 3.4.
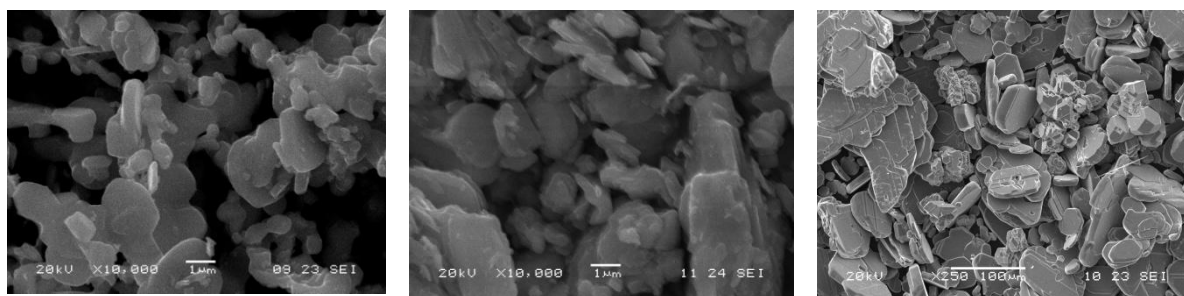
Fig. 3.4: Morphology of the cobaltite particles synthesized through the citrate route (left), solid-state route (middle) and flux-grown (right)

Powder	Processing conditions	Powder characteristics
Solid state (SS)	800°C (ltd1) – 25 h	Density : 4.66 mean grain size D50 = 3.5 μm
Citrate (C)	Fired 2h at 780°C	Density : 4.75 mean grain size D50 = 1 μm
Flux grown (F)	Dwell T = 920°C Solvent ratio : 45%	Density : 4.79 grain size of the flux D50 = 28 μm

Table 3.1: Powder processing conditions

V.3.3.2 Compaction and sintering conditions

Three samples (SS-1, SS-2 and SS-3) were made from the solid state powder and were compacted uniaxially at 354, 287 and 206 MPa respectively.

One sample (C) was pressed at 234 MPa from the citrate powder and one last sample (C+F), which was prepared from a mixture containing 75 wt% of the citrate powder and 25 wt% of the flux-grown powder, was compacted at 192 MPa.

The sintering temperature was estimated, near the sample, between 900 and 920°C. The dweling time was fixed at 15 hours for samples SS-1 and SS-2, and at 5 hours for the other samples. (SS-1) was sintered with no load and underwent a linear expansion of 3% along the normal axis of the pellet. To avoid this expansion a preload of 2 kN was applied on the other samples prior to densification. (SS-2), (SS-3), (C) and (C+F) samples were sintered under a load of 10.6 kN.

A linear shrinkage of 26% was observed for (SS-2) pellet. Its initial diameter being similar to the inner diameter of the mold (about 30 mm), no creeping occurred. As (SS-3), (C) and (C+F) pellet had a much smaller initial diameter (~ 21 mm), they underwent creeping.

Sintering was performed in the furnace of a mechanical testing machine dedicated to high temperature flexural characterizations (Zwick 1474). The set-up is illustrated on figure 3.5.
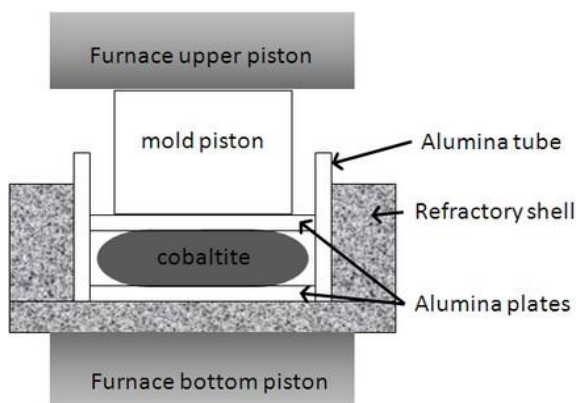
Fig. 3.5: Uniaxial hot pressing setup

V.3.3.3 Ceramic structural properties

Ceramics were characterized in terms of density and open porosity (table 3.2).

Sample	Loading & creeping condition	Density	Open porosity
SS1	No load No creeping	3.25	30.0 vol%
SS2	Under load No creeping	4.63	0.20 vol%
SS3		4.66	0.09 vol%
C	Under load Creeping	4.58	1.11 vol%
C+F		4.67	0.07 vol%

Table 3.2: Physical characteristics of cobaltite ceramics

Hot pressed ceramics are expected to be textured through an alignment of the platelets (powder particles) in the plane normal to the loading axis.

In the following, we call "in-plane" direction, the plane normal to the hot pressing load axis, and "of-plane" direction, the direction parallel to the loading axis. The flexural strength was only measured for sample SS-3 with an applied load parallel to the "out-of-plane" direction: a mean value of 264 MPa was recorded. For SEM observations, samples cutted along the "in-plane" and "out-of-plane" directions were polished (mirror quality) and chemically etched for 5 seconds in an HCl concentrated solution (6N).
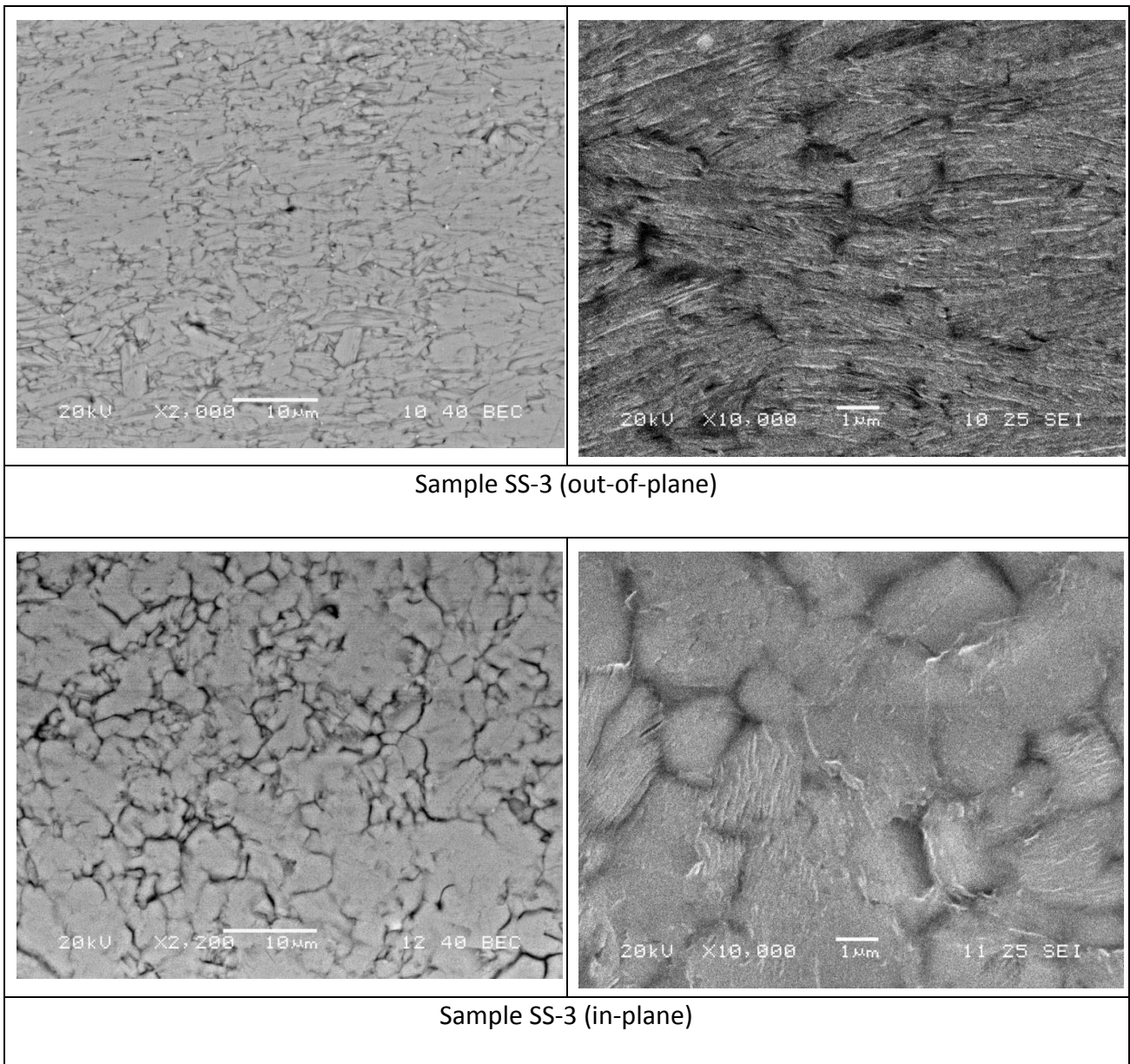
The microstructures are illustrated in the figures 3.6 to 3.9.
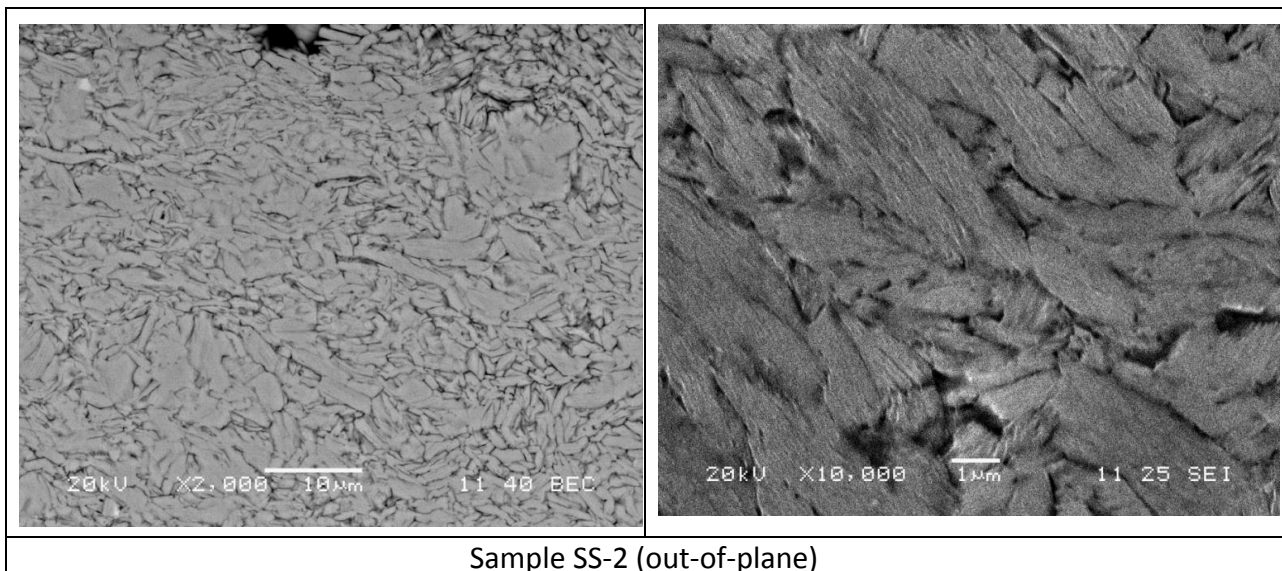
Sample SS-2 (out-of-plane)

Fig. 3.6: SEM micrographs of sample SS-2

No difference was observed between the "in-plane" and "out-of-plane" microstructures of sample (SS-2). Particles were randomly aligned.


Sample SS-3 (out-of-plane)

Sample SS-3 (in-plane)

Fig. 3.7: SEM micrographs of sample SS-3

In the case of (SS-3), a platelet orientation could be observed. The grain size was between 5 and 10 µm. This size is larger than for initial powder particles.

The white stripes are characteristic of the cobaltite lamellar structure. Theoretically, they should be detected only in the "out-of-plane" micrographs. Those observed in the x10000 "in-plane" magnification reveal that several particles do not align properly. Full texturing is thus not achieved.

Starting from the thinner particles processed through the citrate route, a better alignment is achieved. Platelets diameter which were close to 1-2 µm in the powder, increased to about 3 µm in the ceramic.

Sample C (out-of-plane)
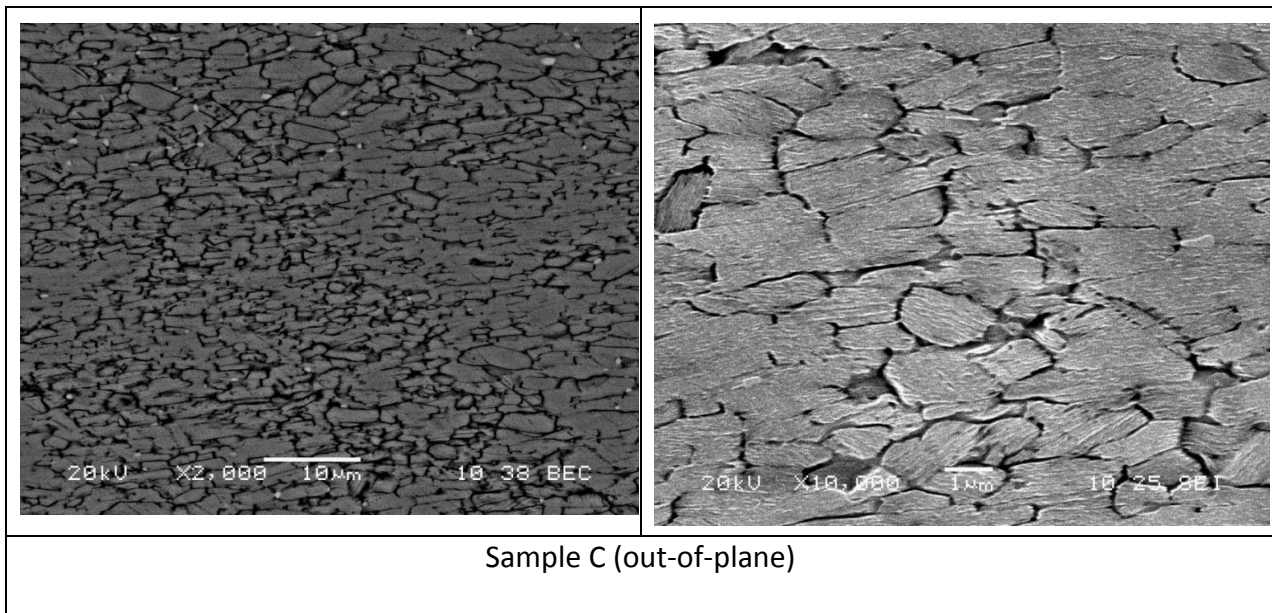
Fig. 3.8: SEM micrographs of sample C

In the case of sample (C+F) micrographs, the large flux-grown plates seem to decrease the effect of the hot-pressing load towards the thinner particles. This screening effect limits therefore the in-plane orientation of platelets. No significant difference was detected between (SS-3) bulk and (C+F) matrix in the x2000 and x10000 magnifications: the expected template effect (inducing an improvement of the texturing through the growth of the thinner particles along the large particles) was not effective.

| Sample C+F (out-of-plane) | Sample C+F (in-plane) |

Sample C+F (out-of-plane)
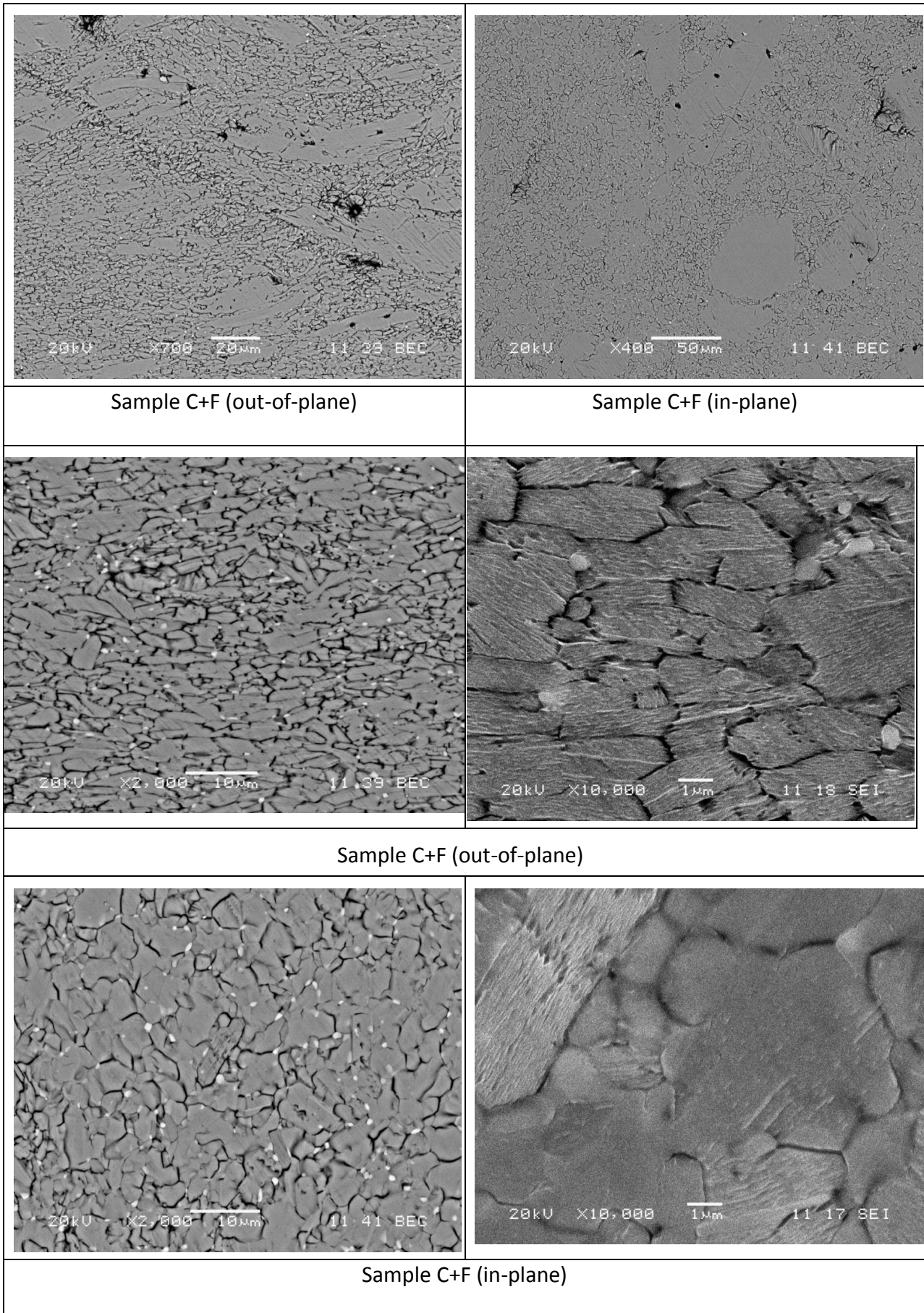
Sample C+F (in-plane)

**Fig. 3.9: SEM micrographs of sample C+F**

V.3.4 Cobaltite thermoelectric properties

Because of texturing, electrical properties of cobaltite are anisotropic.

In-plane measurements were performed for all samples. In this configuration, current as well as ΔT are applied in the plane normal to the hot pressing load direction. Sample SS-3 was also tested in the out-of-plane configuration, where current and ΔT are applied in the direction of the hot pressing load. Electrical conductivity, Seebeck coefficient and power factor are presented in figures 3.10, 3.11 and 3.12.
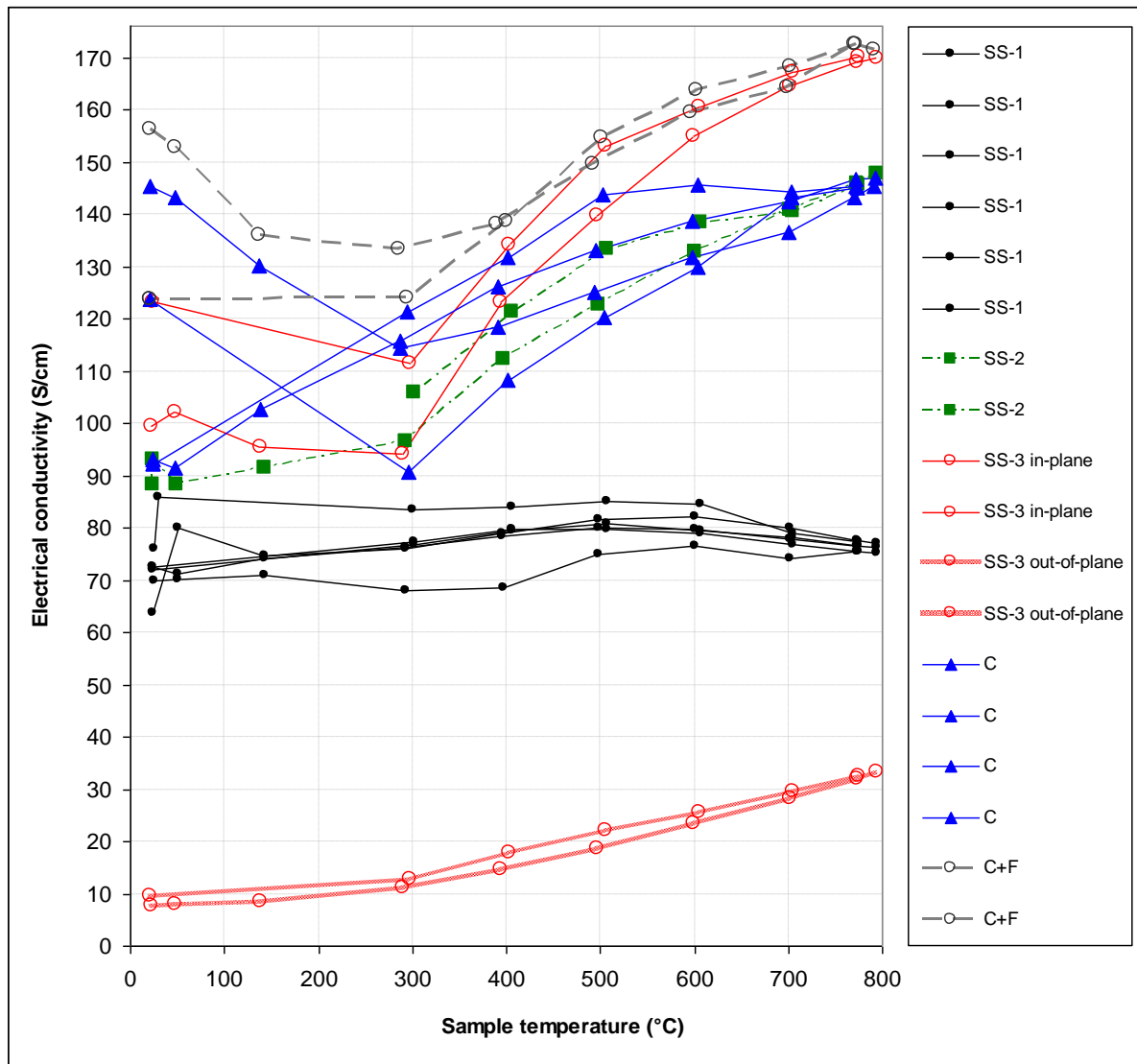
Fig. 3.10: Evolution of the electric conductivity, σ, with temperature for the non-textured and for the textured cobaltites
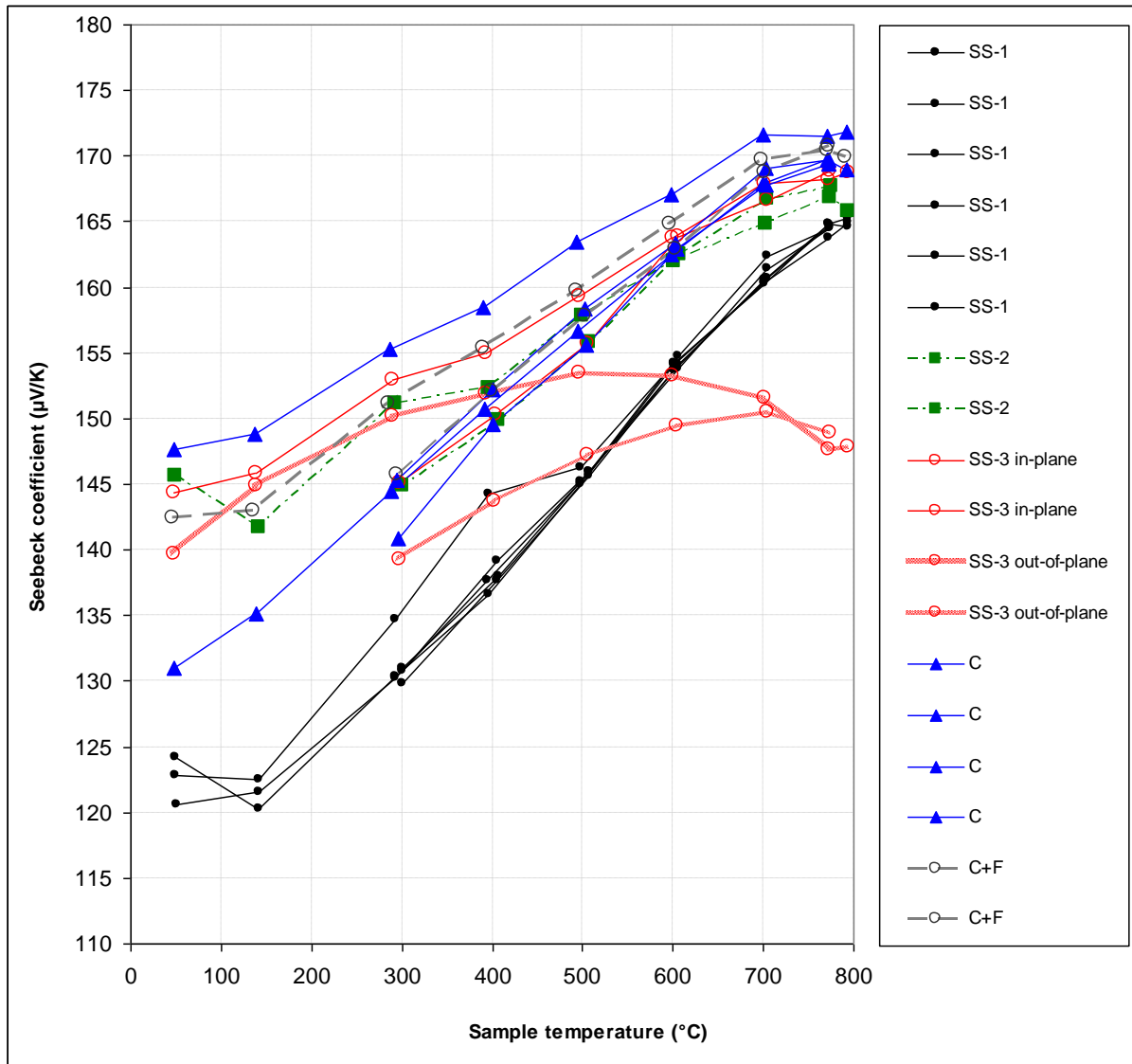
Fig. 3.11: *Evolution of the Seebeck coefficient, S, with temperature for the non-textured and for the textured cobaltites*
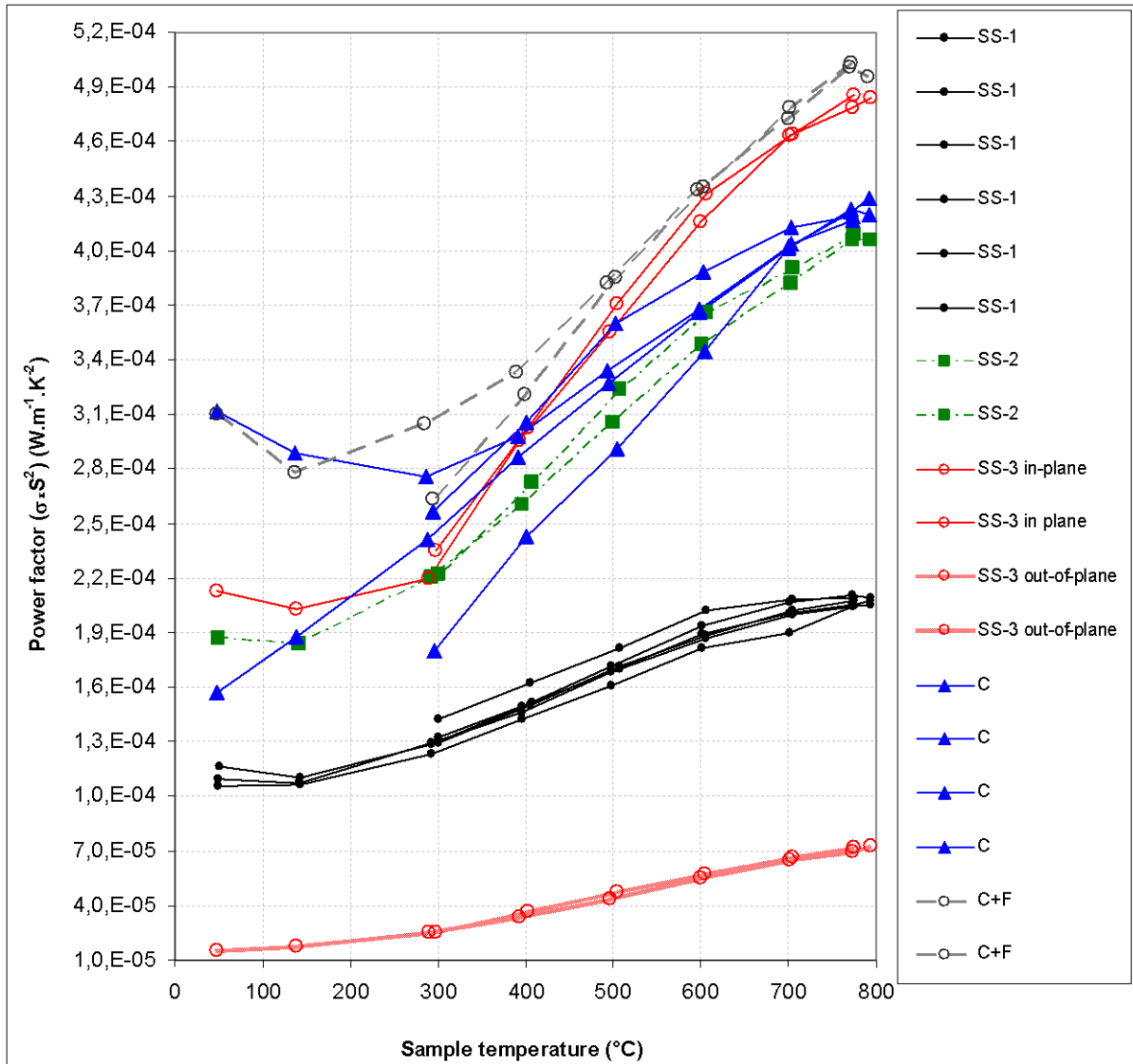
Fig. 3.12: *Evolution of the power factor, $\sigma.S^2$, with temperature for the non-textured and for the textured cobaltites*

As expected, the porous SS-1 sample exhibits poor properties compared to dense ceramics. Texturing and decrease of porosity and texturing lead to a very large improvement of the electric conductivity and a moderate improvement of the Seebeck coefficient.

The most remarkable observation is that properties of the randomly-oriented and porous SS-1 sample are much better than for the dense and out-of-plane-oriented SS-3 ceramic.

To date, the optimal texturing of $Ca_3Co_4O_9$ ceramics has been achieved by Kenfaui et al. (7) who applies much severe hot-pressing conditions (up to 30 MPa) and who uses no mold in order to allow the full creeping of ceramics.

The as-obtained thin foils are stacked without any addition and hot-pressed again to prepare the final material. Platelets are very large (diameter of about 17 μm) and are perfectly oriented. Despite a relative density of only 96 %, this texturing allows to achieve much higher thermoelectric properties: a power factor of 5.5×10^{-4} W m^{-1} K^{-2} is measured at 620°C whereas our best materials exhibit a value of 4.4×10^{-4} W m^{-1} K^{-2}.

Further comparison was done in figures 3.13 and 3.14.
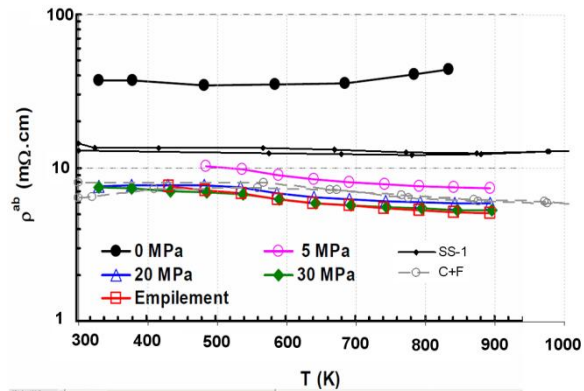

Fig. 3.13: Comparison of the in-plane resistivity between our non-textured SS-1 and textured C+F samples, and the samples prepared by Kenfaui (7)
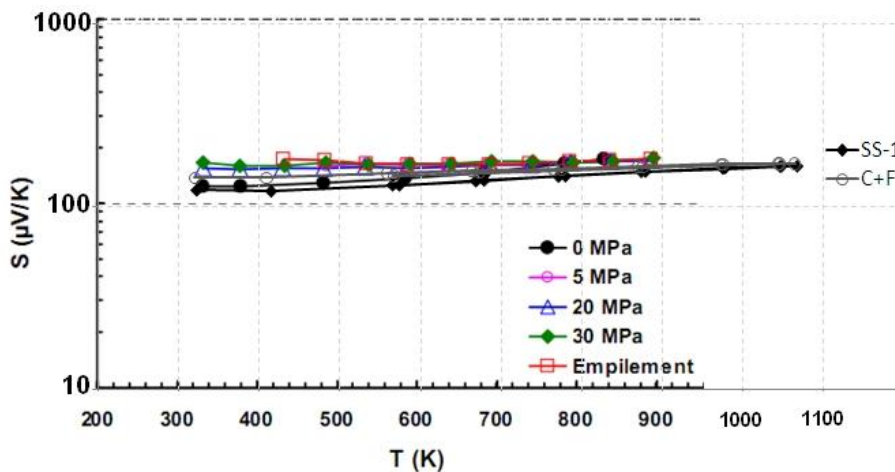
Fig. 3.14: Comparison of the in-plane Seebeck coefficient between our non-textured SS-1 and textured C+F samples, and the samples prepared by Kenfaui (7)

Assuming that our cobaltite ceramics exhibit the same thermal conductivity as those prepared by Prevel (8), the ZT of our materials were estimated and illustrated in figure 3.15.
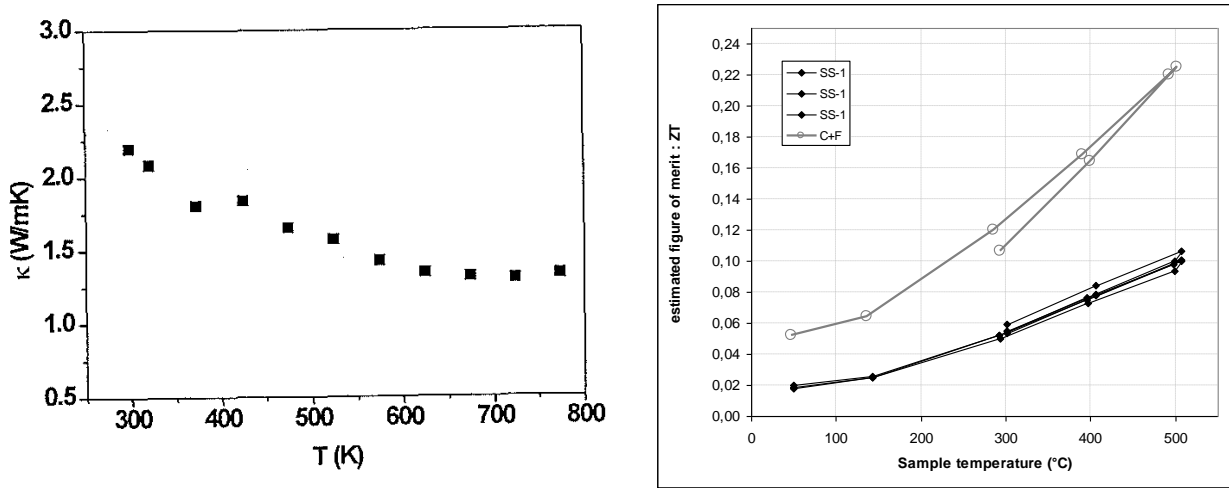
Fig. 3.15:On the left, thermal conductivity of Ca₃Co₄O₉ ceramics versus temperature; on the right, the derived figure of merit, ZT, calculated from the in-plane σ and S values of SS-1 and C+F ceramics; the figure of merit ZT corresponds to the product : $\sigma\,S^2\,\kappa^{-1}$

Porous and non textured ceramics prepared from solid state processed powders exhibit a poor figure of merit. The highest figure of merit was obtained for the C+F system: at 500°C, the ZT reaches a value of 0.22.

V.3.5 Thermoelectric module fabrication and testing

V.3.5.1 Development of the testing bench

The module testing bench, scheduled on the basis of an aluminous refractory tube sliding in a second one, is illustrated on figure 3.16. A furnace is used as the heat source. When the furnace is regulated at 1000°C, the steel plate temperature reaches about 770°C. A refractory steel plate is placed at the entrance of the furnace to achieve a homogeneous radiation. The bench is provided with a brass water-cooling block.
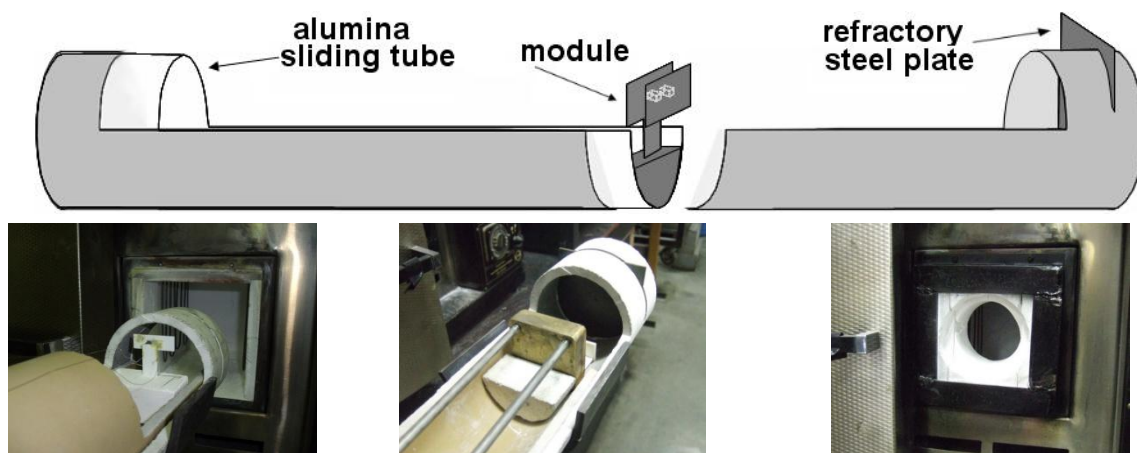
*Fig. 3.16: Thermoelectric module testing bench*

V.3.5.2 Module fabrication and characterization

Substrates used for the fabrication of modules are dense alumina plates of 1 mm thickness. The P-leg of the module was prepared from the sample SS-3. The cutting was done so as to keep the bar axis along the out-of-plane direction. For the N-leg, a manganite ceramic and a zinc oxide ceramic were used. Metallisation was done with two different silver pastes.

A first module was prepared from the cobaltite leg and a ZnO leg fabricated in the laboratory starting from the commercial ultrafine undoped powder (Zano® 10, Umicore). After sintering, the ZnO leg was dense (porosity of 0.4 vol%). As the system is undoped, ZnO leg is non conductive at low temperature and becomes conductive for temperatures higher than 600-750°C. The module n°1 (figure 3.17) was assembled using a silver paste containing glass frit. The apparent open-circuit voltage of this module, measured with the thermoelectric testing bench, is presented on figure 3.18.

Fig. 3.17: Module n°1 before (left pictures) and after annealing (right pictures)
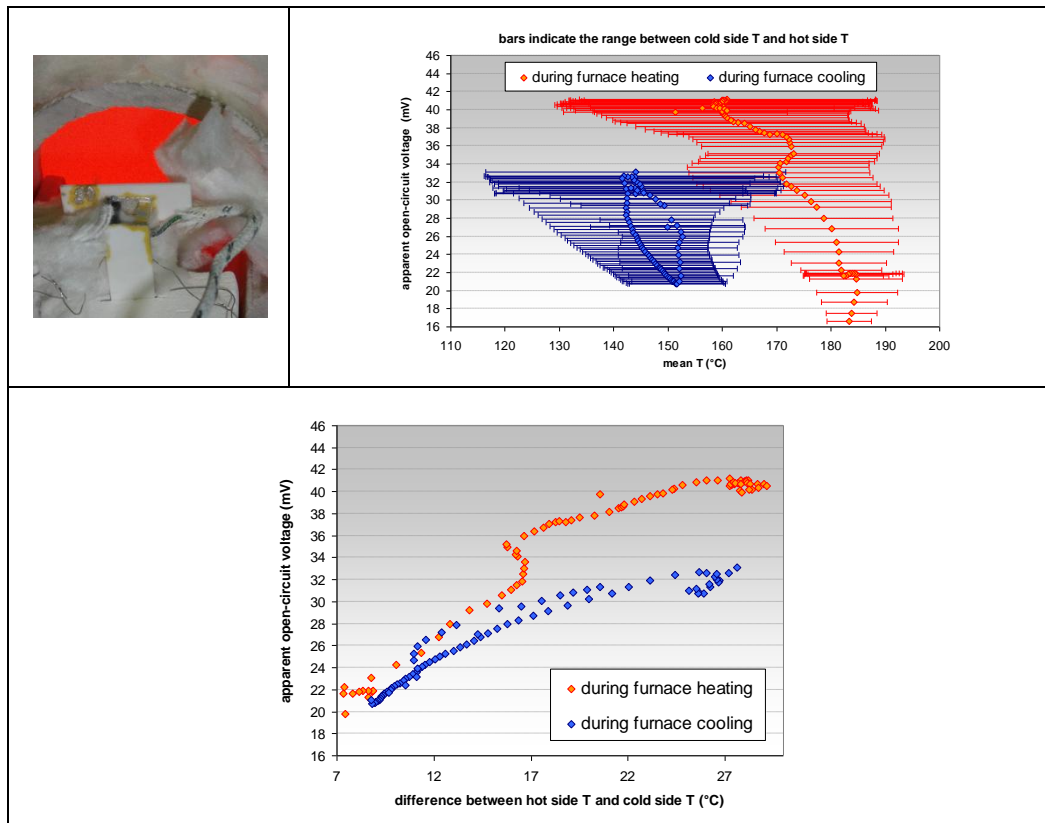
Fig. 3.18: Measurement of the apparent open-circuit voltage of module n°1

The apparent voltage increases as the temperature difference between the hot and the cold side increases, evidencing thermoelectric voltage generation. When the temperature difference was set to a negative value a constant voltage of 17 to 18 mV was detected. In principle, no voltage should be generated under these conditions. The observed constant voltage may correspond to the baseline of the measurements.

Undoped $CaMnO_3$ powder, synthesised through the spray-drying technique, was supplied by the ULg partner. After sintering, the $CaMnO_3$ ceramic was used as the N-type leg of a second module. Assembling was performed using a different silver paste, free of glass frit, following the same procedure as Lemonnier (9). This module broke and could not be tested.

<u>V.3.6 Conclusion and outputs</u>

V.3.6.1. Benefits of hydrothermal synthesis

Traditional hydrothermal route cannot be applied to the synthesis of misfit cobaltite. Our attempts to prepare $Ca_3Co_4O_9$ powders failed systematically. The reason is predicted by the Pourbaix diagram of cobalt: 4+ valency of cobalt ion cannot be stabilized because it is reduced by water. A possibility would be to process the misfit phase by a hybrid hydrothermal-electrochemical method.

The strontium manganite system is more likely to full crystallization. Our processing conditions are however limited, especially in terms of temperature, leading to a very long reaction time. With a suitable equipment (with a lining that avoids reduction of MnO_2 species and withstands higher reaction temperatures) it may be possible to achieve the full crystallization in few hours (less than 10 hours would be competitive). The main disadvantage of the hydrothermal process is the multiple washing steps: a reuse of the KOH aliquot from one batch to the other could be a way to spare water and time.

V.3.6.2 Thermoelectric materials: from the powder synthesis to the module

Fine cobaltite powders prepared from the citrate route lead to a more textured ceramic after hot pressing. But the best thermoelectric performance is achieved when this fine powder is blended with much larger flux-grown particles. To enhance the power factor, three conditions must be simultaneously satisfied: the lowest porosity, the largest grain size (largest platelet diameter) and a good alignment of these platelets perpendicularly to the hot pressing load direction.

Hot-pressed ceramics prepared from the solid state powder and textured by creeping exhibit a thermoelectrical behavior quite as good as in the blended citrate + flux-grown system but

with a main difference: the process starting from the solid-state synthesis route is more simple.

The properties of the textured $Ca_3Co_4O_9$ ceramics prepared at CRIBC are in good agreement with literature. However, as creeping of cobaltites was observed already at 750°C, a better texturing and enhanced thermoelectric properties can be expected if the load is applied sooner (since 750°C instead of 900°C).

A testing bench was fabricated for modules thermoelectric characterization. A good assembly of the module elements was obtained using a silver paste with glass frit. Thermoelectric voltage generation was evidenced on the module prepared from the cobaltite and the ZnO legs.

V.3.6.3 Outlook on thermoelectric materials and benefits of the CHEMAT project

The CHEMAT project was the opportunity for two partners, ULg and CRIBC, to initiate a common work on thermoelectric materials with complementary approaches. ULg developed a new and promising synthesis route leading to fine and pure powders with a controlled stoichiometry and controlled particle size distribution. Synthesis investigations at CRIBC were focused on reference thermoelectric ceramics with the aim to develop its experience on materials characterization and modules fabrication.

The module combining the optimised cobaltite P-leg fabricated at CRIBC and the optimised $CaMnO_3$ N-leg fabricated at ULg could not yet be tested. A new assembly should soon be available and characterized on the thermoelectric testing bench.

New formulations developed at ULg and CRIBC should be investigated in the frame of a future collaboration.

The hydrothermal synthesis was only applied to undoped $SrMnO_3$ powder during the CHEMAT project and the resulting powders were not effective for thermoelectric application. But cerium doping of $SrMnO_3$ is known to increase the power factor and lead to promising thermoelectric performance (the power factor reported by Hashimoto et al. (2) for the composition $Sr_{0.9}Ce_{0.1}MnO_{3-\delta}$ reaches $3.9x10^{-4}$ W K^{-2} m^{-1} at 800°C). Investigations on hydrothermal synthesis, at CRIBC, will be pursued on that system. Future developments at CRIBC will be focused on planar structures developed through innovative processes. Indeed, in the frame of the Convergence program supported by the Walloon Region and the European Regional Development Fund, numerous researches have started on ink-jet deposition and laser surface treatments. CRIBC intends to apply these processes to the

fabrication of planar thermoelectric structures and thermoelectric ceramics with additional functional properties, giving new perspectives of collaboration.

V.3.7 References

(1) "Atlas of Electrochemical Equilibria in Aqueous Solutions", M. Pourbaix, Pergamon, New York, (1966).

(2) "Hydrothermal synthesis of the perovskite manganites $Pr_{0,5}Sr_{0,5}MnO_3$ and $Nd_{0,5}Sr_{0,5}MnO_3$ and alkali-earth manganese oxides $CaMn_2O_4$, 4H-$SrMnO_3$ and 2H-$BaMnO_3$", J. Sporen, R.I. Walton, Journal of Solid State Chemistry 178 (2005) 1683-1691.

(3) "Study on the structural and electrical properties of $Sr_{1-x}Ce_xMnO_{3-\alpha}$ (x = 0.1, 0.3) perovskite oxide", S. Hashimoto, H. Iwahara, Materials Research Bulletin 35 (2000) 2253–2262.

(4) "Structural, Thermal and Electrical Properties of Ce-Doped $SrMnO_3$", S. Hashimoto, H. Iwahara, Journal of Electroceramics 4:1 (2000) 225–231.

(5) "Structural and physical properties of $SrMn_{1-x}Ru_xO_3$ perovskites", S. Kolesnik, B. Dabrowski, and O. Chmaissem (2008) http://arxiv.org/PS_cache/arxiv/pdf/0811/0811.4181v1.pdf

(6) CHEMAT annual report n°3 (2009).

(7) "Texturation et empilement des céramiques $Ca_3Co_4O_9$: Anisotropie des propriétés mécaniques et thermoélectriques", D. Kenfaui, D. Chateigner, M. Gomina et J.G. Noudem, 2ème réunion du GDR Thermoélectricité, ENSCP Paris, 01 juin 2008
http://gdr-thermoelectricite.cnrs.fr/Contributions-Paris2008/P5-Kenfaui.pdf

(8) "Synthèse et caractérisations de céramiques thermoélectriques $Ca_3Co_4O_9$ élaborées par frittage forgeage", M. Prevel, PhD thesis of the University of Caen (France) (2007), Reference n°: 2007CAEN2030.

(9) "Développement d'un générateur thermoélectrique à base de matériaux oxydes", S. Lemonnier, PhD thesis of the University of Caen (France) (2008), Reference n°: 2008CAEN2031.

VI.   DIFFUSION OF KNOWLEDGE

Diffusion of knowledge - CHEMAT Publications

(1)   "Enhancement of the power factor of BiCaCoO-Ag composites prepared by the spray-drying method", by B. Rivas-Murias, H. Muguerra, M. Traianidis, C. Henrist, B. Vertruyen, R. Cloots, Solid State Sciences, 12, 2010, 1490-1495.

(2)   "Improvement of the thermoelectric properties of BiCaCoO cobaltite by chimie douce methods", by H. Muguerra, B. Rivas-Murias, M. Traianidis, C. Henrist, B. Vertruyen, R. Cloots, Journal of Solid State Chemistry, 183, 2010, 1252-1257.

(3)   "Modulated misfit structure of the thermoelectric BiCaCoO cobalt oxide", by H. Muguerra, D. Grebille, E. Guilmeau, R. Cloots, Inorganic Chemistry, 47, 2008, 2464-2471.

(4)   "Structural and electrochemical characterization of mesoporous thin films of NbVO5 upon lithium intercalation", by N. Krins, L. Lepot, R. Cloots, B. Vertruyen, Solid State Ionics, 180, 2009, 848-852.

(5)   "Soft templating synthesized mesoporous thin film as positive electrode design for lithium battery: NbVO5 as a model phase", by N. Krins, J. Bass, D. Grosso, C. Henrist, R. Delaigle, E. Gaigneaux, R. Cloots, B. Vertruyen, C. Sanchez, to be published in Chemistry of Materials.

(6)   "Thin La2Zr2O7 films made from a water-based solution", by V. Cloet, J. Feys, R. Huehne, S. Hoste, I. Van Driessche, Journal of Solid State Chemistry, 182, 2009, 37-42.

(7)   "Transmission electron microscopy analysis of a coated conductor produced by chemical deposition methods", by V. Cloet, T. Thersleff, O. Stadel, S. Hoste, B. Holzapfel, I. Van Driessche, Acta Materialia, 58, 2010, 1489-1494.

(8)   "CeO2 buffer layers for HTSC by an aqueous sol-gel method – chemistry and microstructure", by N. Van de Velde, D. Van de Vyver, O. Brunkahl, S. Hoste, E. Bruneel, I. Van Driessche, European Journal of Inorganic Chemistry, 2, 2010, 233-241.

(9)   "A nitrilo-tri-acetic/acetic acid route for the deposition of epitaxial cerium oxide films as high temperature superconductor buffer layers", by T. Thuy, P. Lommens, V. Narayanan, N. Van de Velde, K. De Buysser, G. Herman, V. Cloet, I. Van Driessche, Journal of Solid State Chemistry, 183, 2010, 2154-2160.

Diffusion of knowledge – new collaborations

One of our "researcher", Natacha KRINS, not financed through the CHEMAT project, has established in the framework of the WP#1, a strong collaboration with the team of Dr Clement Sanchez (Chimie de la Matière Condensée, UMR, UPMC-CNRS 7574, Université Pierre et Marie Curie, Paris 6, Collège de France) leading to a Post-Doctorate from November 2009 until December 2010.

She worked on **Mesoporous SiO₂ thin films containing photoluminescent ZnO nanoparticles**. Mesoporous thin film (MTF) appears as a promising architecture in numerous applications. It offers a large surface area and a facile access to the inorganic network is provided by the highly homogeneous 3D-interconnected pore structure. This architecture

can be achieved using the evaporation induced micelles packing. This one-pot synthesis combines the sol-gel chemistry and the self-assembling method. MTF of numerous crystalline transition metal oxides can be achieved by dip-coating the solution containing the inorganic precursors and amphiphilic block copolymer as structuring agent and applying a well-defined thermal treatment, as for anatase TiO_2, WO_3, Nb_2O_5, V_2O_5 MTF's. However, for some others like ZnO, the synthesis of crystalline MTF remains challenging. In this case, the crystal growth occurs so fast that, whatever the thermal treatment, mesoporous structure collapses upon heating. This project aimed at studying how the addition of silica allows to provide films containing ZnO crystallites homogeneously dispersed in SiO_2 mesoporous matrix and what is the minimum silica content required. This study is based on an in-situ simultaneous SAXS – WAXS – TEA investigation. It was shown that only 30% of silica is required to obtain crystalline ZnO-based MTF. [1]

She worked also on **Thick and Crack-Free Nanocrystalline Mesoporous TiO_2 Films Obtained by Capillary Coating from Aqueous Solutions.** Another part of the project aims at synthesizing MTFs from aqueous solution. In the classical viscous dip-coating approach, the deposition of water solution was prohibited because of its very high surface tension. However, in a recent work, Faustini et al. [2] show that below a critical withdrawal rate, the thickness of the film does not depend of the solvent surface-tension anymore. This regime is called the "capillarity" regime. My work consisted in testing this regime for water-based solution, in particular, investigating the case of TiO_2 MTF. It appears that films of good optical quality were achieved. In drastic conditions of deposition temperature and withdrawal speed (80°C and 10^{-3} mm/s, respectively), 800nm thick film can be achieved for only one layer after a flash treatment of 500°C for 1 minute [3]. It was also observed that "grid-like" anatase TiO_2 MTFs were achieved without any specific aging or slow thermal treatment in contrast with what is required for usual ethanol-based solution [4]. An efficient multilayer deposition process was also developed [3]. The opening of the evaporation induced self-assembling method would allow to extent the synthesis of MTF to other compounds previously inaccessible in organic solvent.

_____

[1]   N. Krins et al., J. Mater. Chem. 21 (2011) 1139.

[2]   M. Faustini et al., J. Phys. Chem. C 114 (2010) 7637.

[3]   N. Krins et al., Chem. Mater. 22 (2010) 6218.

[4]   D. Grosso et al. Chem. Mater. 15 (2003) 4562.

She is now associated researcher of the FNRS, and she is doing, from January 2011 until December 2011 a second Post-Doc in the Advanced Energy Technologies Department, at Lawrence Berkeley National Laboratory, Berkeley, CA, USA (Dr. Thomas Richardson), initiating by this way a new collaboration between ULg and Lawrence Berkeley National Laboratory.

The research she will pursue concerns again the development of mesoporous materials for energy applications. Mesoporous materials have recently attracted much interest in the field of energy storage. Various mesoporous micro-sized particles have been investigated as positive/negative electrode active material in lithium battery (MnO_2 [1], $LiCoO_2$ [2], $LiFePO_4$ [3], $LiMn_2O_4$ [4], TiO_2 [5],...) and it has been recently shown that mesoporous thin films (MTF) are promising in electrochemical supercapacitor applications (TiO_2 [6], Nb_2O_5 [7], MoO_3 [8]). The high insertion capacity and the fast lithium insertion kinetic observed for these mesoporous materials mainly result from (1) the facilitated electrolyte transport through the continuous and homogeneous 3D porous network, (2) the maximized electrode-electrolyte contact area, (3) the decreased penetration depth for ions/electrons according to the small size of the crystals constituting the thin inorganic thin walls and (4) the continuous pathway formed by the interconnected crystals. The good cyclability property is attributed to the ability of the mesoporous inorganic scaffold to accommodate mechanical stresses induced during lithium insertion/extraction. Other characteristics of these systems were shown to play a significant role in the achievement of higher rate capabilities like the orientation of the crystallites, the presence of a conductive carbon coating.

This work aims at studying how the characteristics of the mesoporous architecture individually affect the electrochemical properties of an energy storage system; for example., in which extent do the size of the pores and their interconnectivity affect the transport of a given electrolyte, what is the ideal wall thickness to increase the kinetics transport while preserving good cycling properties, what is the effect of carbon coating on the electron transport, what is the maximal particle size/film thickness to keep a sufficient electronic transport to the current collector, etc. In order to address these questions, we propose to study the electrochemical behavior of anatase TiO_2 mesoporous thin films (MTF) whose pore size, inorganic wall thickness, porous organization and film thickness can easily be tuned using soft templating methods. MTF architecture appears as a good model phase as it constitutes a "clean" electrode exempt of binder or carbon additives. Furthermore, from these MTF, more complex architecture can be achieved like carbon-coated electrode or others presenting hierarchical porous system. It may also be imagined building a 3D energy storage system where positive and negative electrode would be interdigitated.

An extensive knowledge of the mesoporous structure and its cristallinity will be achieved combining, SEM, TEM, tomography and XRD. Electrochemical investigations based on cyclic voltammetry, charge-discharge experiments and electrochemical impedance spectroscopy will allow access to the high-rate capability, the cycling behavior and the relative contributions of pseudo-capacity, classical intercalation capacity and double layer capacity. This is in direct continuity with the work done in the context of the CHEMAT project.

_____

[1]   Y. Ren et al., J. Am. Chem. Soc. 132 (2010) 996.

[2]   P.G. Bruce et al., Angew. Chem. Int. Ed. 47 (2008) 2930.

[3]   Z.C. Shi et al., Electrochimica Acta 53 (2008) 53, 2665.

[4]   J. Luo et al., Chem. Mater. 19 (2007) 4791.

[5]   Y. Ren, Angew., Chem. Int. Ed. 49 (2010) 2570 –2574.

[6]   T. Brezesinski et al., J. Am. Chem. Soc. 131 (2009) 1802.

[7]   K. Brezesinski , J. Am. Chem. Soc. 132 (2010) 6982.

[8]   T. Brezesinski, Nature Materials 9 (2010) 146.

VII.   ACKNOWLEDGMENTS

The CHEMAT consortium would like to acknowledge the "follow-up committee" for its participation during the CHEMAT running research program. During the year 2008, we didn't succeed to organize a meeting with all the follow-up committee members. A decision was made to solicit new members in order to ensure a good return from the industry and public organizations concerning the adequate relation between the research and their expectations.

The "new" follow-up committee was composed as follow:
- Alain STEPHENNE, from the Region Wallonne
- Paul WAUTERS, from Inergy Automobile
- Pierre COOLS, from Thales Alenia Space
- Benedicte ROBERTZ, from UMICORE
- David VANDEVYVER, from Centexbel
- Fabrizio MASERI, from Arcelor-Mittal
- Julien THIRY, from PIMW
- Yves TOUSSAINT, from Green Propulsion

A meeting has been organized at the beginning of year 2009 and at the beginning of year 2010 giving us the possibility to diffuse the scientific reports from year 2007 and 2008 and to evaluate the potential impact of the main results of the research on the transfer of technology from academy to industry!

A few companies (UMICORE, Arcelor-Mittal, Centexbel,...) have marked an interest on the research conducted through the CHEMAT consortium, and have initiated collaborations on different subjects directly connected to the CHEMAT program (Li-ion batteries) or related to the CHEMAT program (materials for photovoltaïcs).